AD NUMBER

AD918237

NEW LIMITATION CHANGE

TO

Approved for public release, distribution unlimited

FROM

Distribution authorized to U.S. Gov't. agencies only; Test and evaluation; Feb 1972. Other requests shall be referred to AF Flight Dynamics Laboratory, [FGL], Wright-Patterson AFB, OH, 45433.

AUTHORITY

AFFDL ltr, 27 Dec 1977

AFFDL-TR-72-13

AD918237

TEST AND DEVELOPMENT OF FLIGHT CONTROL ACTUATION SYSTEM COMPONENTS FOR MILITARY AIRCRAFT

SANFORD M. GOLDSTEIN

HARRY W. SCHREADLEY

DALE G. RAZILL

HYDRAULIC RESEARCH AND MANUFACTURING COMPANY

VALENCIA, CALIFORNIA

TECHNICAL REPORT AFFDL-TR-72-13

D D C

FEBRUARY 1972

AIR FORCE FLIGHT DYNAMICS LABORATORY
AIR FORCE SYSTEMS COMMAND
WRIGHT-PATTERSON AIR FORCE BASE, OHIO

NOTICE

When Government drawings, specifications, or other data are used for any purpose other than in connection with a definitely related Government procurement operation, the United States Government thereby incurs no responsibility nor any obligation whatsoever; and the fact that the Government may have formulated, furnished, or in any way supplied the said drawings, specifications, or other data, is not to be regarded by implication or otherwise as in any manner licensing the holder or any other person or corporation, or conveying any rights or permission to manufacture, use or sell any patented invention that may in any way be related thereto.

Copies of this report should not be returned unless return is required by security considerations, contractual obligations, or notice on a specific document.

AFFDL-TR-72-13

TEST AND DEVELOPMENT OF FLIGHT CONTROL ACTUATION SYSTEM COMPONENTS FOR MILITARY AIRCRAFT

SANFORD M. GOLDSTEIN

HARRY W. SCHREADLEY

DALE G. BAZILL

D D C

APR 15

D

FOREWORD

The effort described in this document was performed by the
Controls Division of Hydraulic Research and Manufacturing Com-
pany under Air Force contract F33615-71-C-1124. The contract
was performed under Project Number 8225, Task Number 822510, en-
titled "Unique and Promising Flight Control Actuation Techniques
for Military Aircraft." Work under the contract was carried
out at Wright-Patterson Air Force Base, utilizing United States
Air Force facilities. The program was monitored by Mr. T. D.
Lewis of the Air Force Flight Dynamics Laboratory (FGL), Wright-
Patterson Air Force Base, Ohio 45433.

The authors wish to express their acknowledgement to the mem-
bers of the Hydraulic Research and Manufacturing Company person-
nel, W. Stoddard, C. Black, and W. Talley, for their assistance
in the execution of the program.

The report covers work performed between 8 December 1970,
and 3 November 1971. The manuscript was released by the authors
in November 1971 for publication as a technical report.

This report contains no classified information extracted
from other classified documents.

This technical report has been reviewed and is approved.

G. H. Purcell
Acting Chief
Control Systems Development Branch
Flight Control Division
Air Force Flight Dynamics Laboratory

ABSTRACT

Test and development activities conducted under this contract were conducted in the following nine areas:

1. Evaluation of a Breadboard Multiplexing System Driving a Fly-by-Wire Actuator. This included comparison of multiplexed actuator loop response to conventional approaches.

2. Evaluate Actuation system of six-degree of freedom motion base. An optimally sized actuator and servo valve were designed, fabricated and tested.

3. A General purpose actuator teststand was evaluated. Structural analysis was accomplished and a general purpose loading actuator was investigated.

4. Various design concepts were explored for the improvement of branch isolation techniques. These included Variable Orifice, Electronic, Active Orifice, Square Root and Non-Linear Spring techniques.

5. Evaluation of a Vickers Inc. Integrated Servopump Actuator Package. This included loaded and unloaded response characteristics with two fluids MIL-H-5606, and MIL-H-83282.

6. Investigation of limit cycle characteristics of a General Electric 666A actuator.

7. Literature Survey and recommendations for a laboratory contamination measurement system choice.

8. Fabrication of a portable flow measurement stand.

9. Design and Fabrication of a transducer Range and Balance Panel.

TABLE OF CONTENTS

LIST OF ILLUSTRATIONS

LIST OF ILLUSTRATIONS

LIST OF ILLUSTRATIONS

LIST OF ILLUSTRATIONS

LIST OF ILLUSTRATIONS

LIST OF ILLUSTRATIONS

LIST OF ILLUSTRATIONS

SECTION I

EVALUATION OF MULTIPLEX DEMONSTRATOR

INTRODUCTION

The digital single line multiplex unit was tested to determine the effect of multiplexing on a hydraulic servoactuator when used in a closed loop flight control system.

A multiplex demonstrator was fabricated by the Fort Worth Division of General Dynamics under Air Force Contract F33615-71-C-1574, "Definition and Demonstration of an Optimum Solid-State Switching and Multiplexing System for Use in a Fly-By-Wire Flight Control System" As part of that contract, a detailed trade study was performed to determine the most efficient design of a Fly-By-Wire multiplexing unit. The resulting multiplex demonstrator unit was delivered to Control Elements Branch, Flight Control Division of the Air Force Flight Dynamics Laboratory, Wright-Patterson Air Force Base, Ohio.

The selected method of multiplexing a quad-redundant system is shown in the block diagram of Fig. 1 for a single branch with time shared voting between branches. This system utilizes a digital, code division multiplex system with self-clocking modulation.

The demonstrator was capable of accepting 4 analog signals (pitch, roll, yaw, and test) and 4 discrete signals into an 8-channel multiplexer which converts the analog signals from a parallel to a serial mode for analog to digital conversion in a 10 bit A/D converter. The basic clock frequency is 62.5 kilohertz, obtained by passing a 1 megahertz crystal controlled clock through a divide by 16 counter. A typical transmitted digital word contains a leading "1" state, a 4 bit address, a 10 bit data word and 1 bit for an odd parity check. In addition to the 16 bits per word, 2 additional bits are required to prepare and load data into the shift registers. This requires a total of 18 bits per word.

The information update rate is the basic clock frequency, 62.5 kilohertz divided by (18 bits per word times 8 words to be sampled sequentially) or 434 samples/second.

1
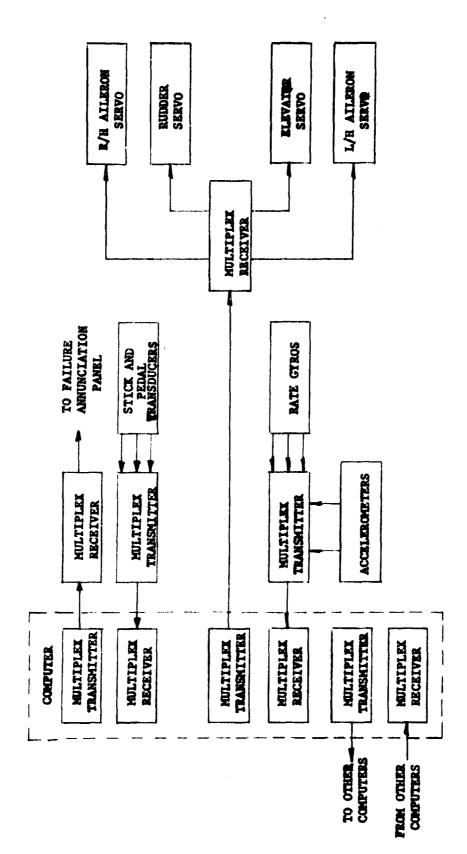
Figure 1. Multiplexing Block Diagram for a Single Branch System

Data is transmitted through 200 feet of shielded, twisted pair cable to receiver #1. The #1 receiver clock is synchronized with the transmitter by a manchester code generated in the transmitter. This produces bi-phase data, which in turn triggers a mono-stable multivibrator in receiver #1. A 2 bit gap detector synchronizes receiver #1 to each word. These digital words are routed to a 10 bit D/A converter. They are then segregated to respective sample and hold output units by use of the 4 bit addresses and a 1 of 10 decoder.

The analog to digital converters are 10 bit converters that utilize 9 bits for a digital word and 1 bit for a sign. The input or output voltage level that the A/D or D/A converters operate with is $\pm$ 10 V DC. Since the total bit count for a 10 bit word is 511 x 2 (for polarity sign change) or 1 out of 1022 (.097%) resolution, this would be .097 x $\pm$ 10 V or 20 V = .0194 volt signal resolution.

Transmitter #2 and receiver #2 in the demonstrator are basically used to monitor redundant surface, stick and pedal positions. Transmitter #2 data word consists of 1 sync bit, 5 bit address, 9 bit data word, 1 parity bit for a total of 16 bits per word + 2 bits for preparing and loading data to shift registers. The clock rate is determined by a 1 megahertz crystal clock divided by 16 which is 62.5 kilohertz. Transmitter #2 transmits 17 position signals, these are a test voltage, elevator position A, B, C, & D, rudder position A, B, C, & D, left aileron position A, B, C, & D, right aileron position A, B, C, & D. The elevator, rudder, right aileron and left aileron (inverted right aileron) B, C, and D inputs are for demonstration purposes. The "A" signal taken from the output of receiver #1 is split into 4 failure switches for the A, B, C, or D channel.

The sampling rate of transmitter #2 is 62.5 kilohertz divided by (18 bits/word x 17 words) or 204 samples per second. The 9 bit data word uses 8 bits for count and 1 bit for polarity. This gives a total count of 256 x 2 (for polarity sign change) or a 512 count for full scale input. The input voltage is $\pm$ 10 V or a total of 20 V. Signal resolution is 1/512 = .194% or .0388 volts.

The output of receiver #2 is directed to a servo monitor "A" channel of each surface monitor and is compared to its B, C, and D channels using an analog comparator. Comparators switch

3

when a 10% or 2 volt error signal is detected. This error detection is sent via transmitter #3 and receiver #3 to the annunciator panel. The error is also used in transmitter #1 to enable or lock the shift registers.

A more detailed description of the multiplex unit is included in Technical Report AFFDL-TR-70-80.

PROCEDURE

The following parameters were investigated through each phase of testing.

      1. Noise level of signals (digital instabilities and analog noise)
      2. Response of system in terms of:
         a. amplitude ratio
         b. phase lag angle
         c. step and pulse
      3. Resolution and threshold
      4. Interface requirements

The following test program was established for the multiplex demonstrator.

I. Measure and Observe the Characteristics of the Multiplex Demonstrator as Received.(Refer to AFFDL TR-70-80 for pin locations, etc.)
   A. Transmitter #1 to receiver #1
     1. Drive system with a function generator at points - J51-1 (elev.), J51-2 (rudder), and J51-3 (aileron)
     2. Monitor system at points J16, J17, and J18 respective to input signal

   B. Transmitter #1 to receiver #1 and back through transmitter #2 to receiver #2
     1. Drive system as in step IA1
     2. Monitor system at points A2A3-1, A2A11-5, and A2A19-5 respective to input signal

   C. Transmitter #2 to receiver #2
     1. Disconnect leads at A2A2A19-J (elev. "A"), K6-6 (elev. "B"), K7-6 (elev. "C"), and

4

K8-6 (elev. "D"), individual leads to
these same points to connect to a func-
tion generator in parallel
2. Monitor system at A2A3-1
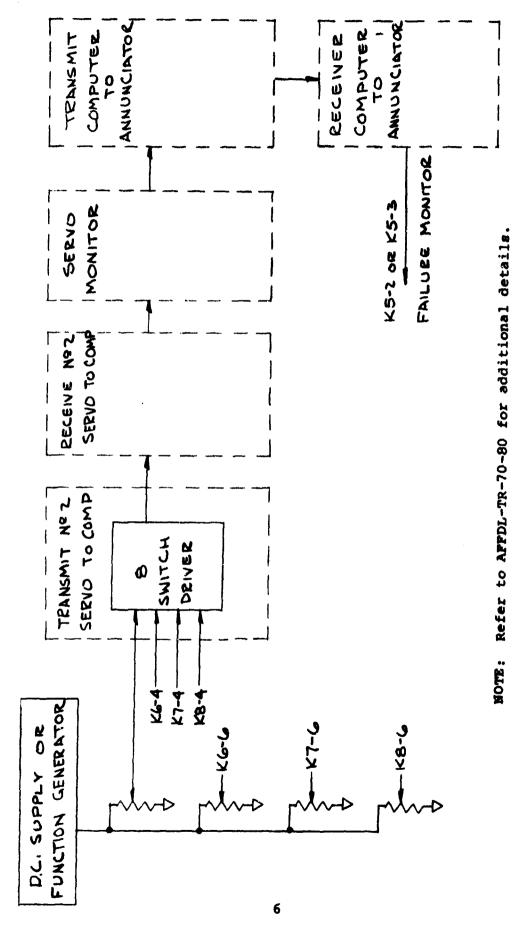
D. Failure detection level of comparators
1. Connect 4 potentiometers to the leads
connected in step IC1 as in Fig. 2.
a. make static (D.C. supply) and dy-
namic checks (function generator)
2. Monitor input differences at potentio-
meters and failures at K5-2 or K5-3 and
failure indicator panel.

II. Measure and Observe the Characteristics of a Closed Loop
Electrohydraulic Actuator System using the Multiplex
Demonstrator in the Transmission Lines

A. Electrohydraulic actuator without multiplex demon-
strator in loop
1. Operate at loop gains of 12, 60, and 120
B. Electrohydraulic actuator with multiplex demon-
strator in loop as in Fig. 3.
1. Operate at loop gain in step IIA1
C. Electrohydraulic actuator with multiplex demon-
strator as in Fig. 4.
1. Operate at loop gains in step IIA1

DISCUSSION OF TEST RESULTS

The multiplex demonstrator was checked as received. The
initial checking was done visually by use of internal inputs
provided on the test panel. Some noise (small random deflec-
tion of the meter) was noticed in servo output positions, al-
though respective input signals were clean.
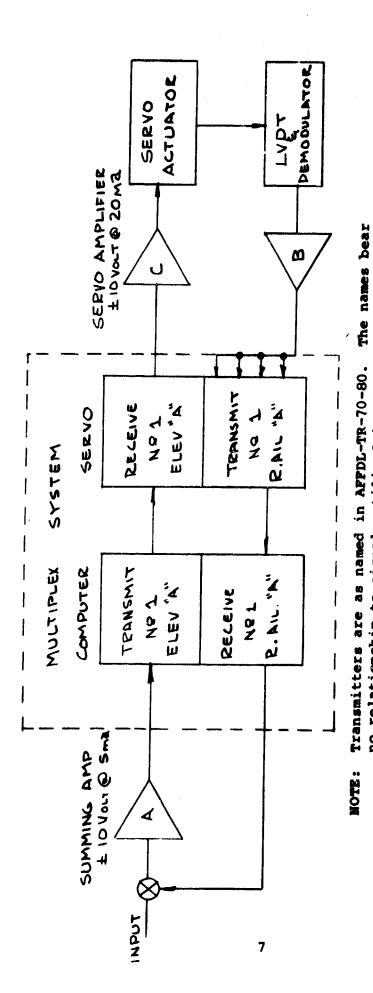
All of the failure simulator switches and corresponding
failure indicating lights on the pilot and maintenance panels
functioned as described. All failures could be reset to a
normal state after removal of failures.

Frequency response testing was accomplished on the trans-
mitter #1 to receiver #1 section, elev. "A", rudder "A", and
right aileron "A" channels as follows:

5

NOTE: Refer to AFFDL-TR-70-80 for additional details.

Fig. 2 – Test Circuit to Monitor Failure Detection

6

NOTE: Transmitters are as named in AFFDL-TR-70-80. The names bear no relationship to signals utilized in the test.

Fig. 3 — Test Setup for Driving a Servo Actuator – Option No. 1

7
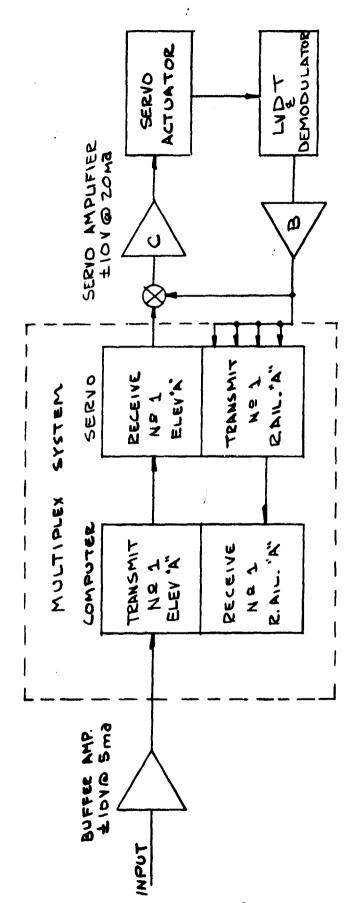
Fig. 4 - Test Setup for Driving Servo Actuator - Option No. 2

A 3 volt peak to peak sine wave from a function generator was used as an input signal to J51-1 (elev. A), J51-2 (rudder "A") and J51-3 (right aileron "A") and monitored at J-16, J-17 and J-18 individually. As the input signal frequency was varied from .01 to 100 CPS, the output signal was compared to the input signal in terms of variation of amplitude, phase lag, and wave shape changes.
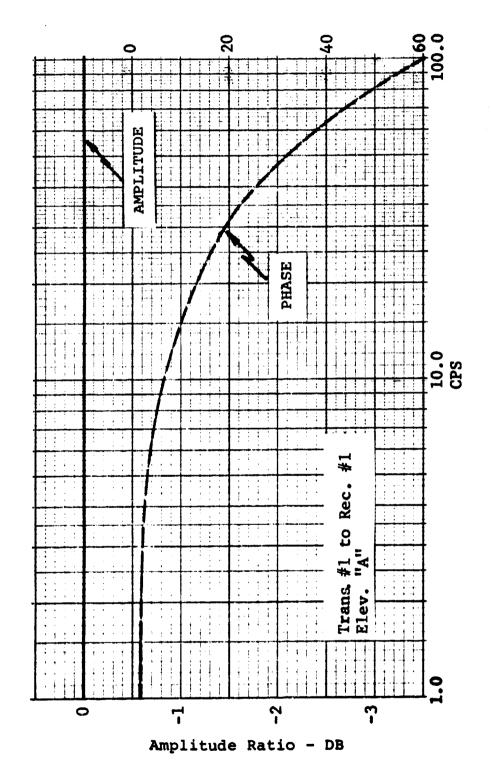
All channels exhibited the same characteristics as shown in Fig. 5, 6, and 7. It was noted that none of the channels exhibited an amplitude change. Only an output phase lag was detected. This phase lag is not directly related to the phase lag that is noticed in an RC circuit or a mechanical equivalent circuit, but a constant time delay of approximately 17 milliseconds contributed by the time required to process the data. Therefore, this had little or no effect on the wave shapes.

Observed noise on each of the outputs from receiver #1 were recorded as follows:

With inputs grounded at transmitter #1, the output noise of receiver #1 was 150 millivolt peak to peak at 62.5 KC with a random level shift of 20 millivolts. The amplitude of a 1 CPS square wave input signal was increased until a recognizable square wave was detected at the output of receiver #1. The corresponding input signal required was .065 V peak to peak. The output signal was approximately .060 V peak to peak with .100 V peak to peak noise on the signal (Fig. 8). Of course, this noise had little effect on the higher level input signals such as 5 to 10 V peak to peak. In order to verify functionality of the demonstrator, a brief check was made using jacks on the demonstrator's front panel. It was found that the 4 least significant bits of the digital words in transmitter #1 were moving at a random rate under constant input conditions.

The original manufacturer of the demonstrator was contacted and advised of this problem. A representative of the supplier confirmed the noise problem during a trip to the FGL laboratory. We were advised that this was the same type of noise observed before delivery. It was decided that testing would continue with the noise problem, although it was causing a reduction in

Fig. 5 - Multiplex Elevator "A" Frequency Response

Phase Lag - Degrees

Amplitude Ratio - DB
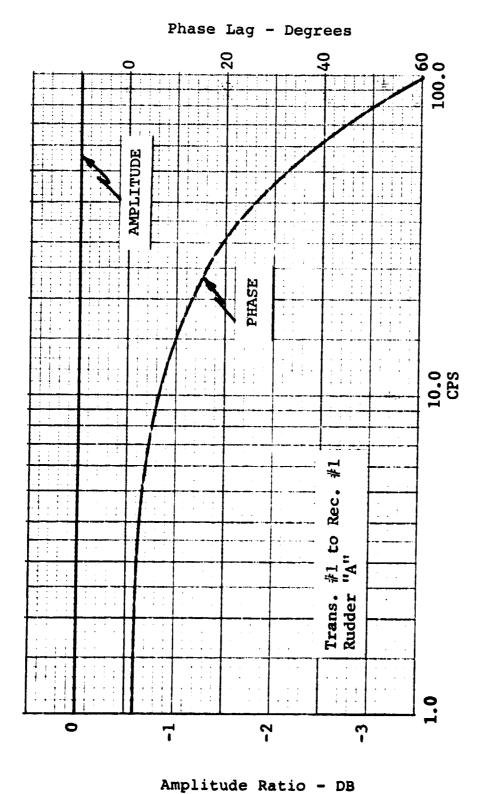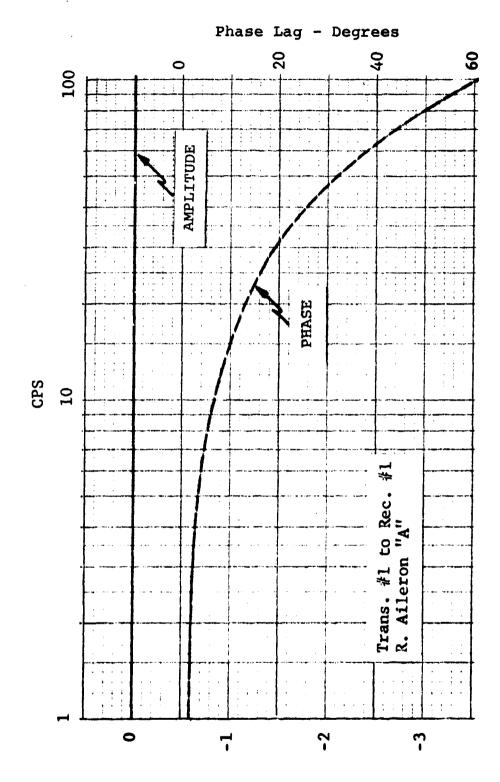
Fig. 6 - Multiplex Rudder "A" Frequency Response

11

Fig. 7 – Multiplex Right Aileron "A" Frequency Response

12

Fig. 8B

Upper Trace - Input - 2 cps square
wave vertical gain .1 Volt/Div.

Lower Trace - Output
Vertical Gain .05 Volt/Div.

Sweep .1 Sec/Div.

Fig. 8A

Upper trace - Input - 2 cps square
wave vertical gain - .05V/Div

Lower Trace - Output
Vertical Gain .05 Volt/Div.

Sweep .1 Sec/Div.

Fig. 8 - Signal Resolution of Transmitter #1 to Receiver #1 (Elevator "A" Channel)

resolution. Instead of .097% resolution, .39% was measured. This resolution is displayed in photographs of Fig. 9.
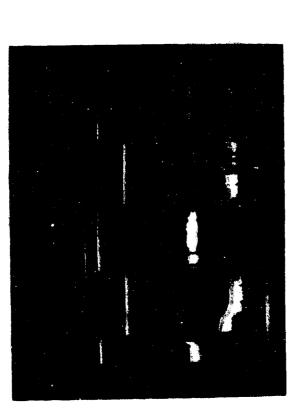
Response tests were performed on the transmitter #1 to receiver #2 section; elev. "A", rudder "A", and right aileron "A" channels. The same method was employed as the transmitter #1 to receiver #1 tests except the output was monitored at points A2A3-1, A2A11-5, and A2A19-5. Fig. 10, 11, and 12 are the frequency response plots generated. Fig. 13 and 14 show noise as observed on the output signal (.200 V peak to peak at 62.5 KC with .100 V level shifting).
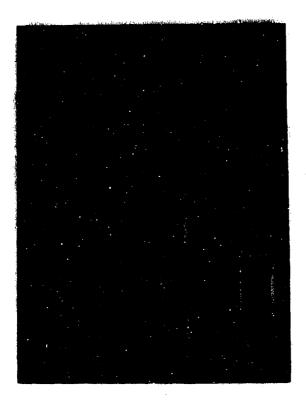
Response tests were performed on the transmitter #2 to receiver #2 section; elev. "A", rudder "A", and right aileron "A" channels of the multiplex demonstrator. Again, the same procedure was used as in the transmitter #1 to receiver #1 test. The input signal was applied to points A2A2A19J (elev. "A"), K6-6 (elev. "B"), K7-6 (elev. "C") and K8-6 (elev. "D"), in parallel and the output signal was monitored at A2A3-1. 4 elevator channels were operated simultaneously to prevent system lock out upon detection of a signal difference by the comparators. All other channels would be the same as elev. "A", as indicated by previous tests. Fig. 15 shows the frequency response. Fig. 16 A and B shows the threshold and noise observed at receiver #2 elev. "A" output (noise level .200 V peak to peak at 62.5 KC with .100 V level shifting).

Comparators in servo monitor section of the multiplex demonstrator were tested for static and dynamic detection levels. The basic test set is shown in Fig. 2. Static detection levels were observed by holding elev. "B", "C", and "D" inputs at zero reference and adjusting a DC bias at elev. "A" input until a visual failure indication was observed. The static levels were found to be +2.53 V and DC -2.33 V DC. This would be 23% to 25% of the demonstrator's ± 10 V maximum input-output signal range.

Dynamic failure detection level was measured using a function generator input at elev. "A" and holding elev. "B", "C",

────────

*The signals in the photographs appear fuzzy and smeared due to a degenerate condition of the memory section of the oscilloscope used for testing.

Fig. 9B

Upper Trace - Input Signal   2CPS
Square Wave - Vertical Gain 1 Volt/Div.

Lower Trace - Output - Vertical Gain
.5 Volt/Div.

Fig. 9A

Upper Trace - "0" Reference for In-
put Signal - Vertical Gain .05V/Div

Second Trace - Input Signal 2 CPS
Square Wave - Vertical Gain .05 V/Div.

Lower Trace - Output .05V/Div.
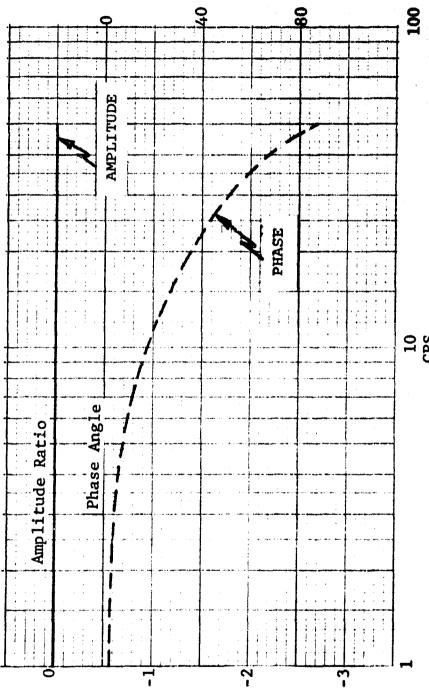
Sweep .1 Sec/Div

Fig. 9A - No Recognizable Output With a .050 Volt Input Signal

Fig. 9B - Minimum Input to Recognize an Output Signal
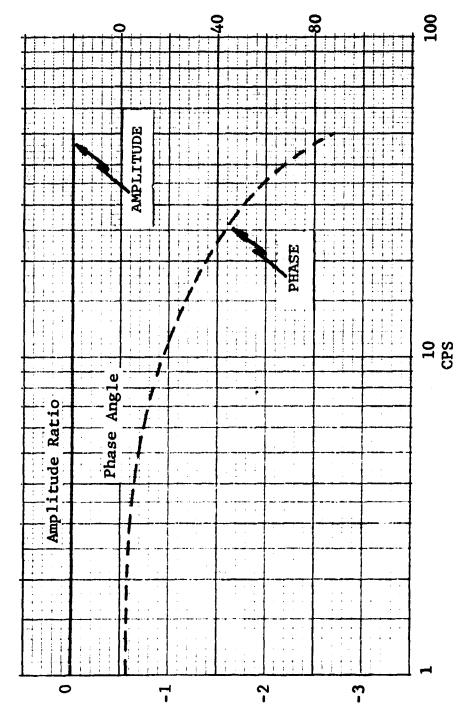
Figure 10. Multiplex Frequency Response - Transmitter #1 to Receiver #2, Elev. "A" Response
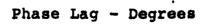
16

Phase Lag - Degrees

Figure 11. Multiplex Frequency Response - Transmitter #1
to Receiver #2, Rudder "A" Response

Amplitude Ratio - DB
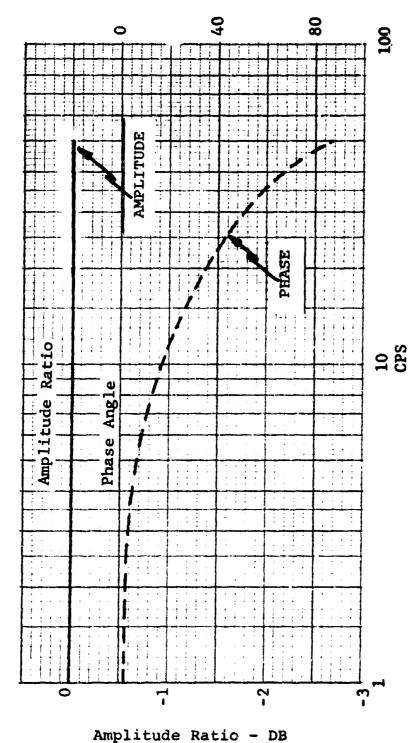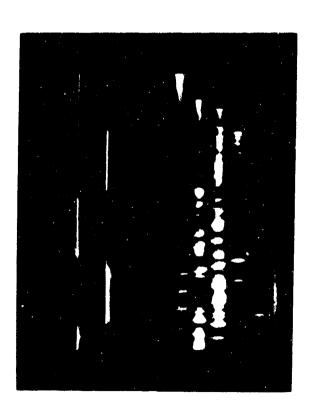
Figure 12. Multiplex Frequency Response – Transmitter #1 to Receiver #2, R. Aileron "A" Response

18
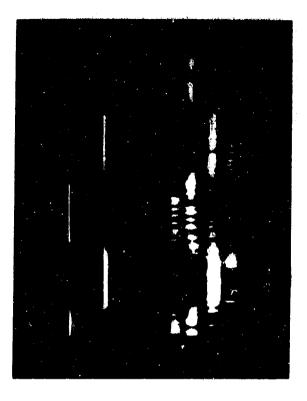
Fig. 13A

Upper Trace - Input 2CPS Square wave
Vertical Gain - .15 Volt/Div.

Lower Trace - Output
Vertical Gain .05 Volt/Div.

Sweep - .1 Sec/Div.

Fig. 13B

Upper Trace - Input 2CPS Square wave
Vertical Gain - .05 Volt/Div.

Lower Trace - Output
Vertical Gain - .05 Volt/Div.

Sweep - .1 Sec/Div.

Fig. 13A - No Recognizable Output With a .05 Volt Input Signal

Fig. 13B - Minimum Input to Recognize an Output Signal

Fig. 13 - Signal Resolution of Transmitter #1 to Receiver #2 (Elevator "A" Channel)

19

Fig. 14A

Fig. 14B

Upper Trace "O" Reference for Input
Vertical Gain - .05 Volt/Div.

Upper Trace - Input 2 CPS Square Wave
Vertical Gain - 1 Volt/Div.

Second Trace - Input 2CPS Square wave
Vertical Gain - .05 Volt/Div.

Lower Trace - Output
Vertical Gain - .5 Volt/Div.

Lower Trace - Output - Vertical Gain
.05 Volt/Div.

Sweep - .1 Sec/Div.
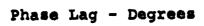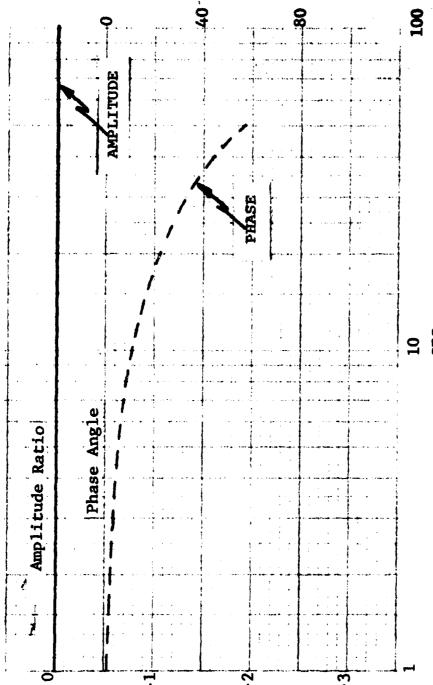
Sweep - .1 Sec/Div.

Fig. 14 A - Minimum Input to Recognize an Output is Improved with a .05
Volt Offset of Input Signal.

Fig. 14 B - Output Noise Shown on a Higher Level Input Signal.

Fig. 14 - Signal Resolution Transmitter #1 to Receiver #2 (Elevator "A" Channel)

20

Figure 15. Multiplex Frequency Response – Transmitter #2 to Receiver #2, Elev. "A" Channel

Fig. 16A
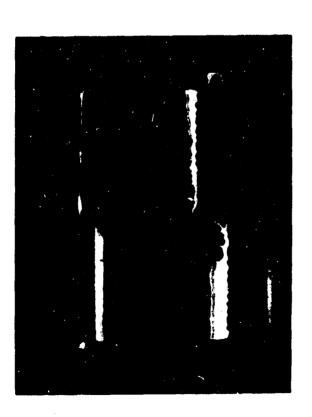
Upper Trace - Input Signal 2CPS Square
Wave - Vertical Gain - .120 Volt/Div.

Lower Trace - Signal Output - Vertical
Gain - .020 Volt/Div.

Horizontal Sweep - .050 Sec/Div.

Fig. 16B

Upper Trace - Input Signal 2CPS Sine
Wave - Vertical Gain - .020 Volt/Div.

Lower Trace - Signal Output - Vertical
Gain - .020 Vertical/Div.

Horizontal Sweep - .050 Sec/Div.

Fig. 16 A - Minimum Input to Recognize and Output Signal

Fig. 16 B - Input-Output Signal Relationship of a Low Level Sine Wave Input

Fig. 16 - Signal Resolution and Threshold of Transmitter #2 to Receiver #2

and "D" inputs at a zero reference. Data was measured by setting various frequencies and increasing the amplitude (V peak to peak) until the monitor panel indicated a comparator disagreement. The dynamic tests were run using both sine and square wave inputs. Results are shown in Fig. 17.

The photographs in Fig. 18 indicate the comparators switching time. To obtain this data, the test was set up as shown in Fig. 2 . A 5 V input step was used to simulate a failure. The output of the comparator and the failure indicating lamp was monitored. The failure indicator was monitored to determine the detection time.

Base Line Tests
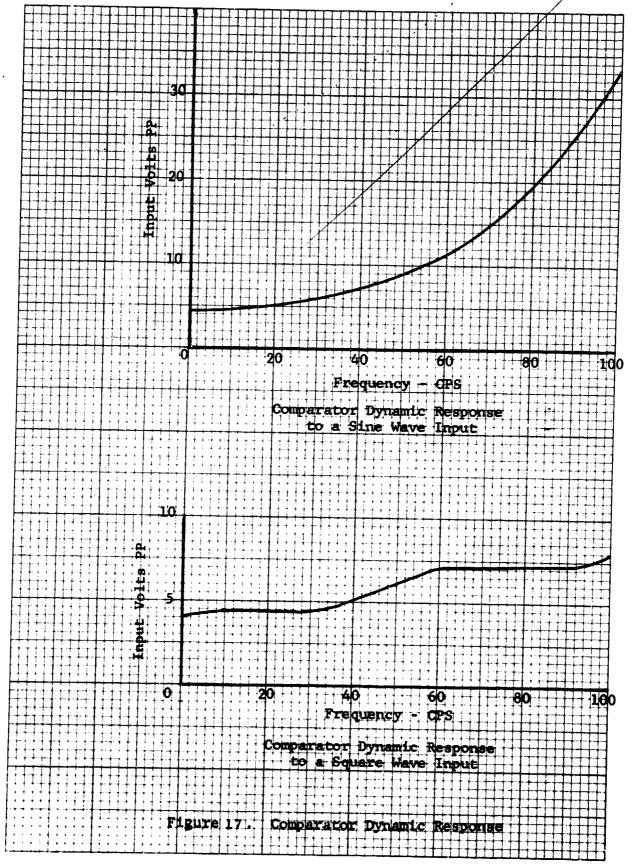
A closed loop electrohydraulic actuator system was set up. It was tested to provide comparison base line data against that obtained with the multiplex demonstrator inserted in the transmission lines. The basic components of the electrohydraulic system are:

> 1 Scheffer Actuator Model #11/8HH5F/FX3-1/2 KM
> 1 Moog Servovalve Model #32
> 1 Schaevitz LVDT Model 2000HR
> 3 Analog Device Amplifiers Model #211
> 1 Ring Demodulator (designed and built by
>   Hydraulic Research & Mfg. Co.)
> Miscellaneous Electronic Components

The electrohydraulic system was set up at 3 loop gains to simulate those typical of flight control systems. These gains were 12.56 rad/sec (2 CPS), 62.8 rad/sec (10 CPS) and 125.6 rad/sec (20 CPS).
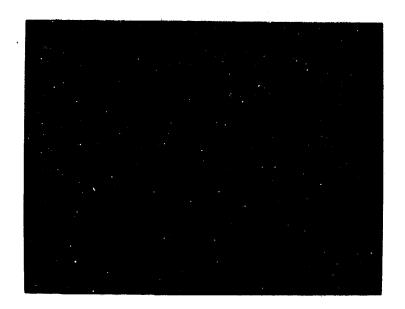
The diagram in Fig. 19 is the basic control circuit for the actuator. Amplifier "A" gain is variable for adjustment of loop gain. Amplifier "B" is an isolation amplifier to remove any loading effect the multiplex system may have on the loop. Amplifier "C" is a fixed gain current amplifier which removes the inductive loading effect of the servovalve.

The required Amplifier "A" gains were calculated using the expression:

Comparator Dynamic Response
to a Sine Wave Input

Comparator Dynamic Response
to a Square Wave Input

Figure 17. Comparator Dynamic Response

24

Upper Trace - Lamp Driver Output
  Vertical Gain - 10 Volt/Div.

Center Trace - Comparator Output
  Vertical Gain - 5 Volt/Div.

Lower Trace - Failure Step Input
  Vertical Gain - 5 Volt/Div.

Horizonal Sweep - .005 Sec/Div.

Fig. 18 - Comparator Switching Time
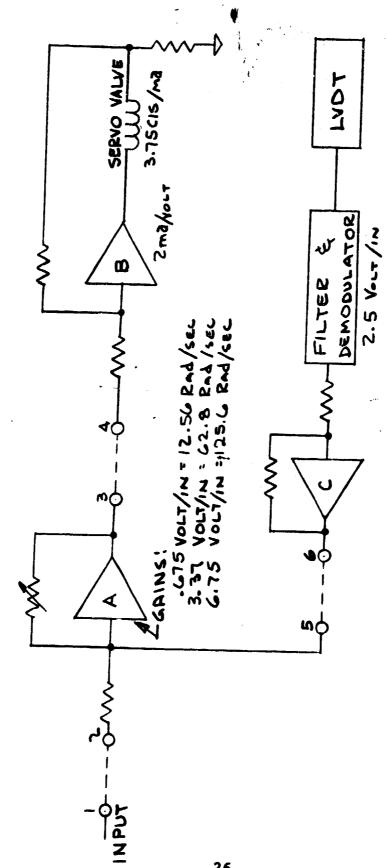
Fig. 19 – Electronic Control Loop

GAINS:
.675 VOLT/IN = 12.56 Rad/sec
3.37 VOLT/IN = 62.8 Rad/sec
6.75 VOLT/IN = 125.6 Rad/sec

SERVO VALVE
3.75 CIS/ma
2 ma/volt

FILTER & DEMODULATOR
2.5 VOLT/IN

LVDT

INPUT

26

$$K = \left(\frac{K_1 \cdot K_2 \cdot K_3}{A} \right) H$$

WHERE: K = Loop gain 12.56 rad/sec
                        62.80 rad/sec
                       125.60 rad/sec

K_1 = Amplifier gain

K_2 = Current amp gain 2 ma/volt

K_3 = Servovalve gain 3.75 cis/ma

H = Feedback gain 2.5 v/in

A = Actuator area .994 in^2

1. K_1 = .675 volt/volt when desired loop gain is
                  K = 12.56 rad/sec (2 CPS)

K_1 = $\dfrac{KA}{K_2 K_3 H}$

K_1 = $\dfrac{12.56 \cdot .994}{2 \cdot 3.75 \cdot 2.5}$

K_1 = .675 volts/volt

2. K_1 = 3.37 volt/volt when desired loop gain is
                  K = 62.8 rad/sec (10 CPS)

K_1 = $\dfrac{KA}{K_2 K_3 H}$

K_1 = $\dfrac{62.8 \cdot .994}{2 \cdot 3.75 \cdot 2.5}$

K_1 = 3.37 volt/volt

3. K_1 = 6.75 volt/volt when desired loop gain is
                  K = 125.6 rad/sec (20 CPS)

K_1 = $\dfrac{KA}{K_2 K_3 H}$

27

$$K_1 = \frac{125.6 \cdot .994}{2 \cdot 3.75 \cdot 2.5}$$

$$K_1 = 6.75 \text{ volt/volt}$$

The base line actuator response curves shown in Fig. 20, 21, and 22 are the result of data taken from actuator testing.

Plug in points 1-2, 3-4, 5-6 shown in Fig. 19 are provided so that a strap may be removed and the multiplex demonstrator can be inserted in the loop.

Multiplex Actuator Tests
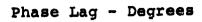
The multiplex demonstrator was inserted in the electrohydraulic actuator loop as follows: the elev. "A" and right aileron "A" channels of transmitter #1 to receiver #1 section were inserted at points 3-4 and 5-6, respectively of Fig. 19. The photograph of Fig. 23 is the actual test set up for the closed loop electrohydraulic actuator testing. The right aileron channel of the transmitter #1 to receiver #1 section was used to maintain a consistent 400 CPS update rate. A 200 CPS update rate is used in transmitter #2 to receiver #2 and this change converted the total system into a true 400 CPS update rate system.
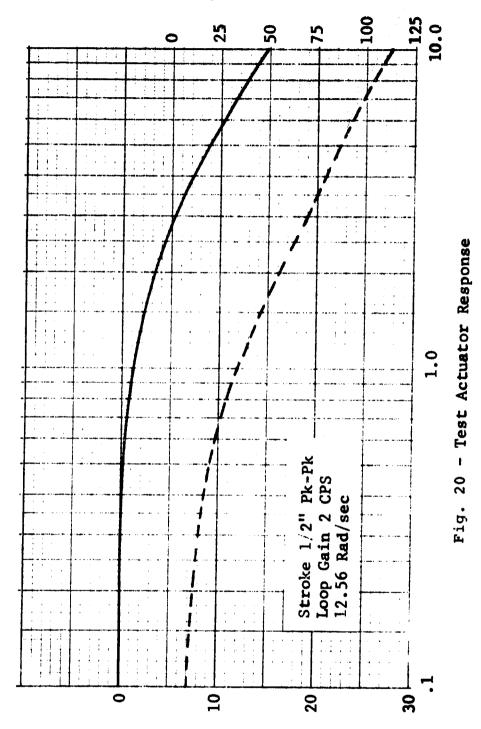
Before readable data could be taken, the noise problem encountered earlier in the test program was resolved as discussed in a later section of this report. Fig. 24, 25, and 26 show the frequency response results. It was noted that when a step input was used, with a loop gain of 125 rad/sec, there was a 10% overshoot and some ringing present on the output signal.

The multiplex demonstrator was inserted in the electrohydraulic actuator loop as follows: elev. "A" channel of the transmitter #1 to receiver #1 section at points 1-2 of Fig. This setup would show effects similar to that which would be found in a mechanical feedback actuator when driven with a multiplexed input signal. Fig. 27, 28, and 29 show the frequency response test results.

SUMMARY OF RESULTS

Throughout the test program the demonstrator performed

Fig. 20 — Test Actuator Response

Stroke 1/2" Pk-Pk
Loop Gain 2 CPS
12.56 Rad/sec

Phase Lag - Degrees

Stroke 1/2" Pk-Pk
Loop Gain 10 CPS
62.8 Rad/sec

CPS

Amplitude Ratio - DB
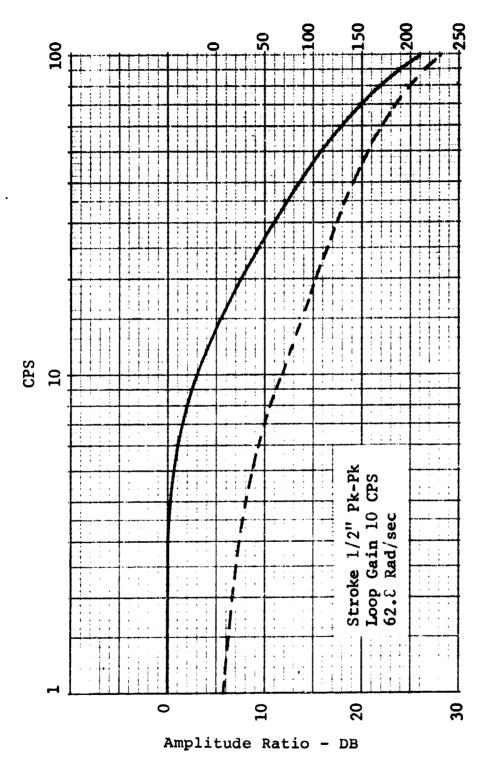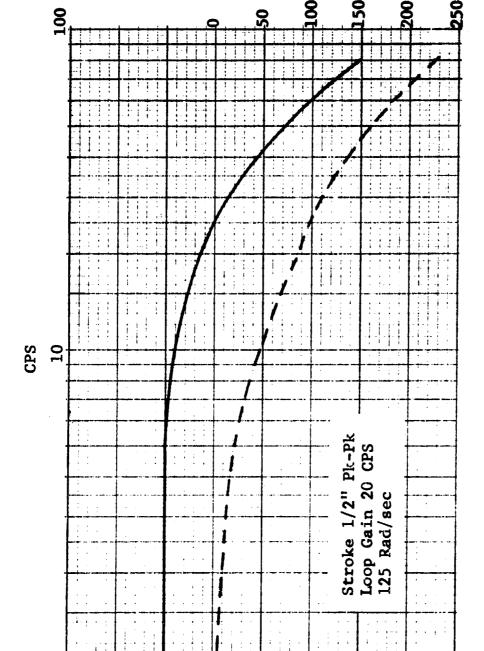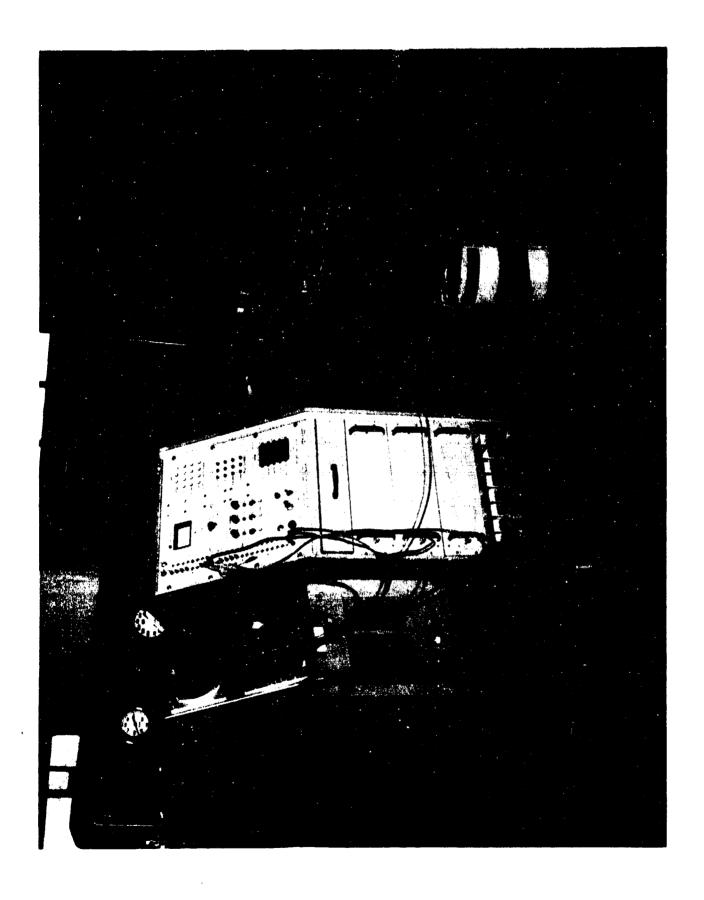
Fig. 21 - Test Actuator Response

30

Figure 22 - Test Actuator Response

31

Fig. 23 – Multiplex Demonstrator in Test Setup

32
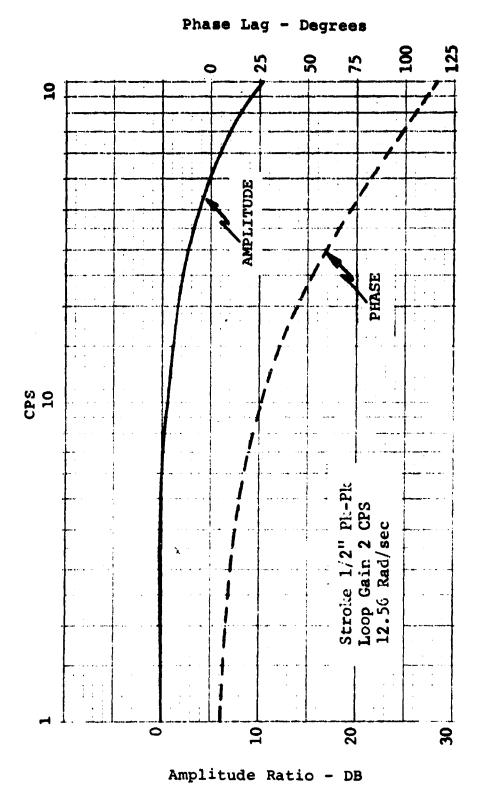
Figure 24 - Test Actuator with Multiplex in Loop

33

Phase Lag - Degrees

Stroke 1/2" Pk-Pk
Loop Gain 10 CPS
62.8 Rad/sec

AMPLITUDE

PHASE

CPS

Amplitude Ratio - DB
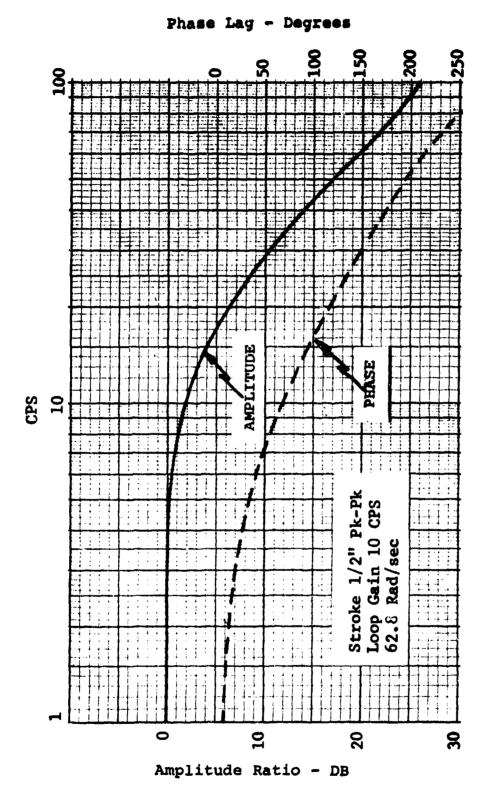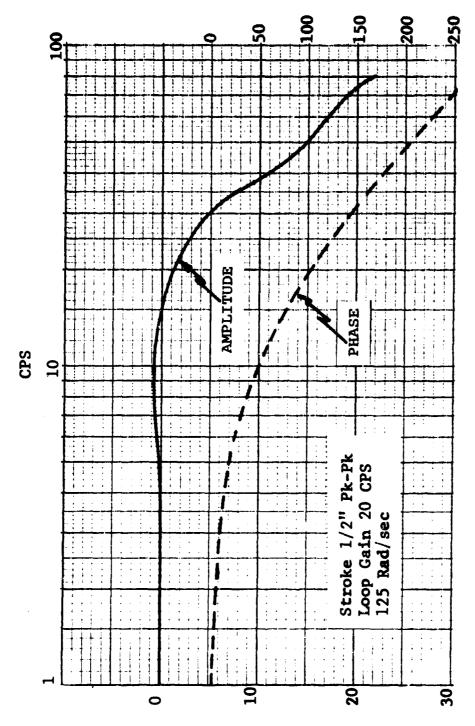
Figure 25 - Test Actuator with Multiplex in Loop

34

Figure 26 – Test Actuator with Multiplex in Loop
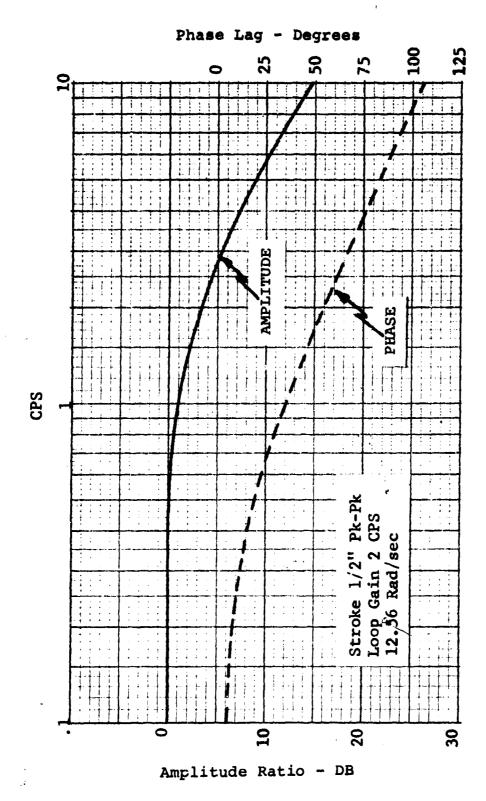
Figure 27 – Test Actuator with Multiplexed Input Signal
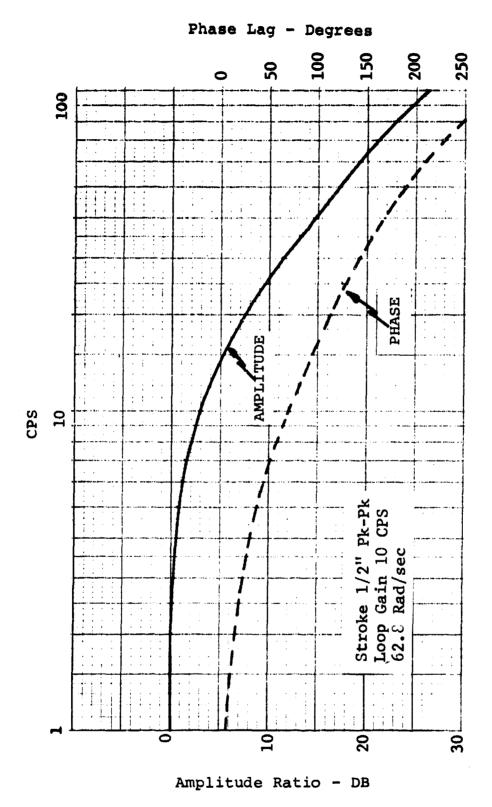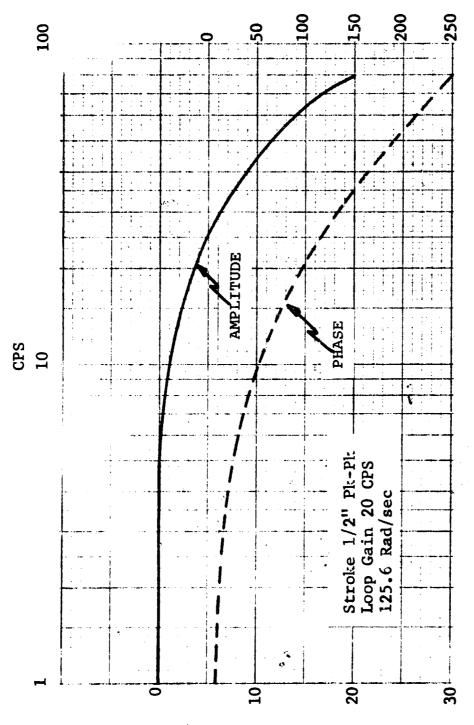
Figure 28 – Test Actuator with Multiplexed Input Signal

37

Figure 29 – Test Actuator with Multiplexed Input Signal

38

satisfactorily. The most significant problem encountered was noise on the reconstituted analog output signal.

During initial investigation, a parallel to serial shift register (NS #DM8590) in transmitter #1 was one source of noise. The bad printed circuit card was switched with an identical PC card in transmitter #2.

After the shift register problem was solved, a decision was made to continue the test program with the existing noise level since it was consistent with that observed by the original contractor. The test program was completed to the point where the multiplex demonstrator was operated in a closed loop actuator system. The actuator was observed exhibiting random movements up to 1/32" of amplitude due to multiplex noise. This random motion was considered excessive for a fair evaluation of the multiplex concept. With the approval of the FGL branch, Hydraulic Research & Manufacturing Company undertook an investigation of the sources of inherent noise in the multiplex unit.

A first problem was apparently poor signal ground. This was resolved by connecting a #10 gauge wire between the main ground buss and the ground buss of each drawer of the multiplex unit. This wire replaced the existing #20 gauge wire and resulted in a reduction of the random digital bit of each word from 4 to 2. The source of the remaining noise was identified as generated in the buffer amplifiers between the transmitter #1 input signal and the 8-channel multiplex switch module. The noise was approximately 200 KC and was sufficient to trigger the A/D converter. The cause of noise was not determined due to the integrated circuit nature of the module. It was believed to be an impedance mismatch, low quality operational amplifier or noise on the power supplies. A solution to this problem was to insert an RC filter on the output of the buffer amplifiers. The filter had a 34 KC break frequency and was made up of a 50 ohm resistor and a .1 f capacitor. The filter had no noticeable effect on output of the multiplex unit. It was found all random bit action of the digital words throughout the transmitter #1 to receiver #2 of the multiplex unit had stopped.

During the testing of the comparators, the light driver for elev. "A" failure indicator of the maintenance panel was inadvertently shorted, causing failure of the light driver integrated circuit. This was replaced.

CONCLUSIONS AND RECOMMENDATIONS

The multiplex unit performed as specified with little
trouble. Further design emphasis could be applied to the re-
moval of noise in the digital system. The main degradation to
a control system employing a multiplexing unit is the addition
of phase shift and its effect on the control system frequency
response. This can be directly improved by an increase of the
sampling rate.

It is recommended that sampling rate be a minimum of 10
times the desired frequency response. Preliminary testing has
indicated that large amplitude limit cycling occurs when the
sampling rate is lowered to 5 times the desired system response.
The trade factors that must be considered are; weight, cost,
reliability, and survivability.

The weight savings potential on a large aircraft is sig-
nificant due to the length of wires required to interconnect a
redundant system. The multiplex packaging scheme itself will
have a weight penalty, since each module or section of the multi-
plex system will require a separate regulated power supply, con-
nectors, and monitor points. Component quality must be high to
prevent instability, noise, and drift problems. The general
solution to these electronic problems is to apply controlled
manufacturing techniques. As a result the cost and weight factors
are increased while the reliability is decreased. Additional
hidden costs of applying a multiplex unit to an aircraft include
installation, increased maintenance and greater aircraft power
requirements. These must be taken into consideration when com-
parisons are made with a hardwired system.

Survivability is another area to be considered during the
trade studies. As an example, on a large aircraft the wire runs
from the flight computer, to the tail section of the aircraft are
quite long. If only a single digital transmission line is used,
the loss of this line could result in the loss of control of both
rudder and elevator. Consequently, it is necessary to employ
redundancy on the digital transmission lines to the aft section
of the aircraft. This must be considered in a total weight trade-
off when compared with a quad-redundant hardwired system.

An advantage of multiplexed flight control system is the
ability to vote at a central monitoring station. A discrete

40

signal obtained from the voting process may be used to disable the failed channel. This signal could also be used to bypass the surface drive actuator or servovalve depending on the type of redundant system employed. This was not within the capability of the demonstration multiplex unit tested.

The method of voting within the multiplex unit tested monitored analog signals with analog comparators. This approach has the disadvantage of being sensitive to dynamic signals as shown in the test results. An alternate method of voting would be to vote in the digital mode. This would negate dynamic considerations and permit the detection level to be set as low as the least significant bit of the digital word. To prevent a channel from an inadvertent shutdown due to line transient, the signal could be sampled twice upon the first indication of a channel mismatch. The time required for the verification of a failure would be approximately 5 milliseconds. If the sample rate is 400 samples/second, there would be no component within the channel unmonitored as long as the system is closed loop or the actuator position is monitored. A digital voting system would increase the accuracy and versatility of a monitoring system.

Other applications of signal multiplexing may be useful, i.e. the multiplexing of aircraft monitoring points such as temperatures. pressures, fluid flow, fluid level, and mechanical linkage positions. These parameters could be monitored using a multiplex unit and digitally voted within performance limits. When these limits are exceeded, the numerical value could be displayed on the pilot's control panel. As an added feature, the pilot could be provided with a manual select switch which would display any parameter selected.

SECTION II

DEVELOPMENT OF A HIGH PERFORMANCE ACTUATION LEG

FOR THE FLIGHT DYNAMICS LAB SPIDER MOTION SYSTEM

INTRODUCTION

This particular task is specifically related to an existing simulator located in Bldg. 195 at Wright-Patterson Air Force Base (WPAFB). There currently exist six actuators, a servosystem, and ball and "U" joints for connecting the actuator legs between the floor and the simulation platform. The general objective of this effort is to provide performance improvement of the existing system while minimizing pumping capability requirements.

Emphasis was given to accomplishing this improvement while utilizing as many of the existing system components as possible. In particular, the special ball and "U" joints were retained. A single high performance leg was designed and fabricated. It was also determined that commercially available servovalves to satisfy performance requirements were beyond the funding scope of this contracted effort. Consequently, a decision was made to design and fabricate at WPAFB a servovalve that would satisfy requirements. This valve and actuator were designed to meet the following performance requirements:

1. Frequency response which exhibits no peaking in excess of 3 db and has phase shift of 150° at 3 Hz minimum.

2. Rate limit shall not occur before ± 2.5 feet amplitude at 1 Hz.

3. Actuator stroke of ± 2.5 feet minimum.

4. A static load capability of 1000 pounds.

A pumping system size was established to permit the high performance leg to undergo three cycles of operation at a frequency of 1 Hz with an amplitude of ± 2.5 feet. The pumping system was also sized to maintain a continuous ± 1 foot stroke

amplitude at 1 Hz.

In order to satisfy the previously listed performance re-
quirements with the existing actuators, a pumping system must
be provided which is capable of delivering approximately 577
GPM. The servovalve on each actuator must be capable of 242
GPM to provide the maximum desired velocities. The basic ac-
tuator design problem was, therefore, one of optimizing the
actuator and servovalve size for the specified load conditions.
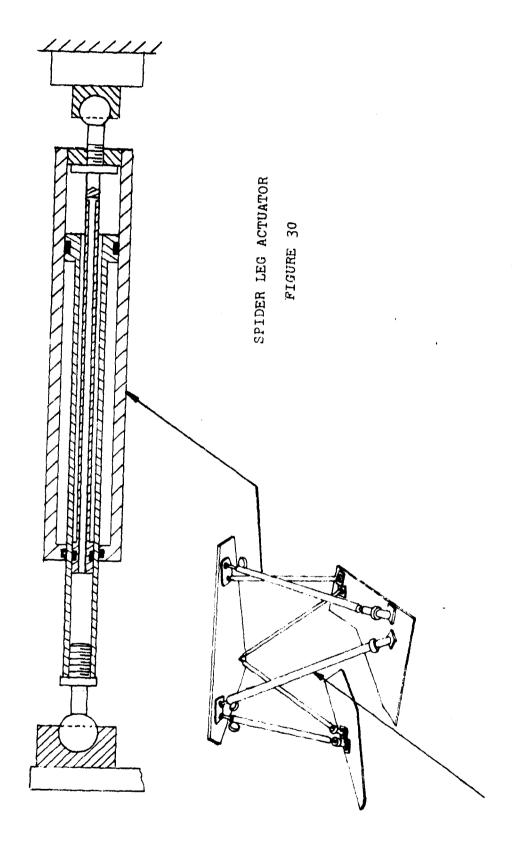
The primary mechanical structural problem was one of
achieving high buckling stiffness. Column characteristics of
the actuator were critical. Since the installation precluded
using an equal area actuator with a tail rod, a single ended
actuator was selected. With this kind of design, the available
column stiffness reduces as the actuator extends. Fig. 19 shows
schematically the type of design chosen. In this actuator a
hollow rod is used to reduce the extend motion driving area.
This rod runs through the center of the actuator and permits a
design with the desired area imbalance. A second benefit was
derived when it is recognized that an internal rod permits the
actuator driving rod diameter to be increased without signifi-
cant weight penalties. By making this driving rod of large dia-
meter, the column buckling stiffness is increased. The internal
hollow rod inside the actuator driving rod permits any oil leak-
age past the seal to be brought back to the pump reservoir.

ANALYSIS AND SIZING INVESTIGATION

An analysis and sizing investigation was conducted for
the Spider Leg actuator in the following five basic areas.

- preliminary sizing was accomplished to permit
  designs to proceed.

- a sizing trade off study was undertaken to
  demonstrate the impact of various specifica-
  tion changes.

- initial preliminary sizing indicated the pos-
  sibility of a stability problem. To this end
  a dynamic simulation was accomplished.

- the feasibility of incorporating dampers
  within the actuator was considered.

43

SPIDER LEG ACTUATOR

FIGURE 30

- a column loading study was made to determine whether rod end sizing and bearing designs were adequate.

PRELIMINARY SPIDER LEG SIZING

Let: A = Required actuator area

     F = Minimum required actuator force

     M = Load mass

     Q_{max} = Maximum rated pump flow

     X_{max} = Peak stroke amplitude @ ω radians/sec

     X_{sat} = Stroke @ ω_s at which pump saturates

     V_{acc} = Accumulator volume

     ω_s = Saturation frequency

For Sinusoidal Motion:

$$(1) \quad X = X_{max} \sin \omega t$$

$$(2) \quad \dot{X} = X_{max}\omega \cos \omega t, \quad \ddot{X} = -X_{max}\omega^2 \sin \omega t$$

The maximum velocity, $\dot{X}_{max}$, occurs when $\sin \omega t = 1$ and

$$\omega = \omega_s$$

Equation 2 becomes:

$$(3) \quad \dot{X}_{max} = X_{max}\omega_s$$

$$(4) \quad \ddot{X}_{max} = X_{max}\omega_s^2$$

$$(5) \quad F = MX_{max}\omega_s^2 + Mg$$

45

$$(6) \quad A = \frac{MX_{max}\,\omega_s^2 + Mg}{P_s}, \quad X_{max}\,\omega_s^2 > 1$$

$$= \frac{M}{P_s}, \quad X_{max}\omega_s^2 < 1$$

$$(7) \quad Q_{max} = AX_{sat}\omega_s$$

An accumulator is used to satisfy peak flow demand above the continuous requirement by which the pump is sized.

Since $X_{max} > X_{sat}$ and a requirement exists for N cycles @ ω_s with maximum stroke of X_{max}, a conservative estimate of V_{acc} can be found by finding the amount of fluid required in excess of pump capacity for N cycles @ ω_s with peak amplitude of X_{max}. This neglects recharging of the accumulator when pump flow is less than Q_{max} during the N cycles.

$$(8) \quad V_{acc} = N \times 4 \times A\left[\int_0^{t_{max}} X_{max}\omega\cos\omega t\, dt - \dot{X}_{sat}t_{sat}\right]$$

$$(9) \quad V_{acc} = 4\,NA\left[\frac{(X_{max}^2\omega_s^2 - \dot{X}_{sat}^2)^{\frac{1}{2}}}{\omega_s} - \frac{\dot{X}_{sat}}{\omega_s}\cos^{-1}\left(\frac{\dot{X}_{sat}}{X_{max}\cdot\omega_s}\right)\right]$$

From 3, $\dot{X}_{sat} = \omega_s X_{sat}$, and 9 becomes

$$(10) \quad V_{acc} = 4\,NA\left[(X_{max}^2 - X_{sat}^2)^{\frac{1}{2}} - X_{sat}\cdot\tan^{-1}\frac{(X_{max}^2 - X_{sat}^2)^{\frac{1}{2}}}{X_{sat}}\right]$$

46

Determine actuator area from Equation (6)

$$A_1 = \frac{\frac{1000}{386} \times 30 \times (1 \times 6.28)^2 + 1000}{3000}$$

$$= \frac{4060}{3000} = 1.36 \ in^2 \quad \text{Min. Blind End Area}$$

$$A_2 = \frac{\frac{1000}{386} \times 30 \times (1 \times 6.28)^2 - 1000}{3000}$$

$$= \frac{2060}{3000} = .69 \ in^2 \quad \text{Min. Rod End Area}$$

Determine Max. required velocity from Equation (3)

$$\dot{X}_{max} = 30 \times 1 \times 2\pi = 189 \ in/sec \ min$$

Determine peak flow required from Equation (7)

$$Q_{max} = AX_{sat}\omega_s = 1.36 \times 30 \times 1 \times 2\pi$$

$$= 259 \ cis$$

$$= 67 \ GPM$$

The pump size is determined from the continuous operation condition from Equation (7)

$$\frac{Q_{pump}}{6} = AX\omega_s$$

$$= 1.36 \times 12 \times 1 \times 6.28$$

$$= 103 \ cis = 26.6 \ GPM$$

$$Q_{pump} = 6 \times 26.6 \ GPM = 160 \ GPM$$

The accumulator size required to satisfy peak flow requirements above pump capability is found from Equation (10)

$$V_{acc/act} = 4 \times 3 \times 1.36 \left[(30^2 - 12^2)^{\frac{1}{2}} - 12 \cdot \tan^{-1} \frac{750^{\frac{1}{2}}}{12} \right]$$

$$V_{acc/act} = 448 - 224 = 224 \text{ in}^3$$

$$V_{acc/act} = 6 \times 224 = 1340 \text{ in}^3$$

There are 231 in^3/gal.

$$\therefore \quad V_{acc} = \frac{1340}{231} = 5.8 \text{ Gal} \quad \text{(Useful volume)}$$

The oil column in the actuator is treated as a hydraulic spring, and its spring rate, K_h, is found from

$$K_h = \frac{4\beta A}{L} \qquad \text{Where} \quad \begin{array}{l} A = \text{min. piston area} \\ L = \text{total length of} \\ \quad \text{oil column} \\ \beta = \text{bulk modulus} \end{array}$$

$$K_h = \frac{4 \times 10^5 \times .69}{60}$$

$$= 460 \text{ \#/in.}$$

Resonant frequency, ω, $= \left(\frac{K_h}{M} \right)^{\frac{1}{2}}$

$$\omega = \frac{460^{\frac{1}{2}}}{1000/386} = 42.2 \text{ rad/sec}$$

$$f = \omega/2\pi = 6.7 \text{ cps}$$

The actuator exhibits a spring mass resonant frequency of 6.7 CPS and may require damping provisions to minimize chatter and/ or oscillation.

Sizing Trade Off Study

A sizing trade off study was undertaken in order to optimize the system pump capacity, accumulator size, valve size and actuator area for the performance requirements specified in Hydraulic Research Report #79400014. A computer program was prepared

on the Tymshare computer system using the equations previously shown in the preliminary sizing study. This program is shown in Fig. 31. Typical results of the print out are shown in Fig. 32 . The total data derived was analyzed and is shown in the summary trade off charts of Fig. 33, 34, and 35. Fig. 33 presents the effect on pump size and accumulator size obtained by varying the peak saturation amplitude up to 30 inches. The load weight is held constant at 1000 pounds and the saturation frequency is varied between 1 and .6 cycles per second. The system pump and accumulator sizes are shown for the specified design point at 160 GPM and 5.7 gallons usable volume respectively.

Fig. 34 shows the variation in system pump size and accumulator size as a function of peak saturation amplitude with the saturation frequency held constant at 1 CPS. The load mass was varied between 5000 and 800 pounds. The existing actuator size and the new required actuator sizes are shown for comparison. Existing actuator sizes would require approximately 640 GPM to meet the specified performance requirements. Reducing actuator area to the optimized level permits the required pump size to be brought down to the 160 GPM level. Fig.35 shows the leg actuator area required as a function of the leg load weight. Saturation frequency is used as a parameter. The existing actuator area shows that the present 4.9 square inches would permit a leg weight of approximately 4800 pounds to be moved at the required stroke and frequency. The resulting penalty in system pump size is significant. The optimized actuator size of 1.36 square inches will move the leg load weight of 1000 pounds at 1 CPS with a minimum system pump size of 160 GPM.

Dynamic Simulation

A non-linear dynamic simulation of the Spider Leg actuator was prepared since preliminary sizing calculations had indicated the probability of a stability problem. The non-linear equations describing the Spider Leg actuator were written by reference to the actuator schematic of Fig. 36. These equations are presented on page 58. Preliminary design values were used to determine the constants in the non-linear equations. These constants are shown in Table 1 are were used to form the scaled equations of page 59. The simulation diagram of Fig.37 was formed from these scaled equations. The problem was then mechanized on an EAI analog computer in the Flight Dynamics

49

FIGURE 31

TRADE OFF STUDY COMPUTER PROGRAM

```
10  PRINT "      ****SPYDER LEG SIZE TRADE-OFF****      "
20  PRINT
30  PRINT
40  FOR M=5000,3000,1000,900,800
50  FOR F=1,.9,.8,.7,.6
60  PRINT IN IMAGE"THE LOAD WEIGHT IS %%%%%. POUNDS":M
70  PRINT IN IMAGE"THE SATURATION FREQUENCY IS %.% CPS":F
80  PRINT
90  PRINT IN IMAGE
"    SATURATION      MAXIMUM       ACCUMULATOR       MINIMUM"
100 PRINT IN IMAGE
"    AMPLITUDE      PUMP FLOW        VOLUME          AREA"
110 PRINT IN IMAGE
"    ---------      ---- ----       ------          ------"
120 PRINT IN IMAGE
"    PEAK INCHES       GPM          GALLONS        SQ. IN."
130 FOR X=30,24,18,12,10,8
140 A=M*30*(F*2*PI)t2/3000/386+1000/3000
150 A1=1/3
160 A=A1 WHILE A<A1
170 Q=A*X*F*2*PI
180 V=12*A*(SQR(900-Xt2)-X*ATN(SQR(900-Xt2)/X))
190 PRINT IN IMAGE
"     %%.%          %%%%.%         %%%.%          %%.%":X,Q*6/3.85,
V*6/231,A
200 NEXT X
201 PRINT
202 PRINT
210 NEXT F
220 NEXT M
  >
```

FIGURE 32

TYPICAL COMPUTER PRINT-OUT

****SPYDER LEG SIZE TRADE-OFF****

THE LOAD WEIGHT IS 5000. POUNDS
THE SATURATION FREQUENCY IS 1.0 CPS

SATURATION AMPLITUDE	MAXIMUM PUMP FLOW	ACCUMULATOR VOLUME	MINIMUM AREA
PEAK INCHES	·GPM	GALLONS	SQ. IN.
30.0	1600.1	.0	5.4
24.0	1280.1	4.3	5.4
18.0	960.1	12.4	5.4
12.0	640.1	23.1	5.4
10.0	533.4	27.1	5.4
8.0	426.7	31.4	5.4
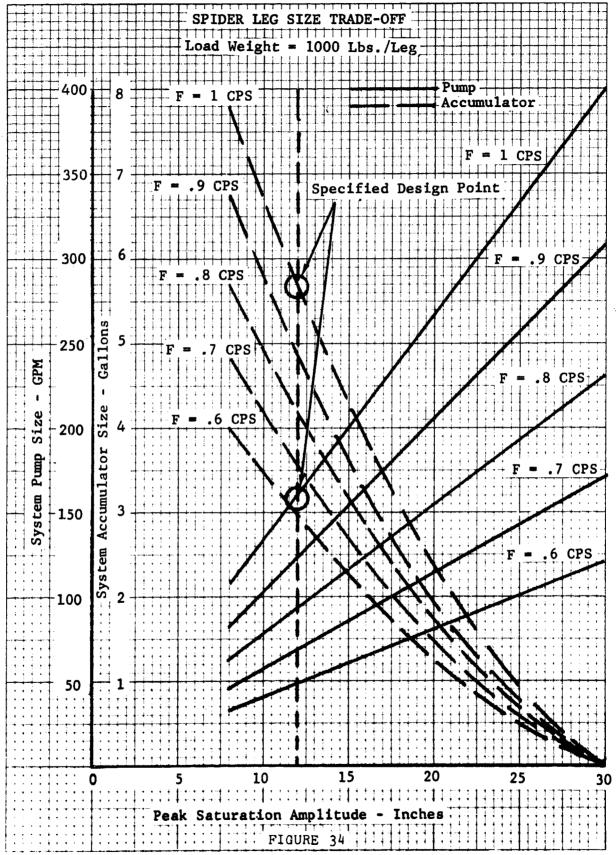
THE LOAD WEIGHT IS 5000. POUNDS
THE SATURATION FREQUENCY IS .9 CPS

SATURATION AMPLITUDE	MAXIMUM PUMP FLOW	ACCUMULATOR VOLUME	MINIMUM AREA
PEAK INCHES	GPM	GALLONS	SQ. IN.
30.0	1183.2	.0	4.5
24.0	946.6	3.6	4.5
18.0	709.9	10.2	4.5
12.0	473.3	18.9	4.5
10.0	394.4	22.3	4.5
8.0	315.5	25.8	4.5
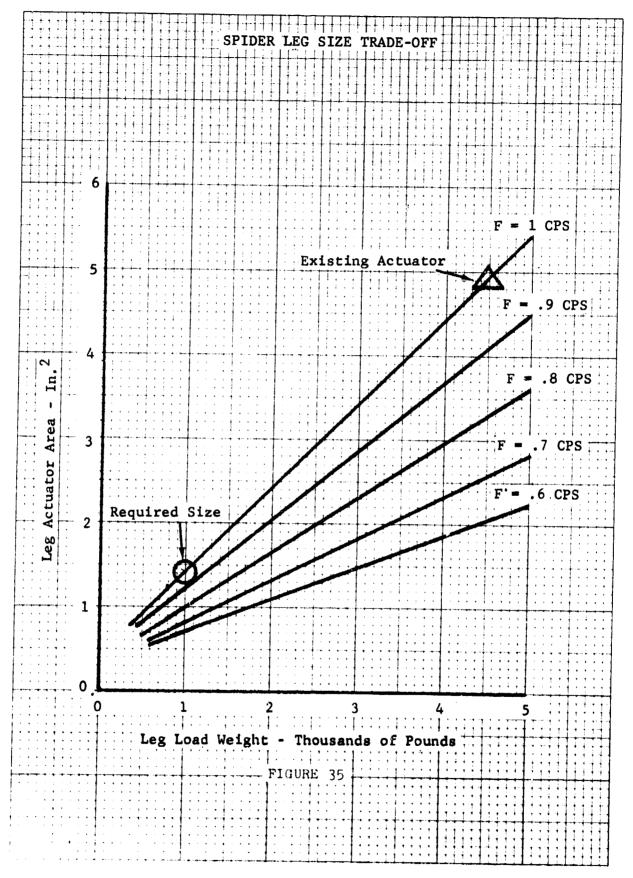
THE LOAD WEIGHT IS 5000. POUNDS
THE SATURATION FREQUENCY IS .8 CPS

SATURATION AMPLITUDE	MAXIMUM PUMP FLOW	ACCUMULATOR VOLUME	MINIMUM AREA
PEAK INCHES	GPM	GALLONS	SQ. IN.
30.0	847.5	.0	3.6
24.0	678.0	2.9	3.6
18.0	508.5	8.2	3.6
12.0	339.0	15.3	3.6
10.0	282.5	18.0	3.6
8.0	226.0	20.8	3.6

FIGURE 33

FIGURE 34

53

SPIDER LEG SIZE TRADE-OFF

Leg Actuator Area – In.²

Leg Load Weight – Thousands of Pounds

F = 1 CPS
Existing Actuator
F = .9 CPS
F = .8 CPS
F = .7 CPS
F = .6 CPS
Required Size

FIGURE 35

54

FIGURE 36

ACTUATOR SCHEMATIC
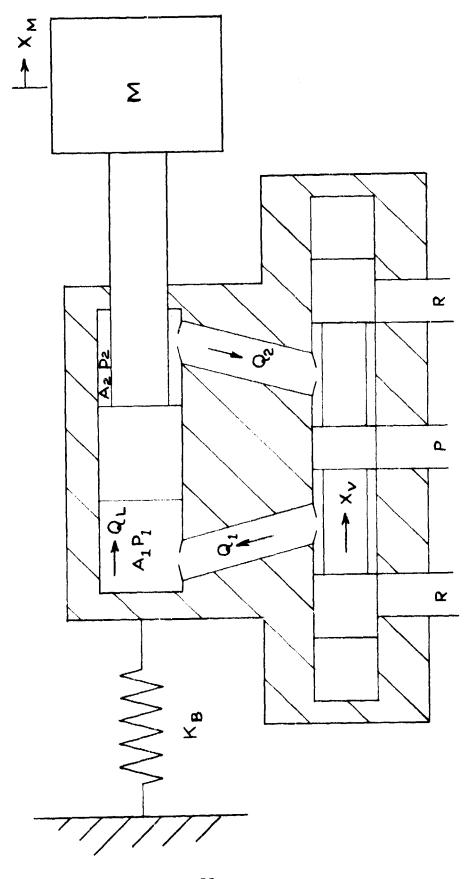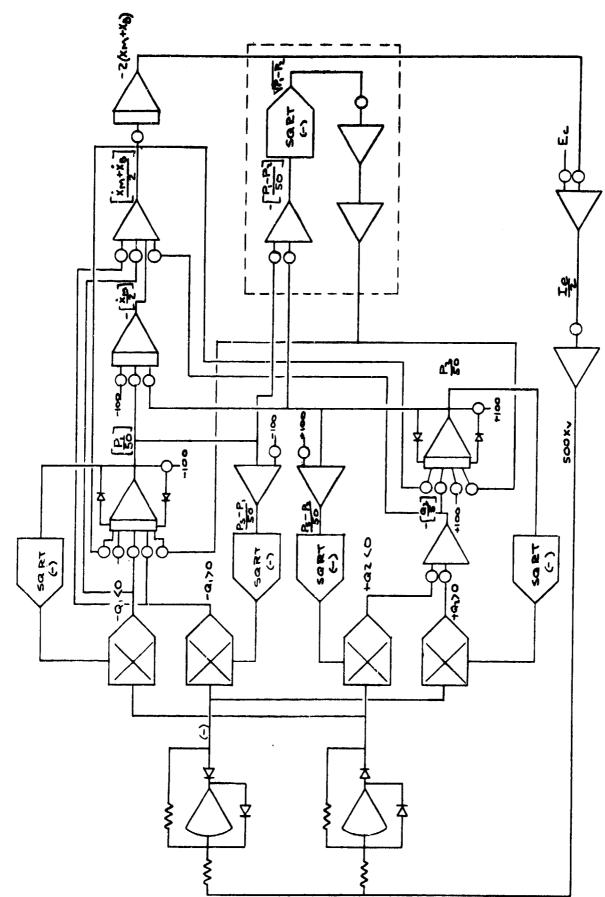
TABLE 1

CONSTANTS

Symbol	Definition	Value
A_1	Blind End Area	1.54 in.^{2}
A_2	Rod End Area	.74 in.^{2}
I_e	Error Current	Ma
K_b	Support Structure Spring Rate	3.2×10^6 #/in.
K_a	Amplifier Gain	7.92 Ma/V
K_{fb}	Feedback Gain	1/3 V/in.
K_{sv}	Servovalve Spool Gain	.005 in/Ma
M	Actuator Load Mass	2.59 # sec^2/in.
P_s	Supply Pressure	3000 psi
V_1	Blind Side Null Volume	114 in.^{3}
V_2	Rod Side Null Volume	25 in.^{3}
W	Total Valve Slot Width	1.1 in.
β	Hydraulic Oil Bulk Modulus	10^5 psi
ω	Nominal Loop Gain	30 RPS

COMPUTER NON-LINEAR SIMULATION DIAGRAM

FIGURE 37

57

Lab. Initial results are shown in Fig. 38 and verify that an instability does exist. The oscillation shown is at an amplitude of ± 1.5 inches at a frequency of approximately 5.7 CPS.

The simulation was then modified to investigate the installation of a damping orifice across the piston of the actuator. This modification is shown by dotted lines in the simulation diagram. A damping orifice of .068 inches diameter succeeded in stabilizing the actuator. Satisfactory response was obtained with a loop gain of 19 radians per second. A series of curves is shown in Fig. 39 which demonstrates the effect of varying the load weight damping orifice diameter and loop gain. It can be seen that Curve 4 with the low loop gain best satisfies the 3 db peaking requirement. Anticipated step response characteristics are shown in Fig. 40 and 41 for 19 and 30 radians per second loop gain. In both cases, a .068 inch diameter orifice was simulated.

SPIDER LEG ACTUATOR NON-LINEAR EQUATIONS

(1) $\quad P_1 A_1 - P_2 A_2 - Mg = M\ddot{X}_m$

(2) $\quad P_1 A_1 - P_2 A_2 = K_b X_b$

(3) $\quad P_1 = P_{10} + \dfrac{\beta}{V_1} \int \left[Q_1 - A_1(\dot{X}_m + \dot{X}_b) - Q_L \right] dt$

(4) $\quad P_2 = P_{20} + \dfrac{\beta}{V_2} \int \left[A_2(\dot{X}_m + \dot{X}_b) - Q_2 + Q_L \right] dt$

(5) $\quad Q_1 = \begin{cases} KX_v \sqrt{P_s - P_1} & X_v > 0 \\ KX_v \sqrt{P_1} & X_v < 0 \end{cases}$

(6) $\quad Q_2 = \begin{cases} KX_v \sqrt{P_2} & X_v > 0 \\ KX_v \sqrt{P_s - P_2} & X_v < 0 \end{cases}$

(7) $\quad X_v = K_v I_e$

(8) $\quad I_e = K_a \left[E_c - K_{fb}(X_m + X_b) \right]$

SCALED EQUATIONS

(1) $\left[\dfrac{P_1}{50}\right] = 28.9 + \int \left\{8.27\left[\dfrac{Q_1}{5}\right] - 5.4\left[\dfrac{\dot{X}_m + \dot{X}_b}{2}\right]\right\} dt$

(2) $\left[\dfrac{P_2}{50}\right] = 31.1 + \int \left\{11.85\left[\dfrac{\dot{X}_m + \dot{X}_b}{2}\right] - 40\left[\dfrac{Q_2}{5}\right]\right\} dt$

(3) $\left[\dfrac{Q_1}{5}\right] = 3.12\left\{.01 \times \left[500X_v\right] \times 10\sqrt{\left[\dfrac{P_1}{50}\right]}\right\} \quad X_v < 0$

$\qquad = 3.12\left\{.01 \times \left[500X_v\right] \times 10\sqrt{60 - \left[\dfrac{P_1}{50}\right]}\right\} \quad X_v > 0$

(4) $\left[\dfrac{Q_2}{5}\right] = 3.12\left\{.01 \times \left[500X_v\right] \times 10\sqrt{\left[\dfrac{P_2}{50}\right]}\right\} \quad X_v > 0$

$\qquad = 3.12\left\{.01 \times \left[500X_v\right] \times 10\sqrt{60 - \dfrac{P_2}{50}}\right\} X_v < 0$

(5) $\left[500X_v\right] = 1.25\left[\dfrac{I_e}{2}\right]$

(6) $\left[\dfrac{I_e}{2}\right] = 3.16\left[5E_d\right] - 2.63\left[2X_m + 2X_b\right]$

(7) $\left[\dfrac{\dot{X}_m + \dot{X}_b}{2}\right] = \int\left\{1.49\left[\dfrac{P_1}{50}\right] - .715\left[\dfrac{P_2}{50}\right] - 19.3\right\} dt + 1.05$

$\qquad \times 10^{-3}\left[\dfrac{Q_1}{5}\right] + 2.31 \times 10^{-3}\left[\dfrac{Q_2}{5}\right]$

(8) $\left[2X_m + 2X_b\right] = .4\int\left[\dfrac{\dot{X}_m + \dot{X}_b}{2}\right] dt$

Spider Leg Actuator Instability
No Damping

FIGURE 38

60

Spider Leg Frequency Response

Curve	Load Wt. Pounds	Loop Gain RPS	Damping Orifice Dia. In.
1	1000	30	.094
2	1000	30	.068
3	500	30	.068
4	1000	19	.068

Frequency - H_z

Amplitude Ratio - DB

FIGURE 39

FIGURE 40
Spider Actuator Step Response
Loop Gain = 19 RPS

Command Signal

Position

Load Pressure

Cylinder 1 Pressure

Cylinder 2 Flow

Piston Velocity

Valve Stroke

62
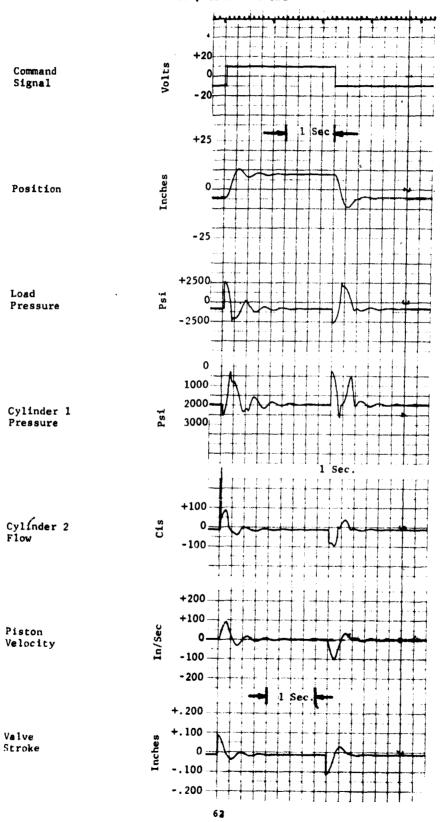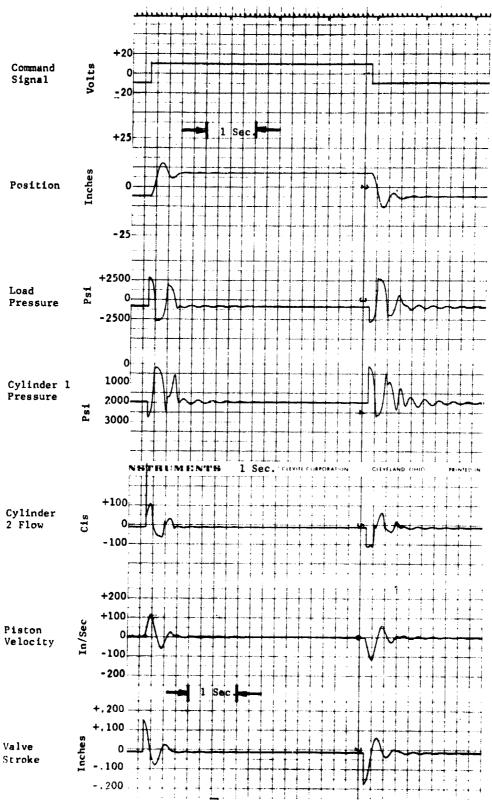
FIGURE 41
Spider Actuator Step Response
Loop Gain = 30 RPS

Damper Feasibility Investigation
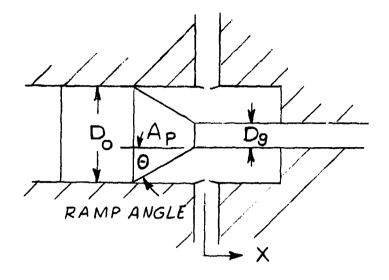
With a design ramp velocity of approximately 190 inches per second and a nominal actuator inertia load of 1000 pounds, it became apparent that catastrophic results could occur if the actuator piston rod was allowed to bottom out within the barrel at high rates of speed. One possible solution was to investigate dampers within the actuator which would prevent the piston from hitting the end of the barrel at maximum velocity. One configuration of this type is shown in Fig. 42.

An investigation was conducted to determine whether or not this would prevent bottoming out without excessive pressure build-up within the barrel. The damper operation was simulated on the analog simulation program available from the Tymshare digital computer. The system equations for the simulation are shown on page   . The simulation diagram is shown in Fig. 43 This diagram was prepared directly from the system equations since amplitude and time scaling are not necessary on this program. In the simulation, the ramp was given an initial velocity of 190 inches per second. The pressure build up was calculated as a function of time as the flow area decreased. The initial design considered a 10° ramp angle. It was found that the cylinder pressure increased from 100 psi and attempted to reach 119,000 psi over a stroke distance of 1.9 inches. The time pressure position profile is shown in the computer print out of Fig. 44. In an attempt to obtain a more realistic pressure peak, the ramp was decreased to 3°. It was found that the pressure went from 400 psi to 16,000 psi within a stroke of 4.6 inches. This profile is shown in the computer print out of Fig. 45.

The apparent trend indicated that to keep the pressure to a reasonable design level, an excessively long and shallow ramp is required. Since the maximum length of the actuator has already been specified, this would then require that the stroke be limited or restricted. Discussions were held with cognizant Flight Dynamics Lab personnel, and it was decided not to install a damper in the actuator. An alternative approach which used stroke limiters on the actuator and pressure relief valves in the installation was to be considered.

Structural Analysis

A structural analysis of the Spider Leg actuator was conducted to determine the design dimensions consistent with the

$$\text{(1)} \quad Q = CAP^{\frac{1}{2}}$$

$$\text{(2)} \quad Q = A_p\dot{X}$$

$$\text{(3)} \quad -PA_p = M\ddot{X}$$

$$\text{(4)} \quad A = \frac{\pi}{4}\left[D_o^2 - (D_s + 2X\tan\theta)^2\right]$$

From (1) and (2)

$$\text{(5)} \quad P = \left(\frac{Q}{CA}\right)^2 = \left(\frac{A_p\dot{X}}{CA}\right)^2$$

Figure 42. Piston Damper
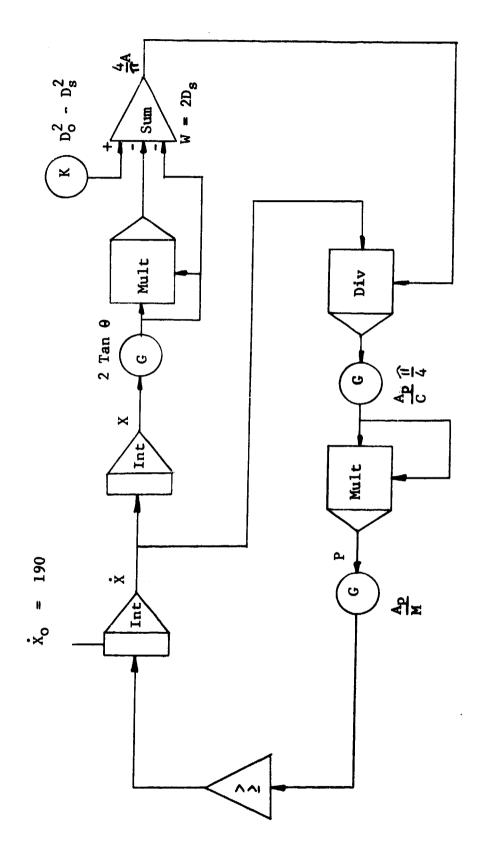
Figure 43. Damper Simulation Diagram

TIME	Pressure psi BLOCK #9	Displacement in. BLOCK #2	Velocity in/sec BLOCK #1
.00000	66.83763	.00000	190.00000
5.00000E- 3	68.90199	.94956	189.82147
1.00000E- 2	75.99715	1.89820	189.63113
.01500	90.63032	2.84582	189.41291
.02000	119.49732	3.79223	189.13946
.02500	182.42685	4.73703	188.75198
.03000	359.32321	5.67930	188.08161
.03500	1300.80308	6.61621	186.30119
.04000	1.19055E 5	7.49384	18.02076
.04500	56.36232	7.50038	.08797
.05000	8.31522	7.50063	.02936
.05500	2.91938	7.50074	.01625
.06000	1.42103	7.50080	.01085
.06500	.82140	7.50085	7.98897E- 3
.07000	.52737	7.50088	6.24567E- 3
.07500	.36450	7.50091	5.08472E- 3
.08000	.26510	7.50094	4.26214E- 3
.08500	.20052	7.50096	3.65211E- 3
.09000	.15639	7.50097	3.18360E- 3
.09500	.12502	7.50099	2.81367E- 3
.10000	.10198	7.50100	2.51496E- 3

Figure 44. Pressure Profile for Damper
with 10° Ramp Angle

67

	Pressure psi	Displacement in.	Velocity in/sec
TIME	BLOCK #9	BLOCK #2	BLOCK #1
.00000	66.83763	.00000	190.00000
1.00000E- 2	67.34828	1.89823	189.64575
.02000	69.43568	3.79289	189.28469
.03000	73.31875	5.68387	188.90797
.04000	79.44150	7.57097	188.50505
.05000	88.59441	9.45384	188.06217
.06000	102.16678	11.33201	187.55999
.07000	122.68834	13.20475	186.96913
.08000	155.08925	15.07094	186.24131
.09000	209.99794	16.92884	185.28941
.10000	313.93239	18.77542	183.93571
.11000	549.51014	20.60486	181.74725
.12000	1292.62324	22.40330	177.30888
.13000	6444.38004	24.12010	162.00315
.14000	1.59238E 4	25.17919	14.32301
.15000	210.79511	25.21242	.76113
.16000	38.22983	25.21691	.27307
.17000	13.82741	25.21892	.15045
.18000	6.73709	25.22014	.09920
.19000	3.87027	25.22098	.07213
.20000	2.46740	25.22162	.05576

Figure 45. Pressure Profile for Damper with 3° Ramp Angle

desired performance parameters and the allowable material stress.
An analysis of the motions and resulting accelerations and stresses
of the Spider Leg actuator revealed that the critical areas of
the design are the column loading effects on the actuator rod
at maximum extension and the hoop stresses caused by the oil
pressure within the various volumes of the actuator design.

The motion analysis of the Spider Leg actuator revealed
that the maximum vertical acceleration would be approximately
3 "g's". Therefore, the actuator will see a load of approxi-
mately 3000 pounds with an undefined eccentricity as a result
of the lateral accelerations of the actuator body. Therefore,
the stress on the rod of the Spider Leg actuator must be deter-
mined by treating the fully extended length of the rod as a
slender column with a load of 3000 pounds applied eccentric to
the nominal vertical center line of the rod. Since the eccen-
tricity is an unknown parameter, it was determined that it would
be desirable to write a computer program to increment the eccen-
tricity of the column load in small steps while evaluating the
resulting column stress by the use of the "secant" formula of
structural mechanics.

The computer program shown in Fig. 46 was written for this
analysis. The initial Spider Leg actuator design layout indi-
cated that an external rod diameter of 1.75 inches would be de-
sirable. Therefore, the computer program was written to define
the required yield strength of the rod material as specified by
the secant formula for eccentrically loaded columns.

The critical parameter for any column design is the slen-
derness ratio, defined as the ratio of the length of a column
divided by the radius of gyration. Since the radius of gyra-
tion is a function of the cross-sectional area of the column,
it is necessary to define the internal diameter of the column
in order to determine the stress as a result of the column load-
ing. Therefore, the computer program was designed to increment
the I.D. of a column and the eccentricity of the column load
and print out a table of values of the required yield strength
of the material for each loading and area dimension.

The resulting data table was analyzed to select the maxi-
mum rod internal diameter consistent with the normal structural

```
0 PRINT"                        SECANT FORMULA FOR CALCULATION OF
20 PRINT "                  ECCENTRICALLY LOADED COLUMN DESIGN FOR
30 PRINT "                          SPIDER LEG ACTUATOR
40 PRINT
50 PRINT IN IMAGE
" OUTSIDE                INSIDE                  ECCENTRICITY          COLUMN
60 PRINT IN IMAGE
" RADIUS                 RADIUS                  FROM C/L              STRESS
70 PRINT IN IMAGE
" -------                -------                 ------------          -------
80 PRINT IN IMAGE
" INCHS                  INCHS                   INCHS                 LBS/SQIN
90 !LET X=INSIDE RADIUS
100 ! LET Y=ECCENTRICITY OF LOAD
101 ! LET R=RADIUS OF GYRATION
120 P=3000
130 S=30000
140 E=3.E7
150 C=0.875
160 L=130
171 FORX=0.1 BY 0.05 TO 0.8
172 FORY=0.1 BY0.1 TO 1.0
173 A=PI*(0.875↑2-X↑2)
175 R=0.5*SQRT(0.875↑2+X↑2)
180 B=P/A*(1+(Y*C/R↑2)*1/COS(L/R*SQRT(P/4*E*A)))
181 GO TO200 IF B>9999999
190 PRINT IN IMAGE
" Z.ZZZ                  Z.ZZ                    Z.Z                   ZZZZZZ";
C X,Y,B
191 NEXT Y
200 PRINT
201 NEXT X
210 PRINT
220 PRINT "END"
>
```

"SECANT" FORMULA COMPUTER PROGRAM

FIGURE 40

mechanics limitations for the column stress versus the slenderness ratio and versus the eccentricity of the resulting column. As a result of this analysis, it was determined that a rod internal diameter of 1.432 inches would result in column stress of less than 4000 pounds per square inch when the actuator rod is extended to a full length of 130 inches and a 3000 pound load is applied at an eccentricity of less than 3/8 inch from the true geometrical center of the actuator rod. The resulting column has a slenderness ratio equal to 200 which permits a maximum column stress of approximately 6000 pounds per square inch as shown in the illustration entitled "Columns of Structural Steel with Different Eccentricities of Load," in Mechanics and Materials, Third Edition, Wiley. This same illustration may be found in several structural mechanics texts or the structural steel handbook and illustrates the manner in which the eccentricity of the load influences the allowable column stress as a function of the slenderness ratio of a given column.

It is important to note that the eccentricity of a load has a much larger influence for columns with a slenderness ratio of less than 120. With a column slenderness ratio of between 200 and 300, the effect of the eccentricity of the load is minimal and causes a variation in the allowable load of less than 500 pounds per square inch for eccentricity ratios from 0.1 to 1.0. Therefore, the safety factor of column design is approximately 1.57:1.

Upon completion of the structural analysis of the column loading effects of the rod of the Spider Leg actuator, the internal pressurization within the rod and the cylinder bore were analyzed along with the deflections that result from the developed stresses. The nominal analytical expressions for the hoop tension in a thick cylinder were utilized for this investigation. These formulas may be found in Formulas for Stress and Strain, R.J. Roark. As a result of this analysis, it was determined that the maximum stress in the actuator rod as a result of the internal pressurization is 2813 pounds per square inch applied in a circumferential direction. The change in the radial dimensions of the rod as a result of the internal pressurization is negligible since the maximum change in any dimension is less than 0.0001 inches.

The maximum stress in the cylinder is 5083 pounds per square inch in the circumferential direction. Again, the resulting

changes in the internal and external dimensions of the cylinder are negligible.

DESIGN AND FABRICATION

Actuator

Actuator dimensions were tentatively selected in the Analysis and Sizing Investigation of the previous section. These dimensions were modified to permit the use of commercially available piston and rod seals. Table II presents a summary of the preliminary and actual dimensions.

All fabrication within the capability of WPAFB was planned to be done at the base and zone machine shops. This included the end blocks, bearings, special nuts, tie rods, and tie rod supports. The tubular barrel and piston required gun drilling and/or honing which could not be done on base.

The material selected for fabrication of the end blocks was AISI 1117. This has a tensile strength of 86,000 psi and a yield strength of 75,000 psi. It exhibits a machinability rating that is 95% of the 1112 screw machine stock. It was selected on the basis of ease of work and strength.

The initial intent was to fabricate the cylinder bore and piston from tubing. It then was to be honed to the cylinder bore size by a commercial honing company. The alloy selected was 4142 with a tensile strength of 100,000 psi and a yield strength of 70,000 psi. However, after many discussions and consultations with experts in the field of honing, it was discovered that the commercially available tubing exhibits a spiral wave created when the tube is pierced by the forming die. Frequently, this die may be slightly off center. During fabrication, the driving rollers on the O.D. of the tube twist the grain structure. The final roller straightening of the tube rounds the O.D. but the axis of the I.D. is not always true. Tubing manufacturers also indicate that a camber exists that typically might be 1/4 inch in a 20 foot length. It was recommended that the commercially procured tubing be gun drilled prior to honing.

It became apparent that there could be little cost saving

TABLE II

ACTUATOR SIZES

	Preliminary			Actual	
	Area	Dia.		Area	Dia.
Bore	3.1400	2.000		3.1196	1.993
Rod	2.4053	1.750		2.4053	1.750
Rod Bore	1.7680	1.500		1.6110	1.432
Blind End	1.3600			1.5091	
Rod End	.6890			.7143	
Piston Bleed Orifice	.00348	.0667			.068

Servovalve Sizes

Design Flow Area	$.2 \ in^2$
Design Valve Stroke	.125 in max
Spool Diameter	.75 in
Slot Width	4 at .40 in.
Valve Porting	1 in diameter nominal
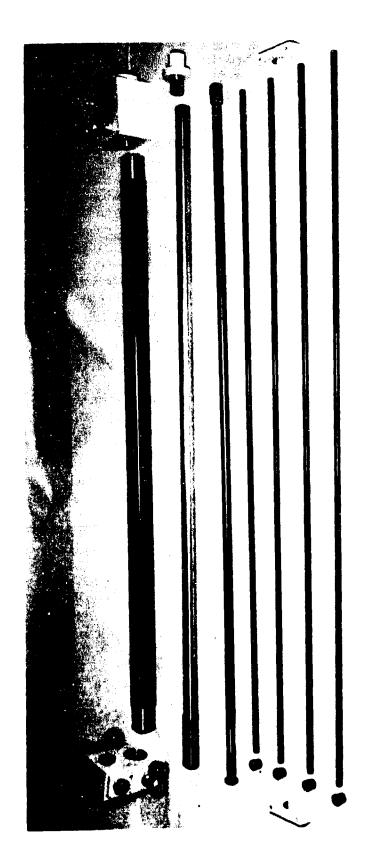
by using commercial tubing, and it was decided to work from
solid bar stock. This would give the optimum in accuracy and
reliability. The bar stock material selected was Stressproof
(trademark registered), a product of LaSalle Steel Corporation.
This is a medium carbon high manganese free machining steel that
has been severely cold worked. No heat treat is necessary and
the material is stress-relieved. It was felt that these char-
acteristics would minimize any tube distortion after gun dril-
ling and honing.

        To find sources for fabricating the tubing a survey of
approximately 24 companies was undertaken. Quotations were so-
licited from the only 5 companies that had equipment capable
of producing the parts. Special equipment was required due to
the long length, 80-7/16 inches. Gun drilling and honing equip-
ment for these lengths are special.

        Machining quotes received with material furnished by Hy-
draulic Research and Manufacturing Company ran as high as $4470
for the body and rod completely finished. It was decided to
split the work effort in order to take advantage of company
specialities. The gun drilling was done by the Howard Dear-
born Company in Berea, Ohio. After drilling the bore and pis-
ton were shipped to Commercial Honing, Inc. in Dover, Ohio, for
final machining. The body was gun drilled to 1.968/1.978 inches
and the rod was gun drilled to 1.406/1.432 inches. Commercial
Honing, Inc. honed the body to 1.992/1.994 inches and the rod
to 1.431/1.433 inches. Total machining costs for the completed
body and piston assemblies was $650. Fabrication of all other
parts for the actuator was accomplished at the WPAFB DMDEE zone
machine shop. The completed actuator parts prior to assembly
are shown in the photograph of Fig. 47.

Servovalve

        The servovalve designed for the FGL Spider Motion actua-
tor is a three stage four way type. It uses an existing com-
mercial two stage flapper nozzle valve as a pilot stage to posi-
tion the power spool. An LVDT is installed on the power spool
and is used to provide electrical feedback for position loop
control. The LVDT selected is manufactured by Schaevitz En-
gineering and is a Model 200 HR. This unit is mounted in an
end cap and subjected to hydraulic pressure. Electrical leads
are brought out through a high pressure connector in the end

74

SPIDER LEG ACTUATOR COMPONENTS

FIGURE 47

75

cap. The pressure connector selected is manufactured by the Conax Company, 2300 Walden Avenue, Buffalo, New York. It is a Model TG-24-A-4-P.

The spool and sleeve assembly were fabricated of 440 C stainless steel by Hydraulic Research and Manufacturing Company, Valencia, California. After fabrication, they were hardened, ground, and lapped. The servovalve body was fabricated by the base machine shop in Bldg. 5 of 2024 T351 aluminum. All other parts were fabricated in the DMDEE zone machine shop. Additional fittings were made so that the basic servovalve body could be used to flow plot the stainless steel spool and sleeve in the lab. The disassembled servovalve is shown in the photograph of Fig. 48. The four lands of the servovalve were flow plotted in the Flight Dynamics Lab hydraulic facility. Grinding dimensions were provided to Hydraulic Research and Manufacturing Company for final grinding. A line-to-line grind condition was initially chosen and arrived at. After grinding by Hydraulic Research and Manufacturing Company, the valve was again flow plotted to verify the land conditions. A second grind would have been desirable to arrive at a slight underlap condition; however, schedule slippages did not permit this to be accomplished.

ASSEMBLY AND TEST

Initial assembly of the actuator was conducted by Hydraulic Research technicians in the Flight Dynamics Laboratory. Initially the rod end seal was a typical commercial "V" ring packing (Periflex brand). This consisted of six pressure rings plus a male and female adapter. The rod wiper seal was manufactured by E.F. Houghton & Company. This was the VIX-SYN wiper, a 90 durometer rubber scraper ring.

A 14 GPM servovalve was connected to the actuator and pressurized to 500 psi. The servovalve was controlled by a battery box and the actuator was operated open loop. Leakage checks were made by gradually increasing the pressure to 3000 psi. When no leaks occurred after two hours, the actuator was connected in a closed loop manner and cycled at a frequency of .2 CPS and an amplitude of $\pm$ 30 inches for ten hours. During this cycling the actuator exhibited excessive chattering in the extend and retract motions. This chattering was attributed to excess stiction from the commercial "V" ring packing.

SPIDER LEG SERVO VALVE COMPONENTS

FIGURE 48

77

In an attempt to relieve the chattering, the six pressure rings were gradually reduced to three, the minimum permissible. Some improvement was noted; however, performance still was not satisfactory. A second packing commercially available and manufactured by the Johns-Manville Company was tried. This was their UNEEPAC 4 multilip W type in common use in industrial actuators. These did not exhibit sufficient improvement over the Paraflex seal to minimize chatter. Next Glyd-ring seals were tried. They are manufactured by the W.S. Shamban and Company, and are made of a modified teflon. These rings are installed over an "O" ring and the manufacturer gives them a friction rating that is 30% of a standard "O" ring in reciprocative motion.

For a rod end seal two Glyd-rings are normally installed with the area between them vented to return. Since this would require extensive modification of the actuator, it was decided to install both Glyd-rings, but not vent the between area. This created a potential shaft leakage problem, but allowed evaluation of the rings for friction and chatter. Upon testing all indication of chatter was eliminated.

A second potential problem arose from the 190 inch per second permissible actuator velocities. It was felt that heat generated could cause excessive wear on the Glyd-rings. Therefore, a bronze filled teflon "V" packing set was ordered from the W.S. Shamban Company. In testing to date, no indication of a thermal problem has been detected and the "V" packing set remains to be evaluated.

The servovalve was initially assembled using a 14 GPM pilot valve. This exhibited excessive mechanical gain and was replaced with a smaller capacity 1-1/2 GPM valve. During check out some sticking of the spool was observed in the null area. This was lapped with a slurry cf 5506 oil and jewellers' rouge and appeared to improve the condition. Under load some indication of null threshold existed. This was attributed to motion of the sleeve within the body due to pressure changes. The sleeve was shimmed and clamped between the end plates and the condition was improved. Continued testing of the servovalve has indicated that a possible spool load problem exists. This is manifest by a motion of the servovalve in the null area under
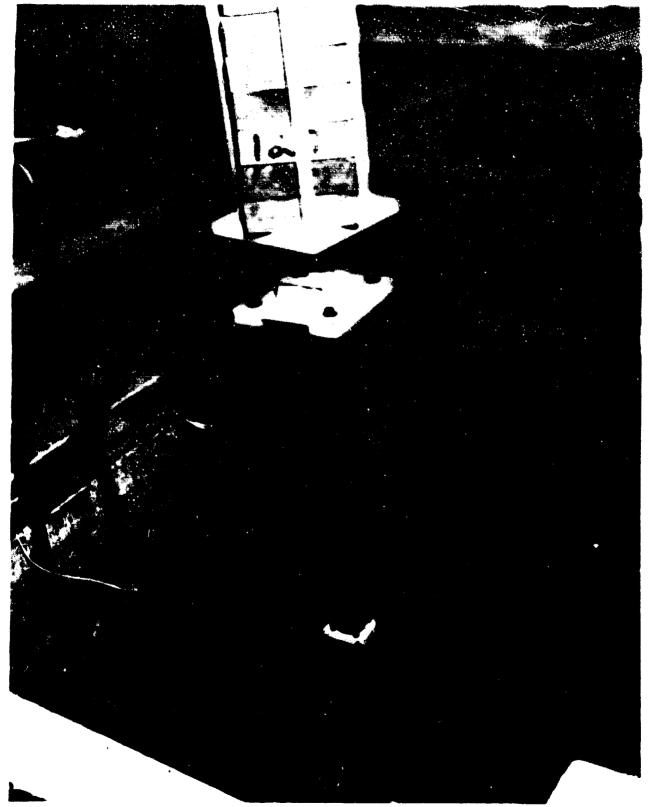
load. Further investigation is recommended.

The actuator was mounted in a 6 foot deep pit, 6 feet by 8 feet wide. A four legged support was lagged to the floor of the pit. The actuator was mounted vertically in the four legged mount and supported on the floor by a welded base also lagged to the floor. This installation is shown in the photograph of Fig. 49 and 50. Since there is no single pumping system of appropriate capacity, it was necessary to interconnect two 20 GPM supplies. The interconnected supplies were plumbed to the valve and actuator using 1-1/4" diameter hydraulic tubing.
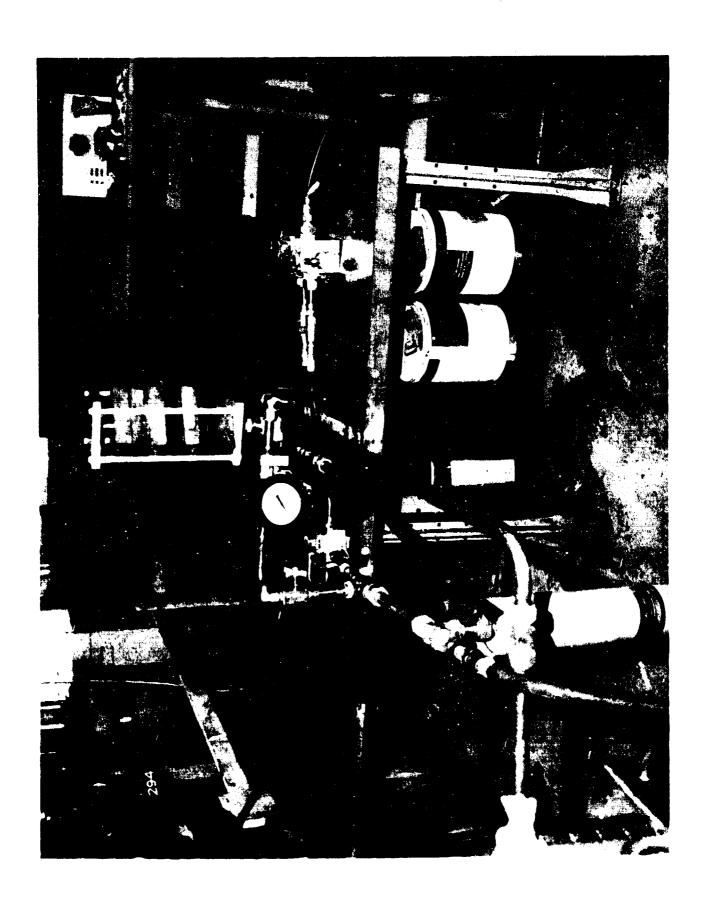
Initially, the actuator was operated using a 14 GPM servo-valve. Initial tests were conducted to determine saturation velocity under no load and no load frequency response. Loop gains were adjusted until the required frequency response characteristics were exhibited by the actuator. Fig. 51 and 52 present the response curves for 12" and 2" peak strokes respectively. An inertia load of approximately 265 pounds was installed on the actuator. Initial cycling tests caused the actuator to break into an oscillation of approximately 5 CPS with ± 2" amplitude. This verified the anticipated instability under no load and a damping orifice of .070 inches diameter was installed. The actuator then exhibited stable characteristics and the frequency response was measured for ± 12" and ± 2" peak amplitudes. These curves are shown in Fig. 53 and 54 respectively.
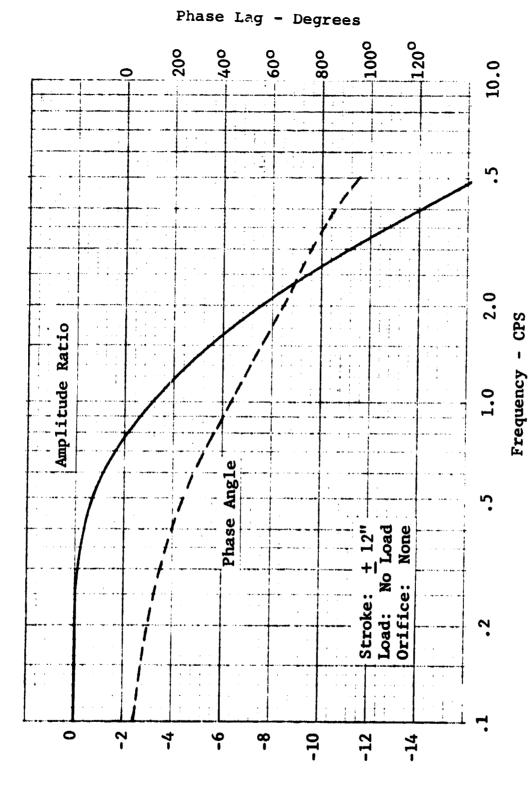
The actuator inertia load was increased in approximately 250 pound increments to a maximum of 1000 pounds with loop gain held constant. Frequency response plots were obtained as each load condition for peak amplitudes of 2" and 12". These curves are shown in Fig. 55 through 60 and demonstrate satisfactory performance can be anticipated under a wide range of load conditions.

SPIDER LEG TEST INSTALLATION
FIGURE 49

SPIDER LEG VALVING TEST INSTALLATION

FIGURE 50

Figure 51. Spider Leg Actuator Frequency Response
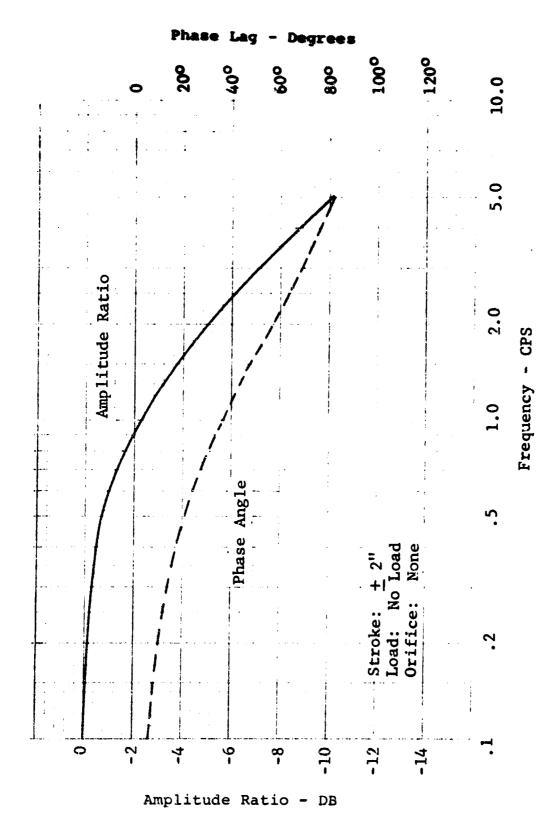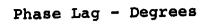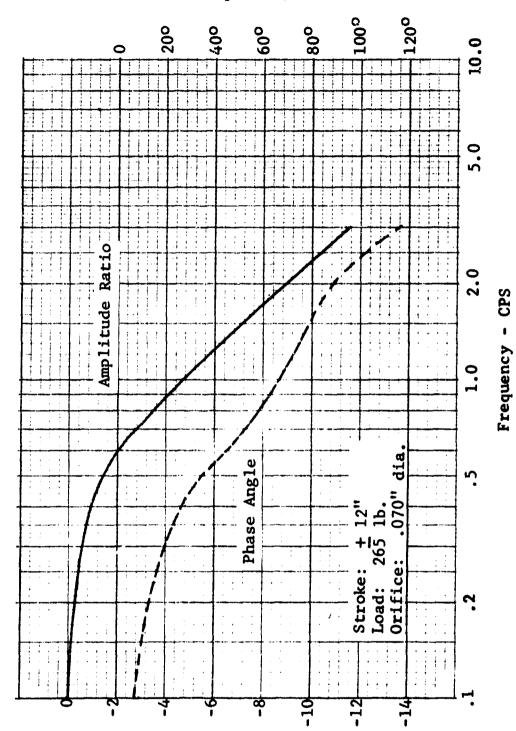
Figure 52. Spider Leg Actuator Frequency Response

Figure 53. Spider Leg Actuator Frequency Response
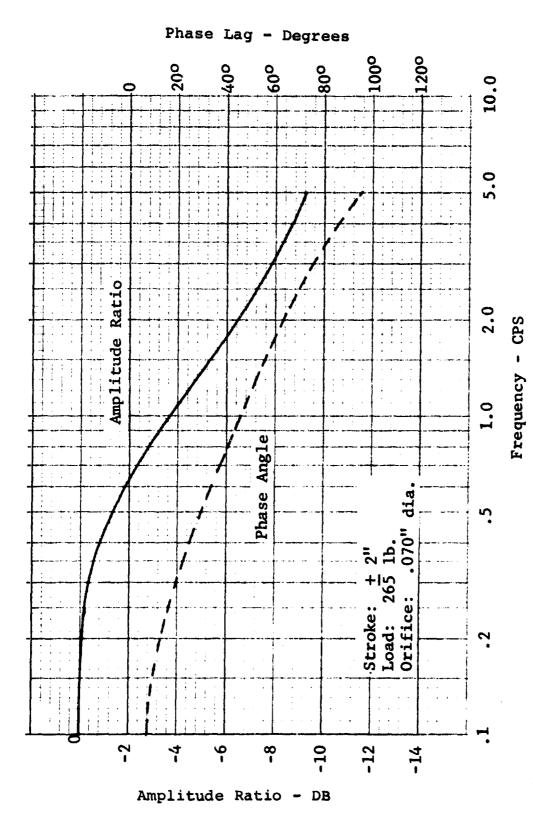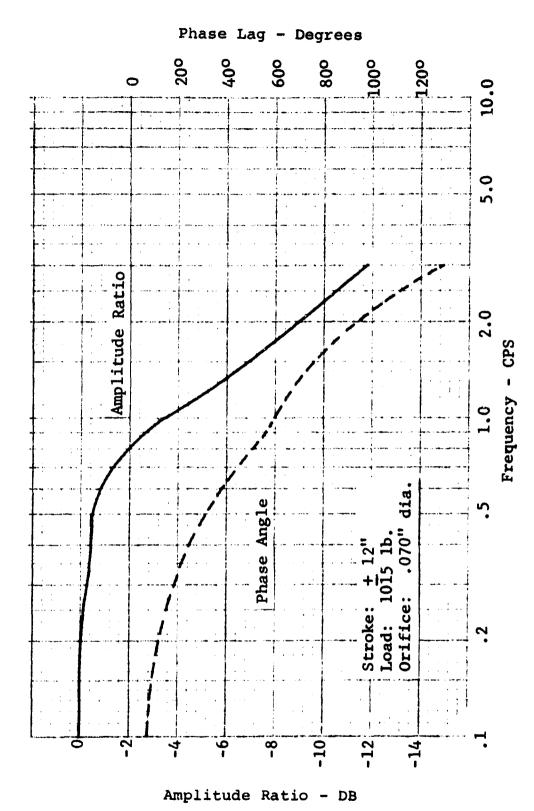
Figure 54. Spider Leg Actuator Frequency Response

Figure 55. Spider Leg Actuator Frequency Response
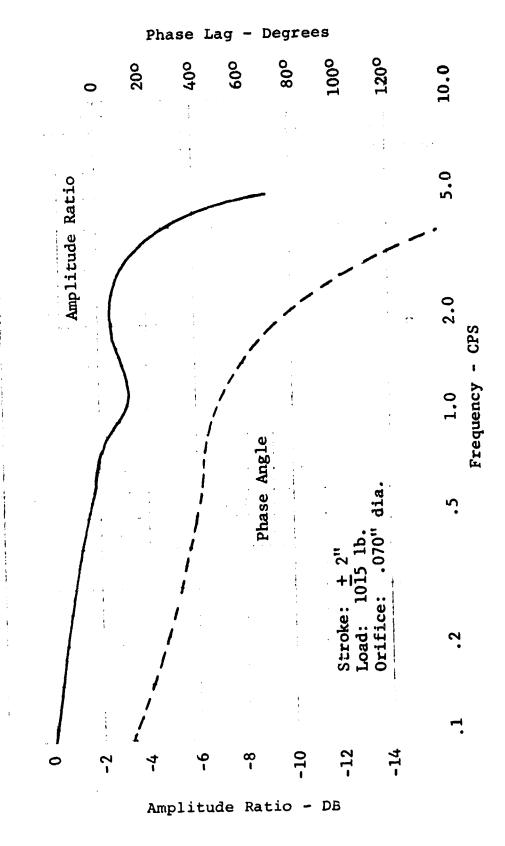
Figure 56. Spider Leg Actuator Frequency Response
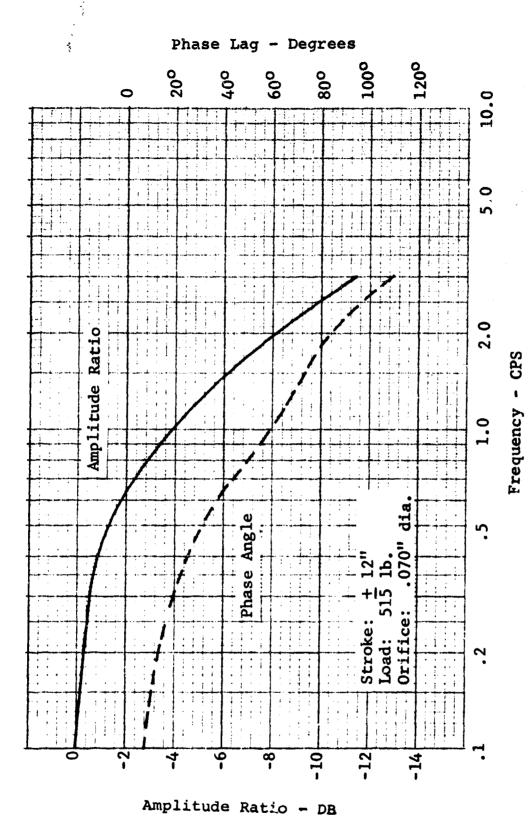
Figure 57. Spider Leg Actuator Frequency Response
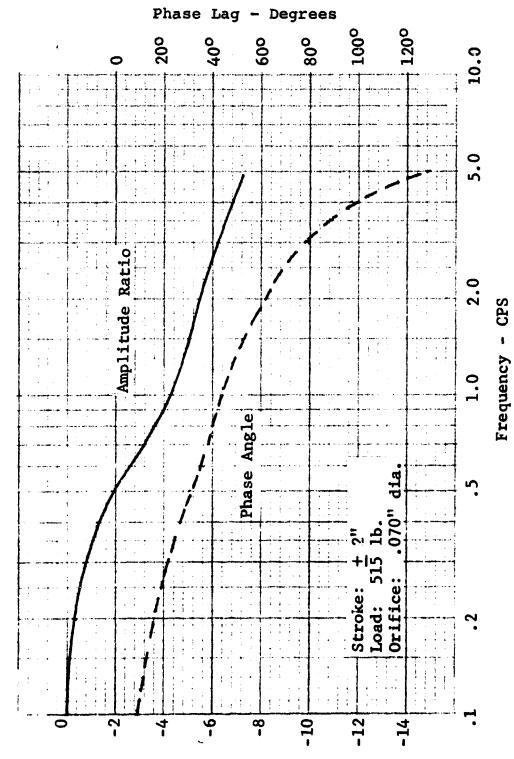
Figure 58. Spider Leg Actuator Frequency Response
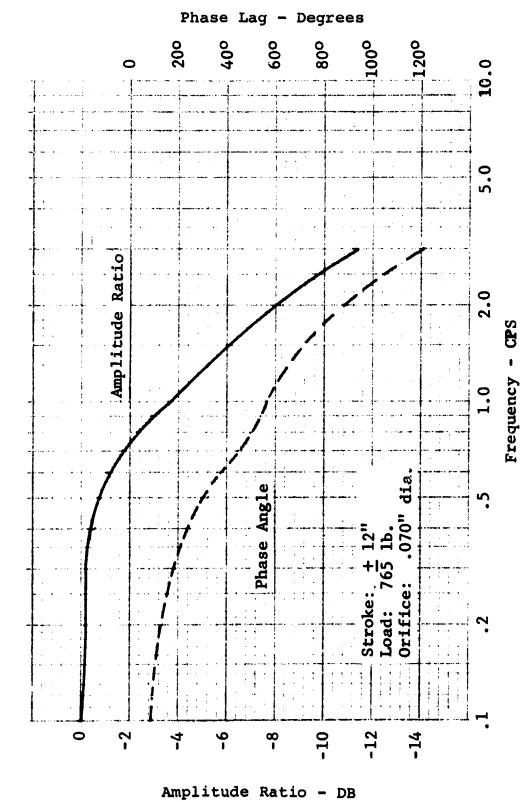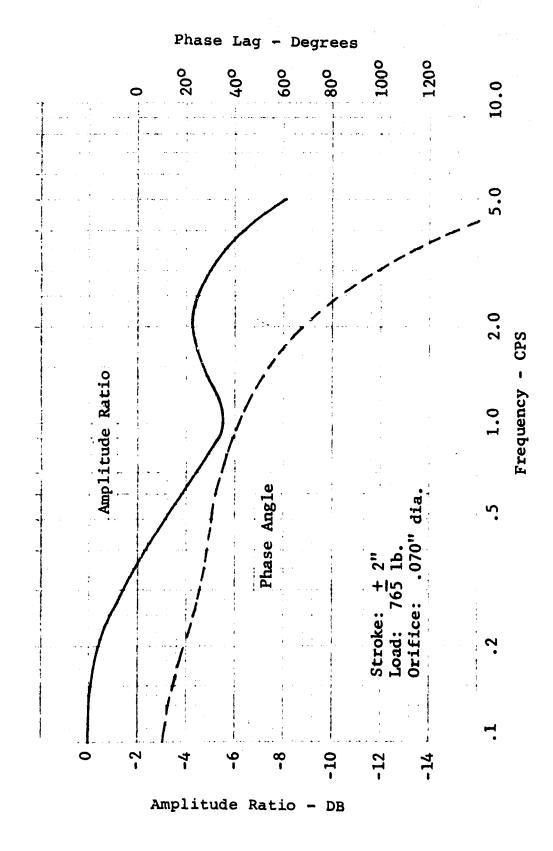
Figure 59. Spider Leg Actuator Frequency Response

Figure 60. Spider Leg Actuator Frequency Response

Stroke: ± 2"
Load: 765 lb.
Orifice: .070" dia.

SECTION III

GENERAL PURPOSE ACTUATOR TEST STAND EVALUATION

INTRODUCTION

The general purpose test stand shown in Fig. 61 is located in the rear of the hydraulics laboratory in Bldg. 195. The general test stand is in the form of a composite beam structure consisting of a steel structural section formed by welding together two wide flange "I" beams and imbedding this structure at a depth of 4-1/8" into a concrete inertia mass. The concrete mass was formed by walling off the portion of a 4 foot deep pit in the rear of the hydraulics laboratory and pouring the section completely full.

For purposes of this evaluation, the general purpose actuator test stand was considered to consist of only the structural "I" beam and the concrete reaction mass as shown in Fig. 62. The degree of coupling between the surrounding walls is questionable since small deflections will exist in the composite structure as a result of applied loads. Furthermore, it was anticipated that the resulting strength and stiffness of this composite structure would be more than adequate to resist the loads that might be created by any test actuators in the near future.

The evaluation of the general purpose actuator test stand was conducted in two distinct phases. The first phase consisted of a structural analysis of the composite member shown in Fig. 62. This was intended to determine the maximum load that could be applied to the structure as a function of the distance between the end restraints, the mounting height of the actuator above the beam surface, and the allowable stress in the concrete and steel composite beam structure. During the second phase a design analysis of the load actuator was made to select, purchase, or construct a load actuator which will develop a reasonable load within the restrictions determined by the first phase. It is also required to have sufficient response to permit the test stand to be used in flutter studies involving a combination of high frequency and high loads.

REACTION MEMBER
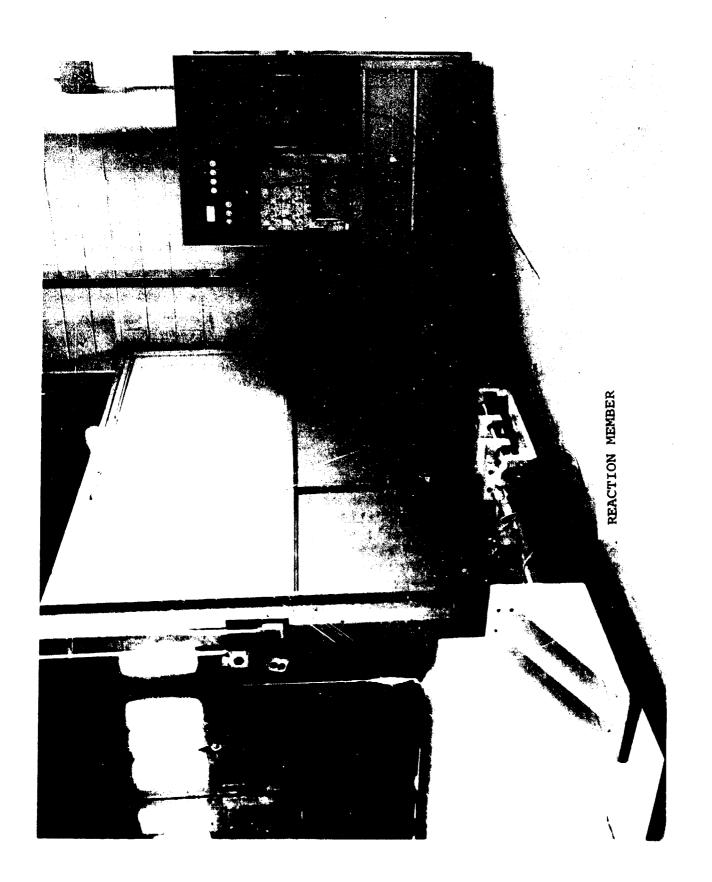
Fig. 61 - General Purpose Test Stand

STRUCTURAL ANALYSIS OF THE GENERAL PURPOSE ACTUATOR TEST RIG

The general purpose actuator test rig structure shown in Fig. 62 may be considered to be a reinforced concrete beam section. Not shown in this figure are a pair of "I" beam feet which are welded normally to the long dimension of the steel beam. These additional members serve to effectively lock the "I" beam section into the concrete mass, thus causing the entire assembly to act as a composite beam member.

For purposes of this evaluation, the surrounding concrete walls which actually enclose this beam were considered to be non-touching. This assumption was made on the basis that the rigidity of the composite beam member is such that the surrounding structure can only contribute additional stiffness. This assumption greatly simplifies the stress analysis.

Fig. 63 represents the beam loading and bending moment diagram. The loads applied to the general purpose actuator test rig are coupled to the beam member by the reaction structure shown in Fig. 61. For purposes of this evaluation, the reaction member is assumed infinitely stiff, i.e., will not contribute deflection under load.

The forces applied to the reaction member may be assumed to be coupled to the beam by virtue of the equal and opposite forces shown in Fig. 63. In addition the same loads create an additional compressive or tensile stress at this point. The ultimate fibers stress may be equated to the sum of the tensile or compressive stress and the stress caused by beam flexure as shown by the following expression:

$$\text{Max. Stress} = \frac{P}{A_t} + \frac{M'}{I_t/C}$$

Where: P   =   Applied Beam Loading
         (t)   =   Tension, (-) Compression
         A_t =   Total Composite Area
         I_t =   Total Composite Moment of Inertia
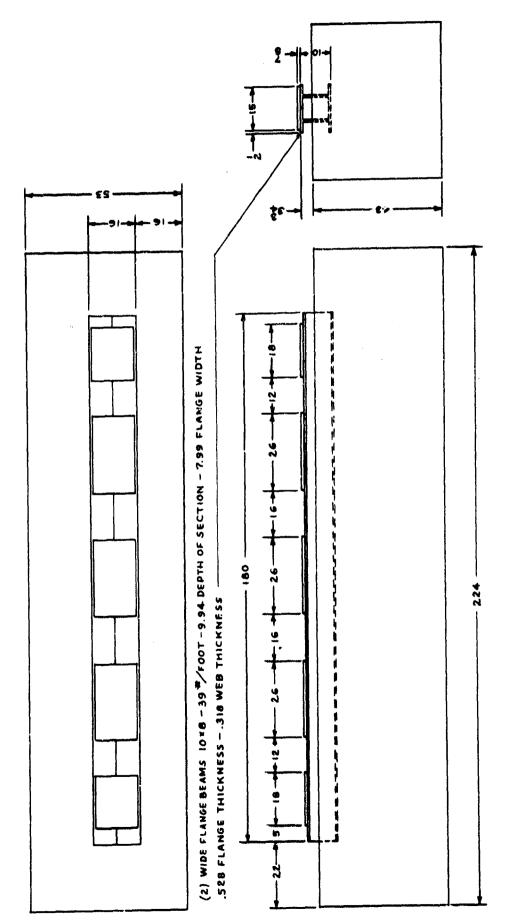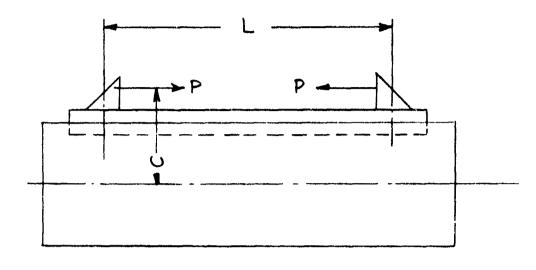
         C   =   Centroid to Neutral Axis
         M'   =   Max. Bending Moment due to Combined Loading Effect
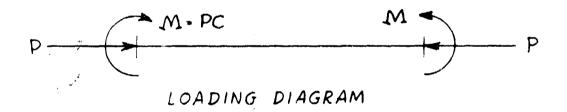
Fig. 62 - Test Stand Support Structure

(2) WIDE FLANGE BEAMS 10×8 – 39#/FOOT – 9.94 DEPTH OF SECTION – 7.99 FLANGE WIDTH
.528 FLANGE THICKNESS – .318 WEB THICKNESS

ACTUAL

LOADING DIAGRAM

MOMENT DIAGRAM
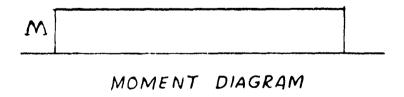
Fig. 63 - Beam Loading Diagram

The direct stress caused by the axial loads and the stress
caused by flexure of beam bending are summed in this case
because they are alike. They both cause in-phase stresses
on the surface of the beam. The bending moment represented
by the term (M) is the bending moment due to the combined
effect of the axial loads and the end couples (PC). The
bending moment (M) may be calculated by use of the following
expression.

$$M = PC / \left(\frac{1 + \cos U}{2}\right)^{\frac{1}{2}}$$

Where: $U = L/J$

$J = \left(\frac{EI}{P}\right)^{\frac{1}{2}}$

$L =$ Length

$E =$ Composite Modulus of Elasticity

$I =$ Composite Moment of Inertia

This expression is valid in beams in which the maximum bending
moment and the maximum deflection occur at the same section.
Referring to Fig. 63, it is obvious that this condition occurs
as a result of the beam loading assumed for this analysis.

The composite beam structure was analyzed by inspection
to determine which direction of beam flexure would cause the
greatest stress. It may be observed thatthe fiber stress in
a beam member is proportional to the distance that a given
stress plane is displaced from the neutral axis or that axis
where the stress is assumed to be zero. The neutral axis of
the composite concrete steel beam would be only slightly higher
than the true horizontal center of the concrete mass. Therefore,
the flexure stresses would be very near the same value at the
top and bottom of the composite beam structure. However, the
direction of the stresses would be opposite.

An analysis of the structural characteristics of the con-
crete structure verified that concrete does not have a defined
yield point as exhibited by the ferrous and nonferrous materials
such as steel or aluminum. These materials exhibit a strain or
elongation proportional to stress until it exceeds a value equal
to approximately 1/2 the ultimate strength of the material. Con-
crete, on the other hand, does not have a finite yield point,
but does display a near perfect relationship between the applied

97

load and resulting strain or elongation until the load exceeds
the rupture strength of the concrete. In a concrete beam sub-
jected to a load which causes a bending moment, the stress at
which the concrete will rupture is defined as the modulus of
rupture and is equal to approximately 250 pounds per square
inch.

It is apparent that the maximum stress that the general
purpose actuator load test structure can withstand will be limit-
ed by the modulus of rupture of the concrete material. The
lower surface of the composite beam member will be in tension
when the applied loads on the upper surface are directed to
create a compressive load. The compressive load that will ex-
ceed the modulus of rupture of the lower surface of the con-
crete and cause a downward or concave deflection of the beam
surface will not produce an excessive tensile stress on the
upper surface of the beam if the load were reversed. Thus,
the maximum load that the general purpose actuator load test
stand can withstand is limited by the modulus of rupture of
the concrete portion of the composite beam, when the direction
of the load causes tensile stress at the lower surface of this
material.

The aforementioned computations are adequate to define
the maximum load that may be applied to the general purpose ac-
tive load system. However, it is desirable to also calculate
the maximum deflection that may be expected in each plane where
the test actuator and load actuator are mounted.

This deflection is readily determined by use of the first
area moment proposition of structural mechanics which states
that the angle between the tangents to the beam and any two
points (A), (B) is equal to the area of that part of the bend-
ing moment diagram between (A) and (B) divided by the product
of the modulus of elasticity and the section moment of inertia.
As shown in Fig. 64, the angle formed by the intersection of
the tangent to the elastic curve of the beam is also equal to
the included angle formed by erecting perpendiculars to the tan-
gents to locate the center of the radius of curvature. Since
the length of the neutral axis theoretically does not change
during application of loads to the beam structure, and since
the tangents to the elastic curve are specified as those tan-
gent to the neutral axis, the radial distance from the neutral
axis to the center of the radius of curvature may be readily
calculated.
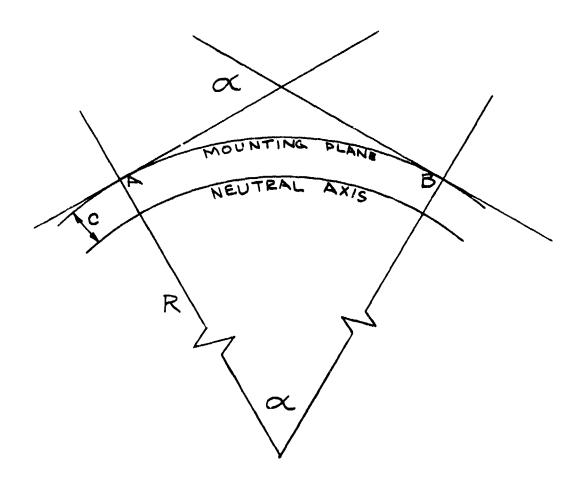
Fig. 64 - Angle Diagram

Therefore, the length of the arc which actually represents the length of any mounting plane in a position above the composite beam may be readily defined for any loading condition by simple geometry techniques. The difference between the arc length of the neutral axis and the arc length in the mounting plane represents the deflection caused by the applied load.

The aforementioned formulas were redimensioned as required to obtain consistency between the units. The computer program illustrated in Fig. 65 was written to determine the maximum stress at the lower surface of the concrete structure, the maximum bending moment at the center of the beam, and the maximum deflection in the mounting plane of the actuator-load system.

The computer program calculates the position of the neutral axis of the composite structure in reference to the lower surface of the concrete portion of the structure. The section moment of inertia of the concrete and steel areas are computed and transferred to the neutral axis. The program then computes the modulus of elasticity and the total moment of inertia and total area of the composite beam structure. The (J) and (U) terms are then computed. The distance from the neutral axis to the nearest possible plane of suspension of the actuator and load system, the actuator mounting height above the reaction beam and the bending moment resulting from the combined effects of a compressive load and the equal and opposite end couples are then computed. The computer program then calculates the angle between the tangents to the radius of curvature of the beam, the actual radius of the curvature of the beam between the two end couples, and the radius of curvature at the desired suspension heights for the test actuator-load system.

The length of the segment of the arc between the reaction members is then computed and subtracted from the arc length at the neutral axis to determine the deflection resulting from the applied load. The program then computes the maximum stress at the lowest plane in the concrete section of the composite structure. The print out lists the applied load, distance between the surface of the end restraints, the actuator and load system mounting heights above the surface of the steel structural member, the maximum stress at the lower surface of the concrete beam, the maximum bending moment at the center of the beam, and the maximum longitudinal deflection in the actuator-load system mounting plane. The program iterates by incrementing the actuator-load system suspension height, the distance

100

```
1 PRINT"
  *** GENERAL PURPOSE ACTUATOR TEST STAND STRUCTURAL ANALYSIS ***"
2 PRINT
3 PRINT
4 PRINT
5 PRINT
10 PRINT"
BEAM      ACTUATOR    ACTUATOR    MAXIMUM    MAXIMUM    MAXIMUM"
20 PRINT"
COMP      SPAN        MOUNTING    STRESS     MOMENT     DEFLECTION"
21 PRINT"
LOAD      LENGTH      HEIGHT      (POUNDS)/  AT L/2     ON ACT C/L"
22 PRINT"
(LBS)     (INCHS)     (INCHS)     (SQ/IN)    (IN LB)    (INCH)"
23 PRINT"
----      -------     --------    -------    -----      --------"
40 PRINT
50 FOR P=10000 BY 10000 TO 80000
60 FOR L=48 BY 12 TO 132
70 B=53
80 H=43
90 AS=22.96
100 YS=H-1.25
110 A1=B*H
120 Y1=H/2
130 Y=((AS*YS)+(A1*Y1))/(AS+A1)
140 I1=((B*(H↑3))/12)+A1*((Y-Y1)↑2)
150 IS=419.4+AS*((YS-Y)↑2)
160 E1=3.5E6
170 ES=3E7
180 E=(E1*I1)+(ES*IS)
190 I=IS+I1
200 A=AS+A1
210 J=SQRT (E/P)
220 U=L/J
230 FOR C=43-Y+3.67 BY 3.82/2 TO 43-Y+16.315
235 H=C-((43-Y)+3.75)
240 M=(P*C)/SQRT(((1+COS(U))/2))
250 M1=M/(1-.125*((P*(L↑2))/E))
251 T=2*(M1/(P*J))*((1-COS(U))/SIN(U))
252 R=L/T
253 R=R-C
254 L1=R*T
255 X=L1-L
260 S=(P/A)+M1/(I/Y)
270 PRINT IN IMAGE"
XXXXX     XXX      XX.XX      XXXX    XXXXXXX    X.XXXXX.":P,L-24,
4 S,M,X
280 NEXT C
290 PRINT
300 NEXT L
310 NEXT P
320 PRIN
```

FIG. 65 – STRUCTURE ANALYSIS COMPUTER PROGRAM

between the end restraints, and the applied load within the limits chosen.

Fig. 66 is a sample of the data print out of the computer program. Only one specific actuator-load system mounting configuration is represented. This particular configuration is most commonly used to evaluate various actuators.

The axial load-deflection characteristics of the general purpose actuator test stand was measured by the mechanism shown in Fig. 67.

A pair of 70 inch long, thin wall stainless steel tubes were selected which would slip together to form a telescoping assembly. The ends of the tube assembly were fitted with hardened rounded point protrusions designed to make contact with the end restraints. A 2 inch deflection LVDT assembly was fitted within the tubes and spring loaded in such a manner as to cause the tubes to tend to extend or to increase in length.

The LVDT assembly was excited and calibrated at a gain of 22 volts per inch. The deflection measuring instrument was supported on stanchions and placed between the end restraints. The rounded contact points at each end of the assembly made contact at a position of 8.74 inches above the reaction beam surface.

The test stand structure was statically loaded with a series of tension and compression loads. The resulting deflection of the test stand structure was measured with the LVDT system. An analysis of the load deflection data revealed that the measured spring rate of the test stand at the particular actuator span and mounting height utilized for this analysis was 1.25 million pounds per inch. This compares to a calculated spring rate of 1.12 million pounds per inch for the selected mounting configuration. This is attributed to a restraining effect from the pit walls.

LOAD ACTUATOR DESIGN ANALYSIS

The load actuator currently utilized in the general purpose actuator test stand is a stabilator actuator of an F4 aircraft. The control valve was removed and replaced with a servovalve manifold to permit each half of the dual tandem actuator to be controlled by separate pressure control servovalves. The

Beam Comp Load (Lbs)	Actuator Span Length (Inches)	Actuator Mounting Height (Inches)	Maximum Stress (Pounds)/ (Sq, In,)	Maximum Moment at L/2 (In. Lb)	Maximum Deflection on Act, C/L (Inch)
10000	96	4.92	25	337664	-.00590
20000	96	8.74	49	675777	-.00180
30000	96	8.74	74	1013677	-.00271
40,000	96	8.74	99	1351585	-.00361
50,000	96	8.74	123	1689501	-.00451
60,000	96	8.74	148	2027426	-.00541
70,000	96	8.74	173	2365358	-.00632
80,000	96	8.74	197	2703298	-.00722

Figure 66. General Purpose Actuator Test
Stand Structural Analysis
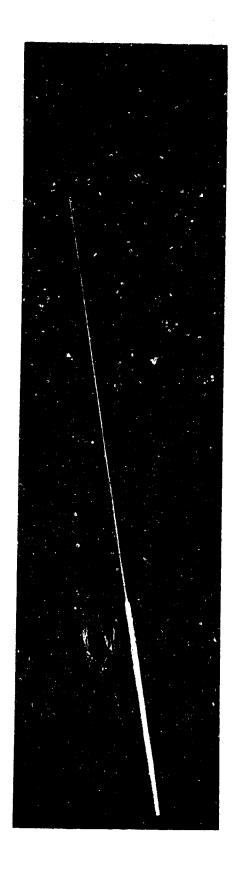
Fig. 67 – Beam Deflection Transducer

pressure control servovalves were utilized in a servoloop which derives feedback from a pressure transducer across the piston. Thus, it is possible to electrically program loads.

The rod eye termination at the end of the actuator rod is marginal. Considerable compliance has been detected in this rod eye and it was replaced with a high strength design fitted into the same physical envelope. The rod bearing supports within the actuator are marginal at any position near the full extension of the load actuator. The actuator rod stiffness as a column leaves much to be desired and, when combined with the poor bearing supports, results in a large visible deflection under high capacity loads at a major extension of the actuator. As a result of the above observations, it is determined that it would be desirable to design a new load actuator.

The load actuator should be an equal area design with rod extensions from either end of the actuator. The actuator rod should be stiff in terms of the column deflections that may be expected. The rod ends should be equipped with different threaded configurations (male thread and female thread) to facilitate interface connections between the load actuator and the test actuator system. The actuator end caps should contain machined, large diameter trunion mounts which will permit the actuator to be restrained by mating clevis blocks which may be physically attached to the end restraints. The trunion mounts at each end of the cylinder will permit the cylinder to be reversed facilitating interface connections.

Special low compliance rod eye terminations should be designed, utilizing high strength materials to provide a minimal compliance structure or restraint for the normal rod end bearings obtained from commercial sources. Commercial rod eye bearings which do not utilize an organic separator or similar low friction interface device between the spherical ball and the mating seat should be utilized for this design.

Fig. 69 presents an illustration of a design which embodies all of the desirable characteristics. The load actuator design shown in Fig. 68 was dimensioned as indicated in the following actuator description. Hydraulic cylinder manufacturers were requested to quote one prototype item.

SHOWN 90° OUT OF POSITION
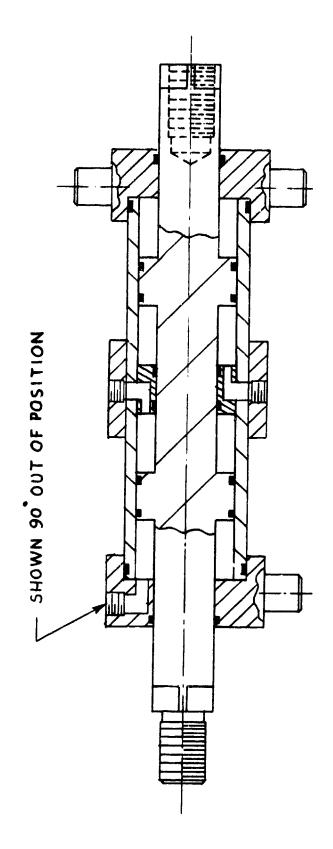
Fig. 68 - Load Actuator Design

Actuator Description

The actuator shall be a dual tandem, equal area design with double rod extension. The cylinder bore will be 4 inches and the rod diameter will be 2-1/2 inches. The cylinder stroke will be ± 5 inches or 10 inches total travel. The interface seal between the front and rear cylinders shall contain a central cavity vented to ambient to prevent any cross-transfer of fluid between the two cylinder sections.

The rear of the cylinder shall be equipped with a trunion mount of 3/4 inch diameter machined directly on the cylinder head. The front cylinder head shall contain identical trunions. The cylinder rod shall be equipped with the standard style 2, 1-7/8-12 male thread on the forward end and standard style 4 female threads at the opposite end.

The normal air bleeds, vents and cushions shall be excluded from this design. Standard SAE porting is acceptable, however, the minimum size shall be equivalent to an AN-12. Port location shall be restricted to the cylinder end caps and all ports shall enter from the same surface.

The above listed description of the specially designed general purpose actuator test system, load actuator was submitted to the cylinder manufacturers along with the drawing of a specially designed rod eye shown in Fig. 69. This illustration depicts the female rod eye member for the load actuator. The manufacturers were requested to submit a cost to produce two such rod eye configurations with this male thread unit dimensioned in such a manner as to produce a maximum stress of 80,000 psi in the threaded section.

All cylinder manufacturers with the exception of Sheffer Corporation, Cincinnati, Ohio, elected to no bid the prototype item. Sheffer Corporation submitted a bid of $1200 for the actuator and $200 for each rod eye configuration. All costs may be discounted 7% and a delivery period of 6 - 8 weeks was given.

CONCLUSIONS AND RECOMMENDATIONS

The structural analysis performed on the general purpose actuator load test stand resulted in a complete tabulated listing

MORSE SPHERCO BEARING
#COR-12 - 54000# RADIAL STATIC LOAD CAP.

MATERIAL - LASALLE STEEL CO. STRESSPROOF® - 100 000 YIELD STRENGTH
ROCKWELL C-27
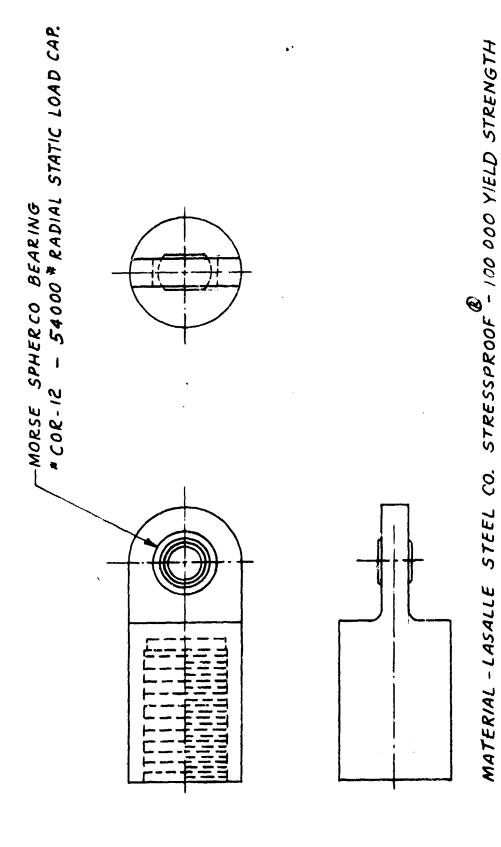
Fig. 69 - Actuator Rod End

of the load stresses and deflections over a load range from 10,000 to 80,000 pounds at various mounting heights and spans. The empirical results correlated with the actual measured stiffness of the load system in one specific mounting configuration. It was shown that reasonable correlation was achieved.

The analysis of the general purpose actuator test stand load actuator did reveal that it was necessary to design and/or procure a new actuator specifically designed to perform the loading task.

It is recommended that the data print out be retained. The spring rate of the composite structure should be determined by measuring the strain that appears at the surface of the reaction member, thus avoiding measurement errors that may result from the relative motion between the end restraint and the composite reaction structure.

It is recommended that a trade off study be made to determine whether to make or buy the new load actuator.

It is recommended that a low mechanical compliance, high resolution, high dynamic response load cell be selected to directly measure the load forces developed by the specially designed load actuator. This will eliminate any errors resulting from measurement of developed force by use of a differential pressure transducer across each drive area.

It is recommended that the high flow rate pressure control valve that was fabricated under past contractual efforts be assembled and refurbished to provide the high flow requirement of the new load actuator.

SECTION IV

HYDRAULIC BRANCH ISOLATION

INTRODUCTION
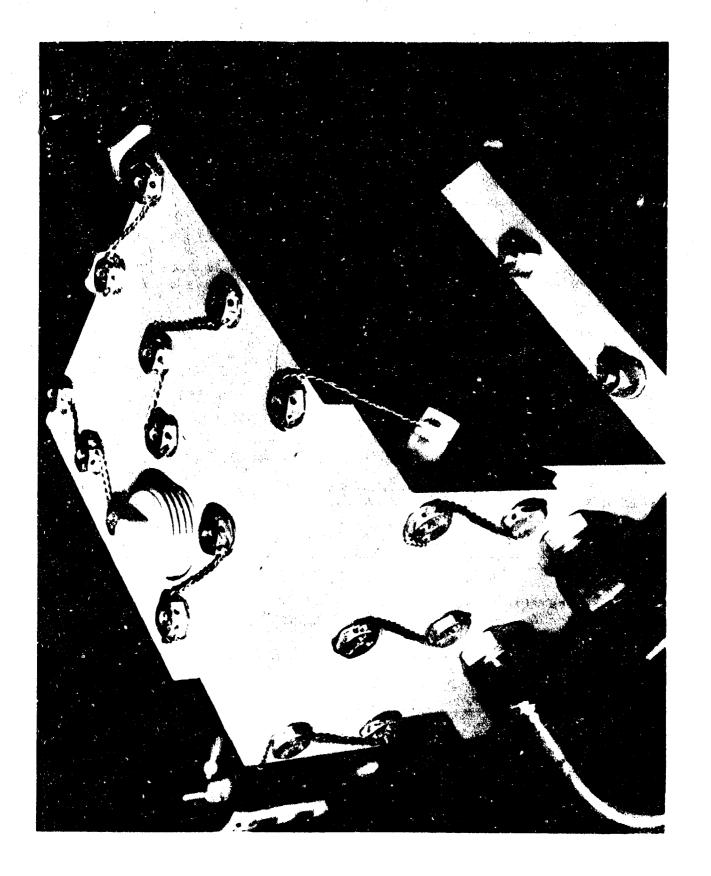
Hydraulic branch isolation refers to the technology utilized to isolate a branch of a hydraulic system in the event a leak occurs.

The advent of very large aircraft has increased the complexity of the hydraulic system to the point that some hydraulic branch isolation device should be utilized to enhance the reliability of the control system. Several devices have been developed to accomplish this task. The mechanizations vary from the simple flow surge device commonly referred to as a hydraulic fuse to the more recent flow comparison instruments and reservoir level sensors.

Under contracts F33615-68-C-1638 and F33615-70-C-1221, Hydraulic Research and Manufacturing Company conducted a continuing research program to improve the design of hydraulic branch isolation mechanizations. This research study began with the design and analysis of an improved hydraulic fuse and has progressed to the design, development and successful flight test of a flow comparison instrument shown in Fig.70 and hereafter referred to as the Flow Difference Sensor (FDS). This effort is documented in TR-69-119. This mechanization was capable of detecting a flow imbalance of 1.5 GPM over a range of 0 - 15 GPM. The device was designed for operation with an F4 stabilator actuator.

The FDS was utilized in conjunction with an F4 aileron actuator in a series of laboratory tests to evaluate the long term operating characteristics of the actuator and the vulnerability of the actuator to small arms ballistic impact. During this series of tests it was observed that several significant leaks occurred which did not cause the FDS to operate and isolate the actuator from the hydraulic source. The magnitude of these leaks was measured and found to be below the 1.5 GPM detection level. Consequently, it became desirable to investigate design of branch isolation devices for a lower detection level. To this end a program was established with the following objectives:

    1. Define the performance specifications for a wide range hydraulic branch isolation device.

110

Fig. 70 - Flow Difference Sensor

2. Determine the state-of-the-art in leak detection technology.

3. Design, develop, analyze and laboratory evaluate selected mechanizations that are capable of achieving the performance specifications defined in (1).

4. Recommend one or two mechanizations for future development.

PERFORMANCE SPECIFICATION FOR HYDRAULIC BRANCH ISOLATION DEVICE

The following specifications were developed in consideration of the environment in which the device will operate and its anticipated usage.

1. Fluid MIL 5606
2. Flow range - 0.1 - 15 GPM
3. Maximum pressure drop at 15 GPM - 100 psi
4. Flow sensor response - linear
5. Detection level - 0.25 to 0.5 GPM
6. Acceleration and vibration - per MIL STD 810B

The maximum pressure drop of 100 psig was selected in consideration of the maximum allowable supply pressure drop attributable to valves and other devices presently installed in aircraft hydraulic systems. The flow sensor pressure-flow response should be linear in order to permit a low detection level over a wide flow range. The desired level of 0.25 to 0.5 GPM was selected upon review of the results of the gunfire and life tests conducted with several actuators in previous contractual efforts.

The operating temperature range of the device is defined by the intended usage in an aircraft flight control system.

The viscosity sensitivity of any mechanization must be minimized to prevent any significant change in performance characteristics over the wide operating temperature range.

The response of the device will most likely be limited by the need to provide a time delay prior to the initiation of the shutdown sequence. This delay may be required to prevent inadvertent operation of the device due to flow discontinuities, entrained air or surge phenomenon. Past experience has shown that

the time delay period should be 50 - 100 milliseconds. This will provide acceptable response.

The resolution of the device is defined as the change in flow rate which will produce a perceptible change in the sensing mechanism output. Ideally, the resolution should be an order of magnitude better than the desired detection level.

The acceleration and vibration criteria are defined by the intended usage of the device in an aircraft hydraulic system. Therefore, the vibration and acceleration test schedules of MIL STD 810B should apply.

DETERMINATION OF THE STATE-OF-THE-ART IN LEAK DETECTION TECHNOLOGY

The state-of-the-art of leak detection technology was determined by a combination literature search and patent survey. The literature search was limited to information specifically categorized under the heading "Leak Detection Equipment or Techniques." Literature search sources were limited to the NASA Tech Briefs, the abstracted transactions and publications of ASME and SAE societies, and sundry commercial equipment catalogs and technical magazines or abstracts.

The literature search did not reveal any mechanization or concept which could be explicitly applied or utilized to detect leaks within an aircraft hydraulic system. Most of the information assimilated during the literature search phase of this effort was related to techniques or equipment which might be used to determine the source, rate, and amount of a gas leaking into or out of some containment volume.

The files of the U.S. Patent Library were surveyed for mechanizations which control the flow of fluid through a connected device or detect a leak in a connective system or apparatus. Copies of the following patents were obtained for detailed study and analysis.

Patent Number	Date	Inventor
2732858	1/31/56	G.C. Noon
3006407	10/31/61	J. Shew
1633114	6/21/27	C.E. Loose
2428150	9/30/47	H. Fields, Jr.

Patent Number	Date	Inventor
2493906	1/10/50	H.W. Wishart
3001799	9/26/61	R.W. Plume
2744533	5/8/56	W.L. Parker

It was observed that patents #2732858, #3001799, and #3006407 were not applicable to leak detection technology since they were essentially proportional flow control devices.

The remaining patents all refer to leak detection and shut-off mechanizations for detecting leaks within an external seal and a hydraulic system. With the exception of patent #2744533, the remaining mechanizations can be functionally categorized in two groups. The first group is intended for operation with single acting cylinders. A spring returned displacement piston with a through orifice is contained in a large volume which is greater than the displacement volume of the attached actuation subsystem. In normal operation the displacement piston merely shuttles back and forth within the enclosed volume. If a significant leak should occur within the actuation subsystem, the displacer piston will be permitted to travel to the end of the bore at which point an attached closure valve will actuate and hydraulically lock in position, blocking flow to the attached actuator subsystem.

The second group of devices or mechanizations utilizes a return side pressure biased pilot valve stage to hold open a closure valve in the supply line. As long as the pressure in the return line is maintained at some level above that required to operate the pilot valve the operation of the device will not be affected. However, if a substantial leak should occur that lowers the return side pressure below this critical value, the pilot stage will cause the supply side closure valve to operate and block the fluid to the branch systems.

The mechanization described in patent #2744533 is illustrated in Fig. 71. The similarity between this mechanization and the current F4 aileron actuator FDS is most unusual. This mechanization utilizes two flow sensing elements placed in series with the supply and return lines of an attached branch actuator. The flow sensing elements consist of tapered cones seating in slightly more divergent conical seats. These flow sensing elements are displaced as a function of the flow rate through each

114

May 8, 1956   W. L. PARKER   2,744,533

HYDRAULIC FUSE

Filed April 23, 1951
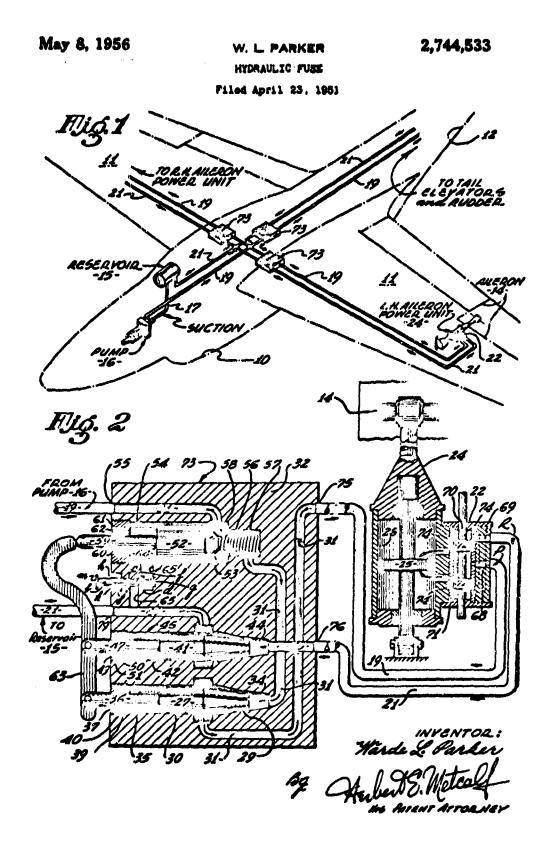
Fig. 71 - Patent 2744533

115

orifice assembly. The resulting motion is coupled to a differential linkage which couples the output motion to a closure valve in the supply line.

In general the literature search and patent survey did not reveal any techniques or apparatus which would enhance the state-of-the-art of hydraulic leak detection technology. However, it was determined that the state-of-the-art in hydraulic branch isolation technology is as defined by the past and current research efforts in the AFFDL/FGL hydraulics laboratory.

Therefore, the hydraulic leak detection by flow comparison concept was selected for continued development and the remaining effort was redirected toward investigating those techniques which might be utilized to more accurately sense the flow in the pressure and return lines of an aircraft branch actuator subsystem.

FLOW SENSOR ANALYSIS

At the inception of this effort it was readily determined that the sharp edged orifice was the only flow sensing element which was effectively insensitive to the viscosity of the flowing fluid. Its nominal pressure-flow characteristic is non-linear. (The flow developed differential pressure is proportional to the square of the flow rate in volume per unit time dimensions, multiplied by a fixed numerical constant.) It is desirable to obtain a linear response wherein the flow developed differential pressure is proportional to the flow rate in volume per unit time dimensions multiplied by a numerical constant. Therefore, it is necessary to extract the square root of the differential pressure signal from the sharp edged fixed orifice sensing element to obtain the desired characteristic.

Based on the information assimilated during the literature search, patent survey and experience obtained under similar development efforts, the following mechanizations were conceived as being candidate methods for extracting the square root of the flow developed differential pressure signal.

      1. Hydromechanically linearized variable orifice assembly.

      2. Electronically linearized fixed orifice assembly.

116

3. Active orifice techniques.

4. Square root linkage.

5. Non-linear spring.

Hydromechanical Linearization

In this concept the hydraulic fluid flow is separated into 1 or more parallel flow paths and caused to pass through a combination of fixed and variable sharp edged orifices to produce a linear pressure-flow response.

The variable orifice assembly consists of a variable orifice utilizing the standard plug valve configuration except the plug is restrained against the seat by a spring. The initial deflection of the spring (i.e. the spring preload) may be adjusted to prevent the flow of fluid through the variable orifice assembly until the force developed by the applied pressure multiplied by the exposed area of the poppet face is adequate to cause the poppet to move away from the seat, thus permitting flow of fluid through the variable orifice.

The differential pressure related to the flow of fluid through a fixed and a variable orifice is shown in Fig. 72. For the variable orifice the developed differential pressure is proportional to the flow rate in volume per unit time dimensions raised to the 2/3 power and multiplied by a numerical constant. Thus, it may be observed that the pressure-flow response of the fixed orifice and the variable orifice assemblies are dissimilar to the extent that the characteristics may be combined over a limited range to produce a piecewise linear response. Furthermore, sets of fixed and variable orifices may be effectively combined in a series-parallel configuration to produce a linear response over a fairly wide range.

In order to properly design any mechanism it is necessary to have a complete understanding of the analytical expressions which depict the operation of the device. Therefore, a computer program was initiated to analytically model the pressure-flow response of a two stage variable orifice assembly containing

Fig. 72 - Fixed and Variable Orifice P-Q Curves

The figure shows a graph with Q (VOL./TIME) on the vertical axis and P on the horizontal axis. Two curves are plotted:

$$P = K_1 (Q)^2$$

$$P = K_2 (Q)^{2/3}$$

fixed orifice parallel flow paths. This mechanization is illustrated in schematic form in Fig. 73. The incoming flow is divided into two flow paths formed by passage diameters D_1 and D_3. The flow through the D_1 passage consists of a partial flow Q_2 and Q_1. Q_2 is the flow which passes through a fixed orifice in the poppet of the valve or variable orifice assembly. Flow Q_1 is the flow that passes through the variable orifice formed by the valve seat and the conical base of the valve poppet element. The variable area orifice thus formed will have a throttling effect on the Q_1 partial flow which will be proportional to the spring rate K, the spring preload X_1, and the port entrance diameter D_1 as defined in AFFDL-TR-69-119.

The remaining incoming flow passes through the passage formed by the D_3 diameter where it is separated into the Q_3 and Q_4 partial flows. The operation of the second stage of the variable orifice assembly is identical to that of the first stage with the exception that the second stage physical parameters such as the fixed orifice diameter D_4 and the spring rate K_1 are adjusted to achieve specific performance characteristics.

The computer program shown in Fig. 74 was developed to analytically model the pressure versus flow response of the two stage variable orifice assembly illustrated in schematic form in Fig. 73. Each flow rate, displacement dimension, or physical system dimension such as orifice diameter is clearly labelled and related to the computer program. Fig. 75 is a sample of the computer print out of the predicted pressure-flow response related to the physical dimensions noted in the print out and established in the actual evaluation hardware shown in Fig. 76. The physical dimensions of the variable orifice mechanism and the desired orifice stops are the required inputs for the program. The computer program increments the developed differential pressure in 5 pound per square inch intervals and calculates the total flow through the two stage variable orifice assembly, the first stage variable orifice deflection in inches, and the second stage variable orifice deflection in inches. The computer program also calculates the desired or ideal flow rate from each differential pressure in order to provide a direct comparison between the calculated total flow through the system and the desired flow. It is then a simple matter to vary the physical dimensions of the system to achieve the desired linear response. It is important to note that excellent correlation has been achieved. The actual pressure-flow response from the test item has
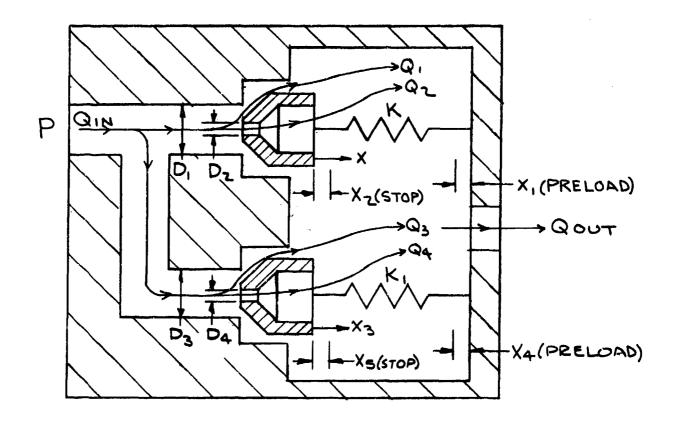
Fig. 73 - 2 Stage Variable Orifice Schematic Diagram Assembly

```
1 PRINT" INPUT DESIRED PRESSURE-FLOW RESPONSE AS (E),MAXIMUM"
2 PRINT" FLOW IN GPM & (F),MAXIMUM PRESSURE DROP DESIRED"
3 INPUT E,F
4 PRINT
5 PRINT
6PRINT
7 PRINT IN IMAGE
"  ***   COMPUTER PROGRAM TO ANALYTICALLY MODEL THE PRESSURE ***"
8 PRINT IN IMAGE
"      VS FLOW RESPONSE OF A TWO STAGE VARIABLE ORIFICE"
9 PRINT IN IMAGE
"      ASSEMBLY CONTAINING FIXED ORIFICE PARALLEL FLOW PATHS"
10 PRINT
11 PRINT
12 PRINT
13 PRINT IN IMAGE
"                                        FIRST          SECOND"
14 PRINT IN IMAGE
"                                        VARIABLE        VARIABLE"
15 PRINT IN IMAGE
"              CALCULATED     DESIRED    ORIFICE         ORIFICE"
16 PRINT IN IMAGE
"  PRESSURE      FLOW         FLOW      DEFLECTION      DEFLECTION"
17 PRINT IN IMAGE
" LBS/SQ.IN.     GPM          GPM         INCHS           INCHS"
18 PRINT IN IMAGE
"  ---------     ------      -------     ----------     ------------"
19 D=.5 ! FIRST VARIABLE ORIFICE ENTRANCE DIAMETER IN INCHS
20 D3=.5 ! SECOND VARIABLE ORIFICE ENTRANCE DIAMETER IN INCHS
30 K=606 ! FIRST VARIABLE ORIFICE SPRING RATE
40 K1=910 ! SECOND VARIABLE ORIFICE SPRING RATE
50 D2=.12 ! DIAMETER OF FIXED ORIFICE IN FIRST VARIABLE ORIFICE
60 D4=0   !     "       "       "      "       "  SECOND      "         "
70 X1=0 ! FIRST VARIABLE ORIFICE PRELOAD IN INCHS
80 X2=.013 ! FIRST VARIABLE ORIFICE STOP-OUT IN INCHS
90 X4=.0095 ! SECOND VARIABLE ORIFICE PRELOAD IN INCHS
95 X5=.025  ! SECOND VARIABLE ORIFICE STOP-OUT IN INCHS
100 FOR P=5 BY 5 TO F
101 A=.785*P
102 B=-(K+1.57*D*P)
103 C=(-K*(X1))+(.785*(D↑2)*P)
110 X=(-B-SQRT((B↑2)-4*A*C))/(2*A)
111 IF X>0 THEN X6=X ELSE X6=0
112 B1=-(K1+1.57*D*P)
113 C1=(-K1*(X4))+(.785*(D↑2)*P)
120 X3=(-B1-SQRT((B1↑2)-4*A*C1))/(2*A)
121 IF X3>0 THEN X7=X3 ELSE X7=0
130 IF X6<X2 THEN Q1=(103*1.11*X6*((2*D)-X6)*SQRT(P))/3.85 ELSE
Q1=(103*1.11*X2*((2*D )-X2)*SQRT(P))/3.85
140 Q2=(103*.785*(D2↑2)*SQRT(P))/3.85
150 IF X7<X5 THEN Q3=(103*1.11*X7*((2*D3)-X7)*SQRT(P))/3.85 ELSE
Q3=(103*1.11*X5*((2*D3)-X5)*SQRT(P))/3.85
160 Q4=(103*.785*(D4↑2)*SQRT(P))/3.85
170 Q=Q1+Q2+Q3+Q4
180 Q5=(  F)*P
185 IF ∴ >X2 THEN X8=X2 ELSE X8=X6
186 IF ∴ >X5 THEN X9=X5 ELSE X9=X7
190 PRINT IN IMAGE
"   ZZZ        ZZ.ZZ        ZZ.ZZ         .ZZZZ           .ZZZZ"
"↑ P, Q, Q5, X8, X9
200 NEXT P
```
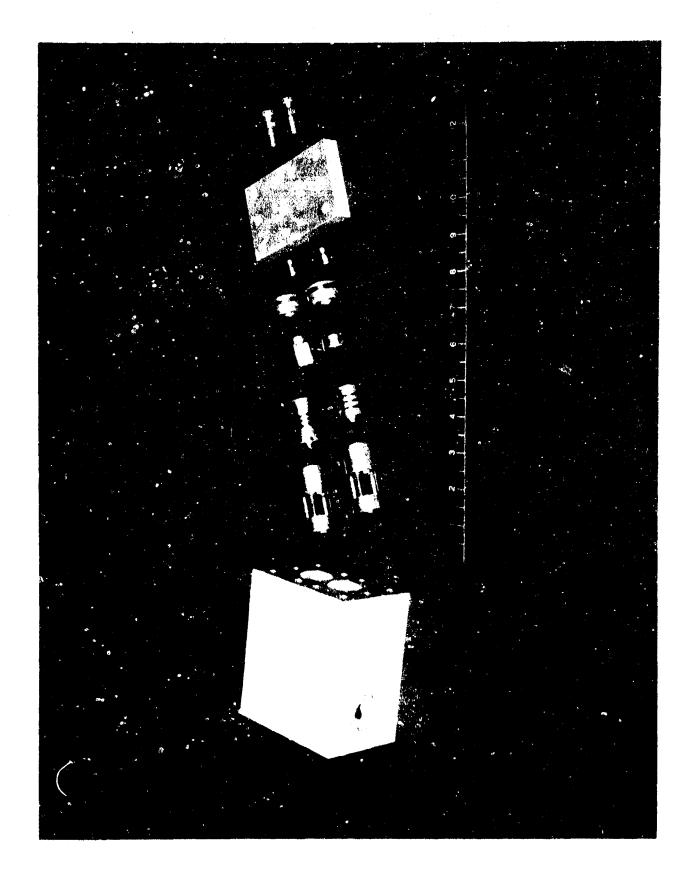
Fig. 74 – Two Stage Variable Orifice

Computer Program

*** COMPUTER PROGRAM TO ANALYTICALLY MODEL THE PRESSURE ***
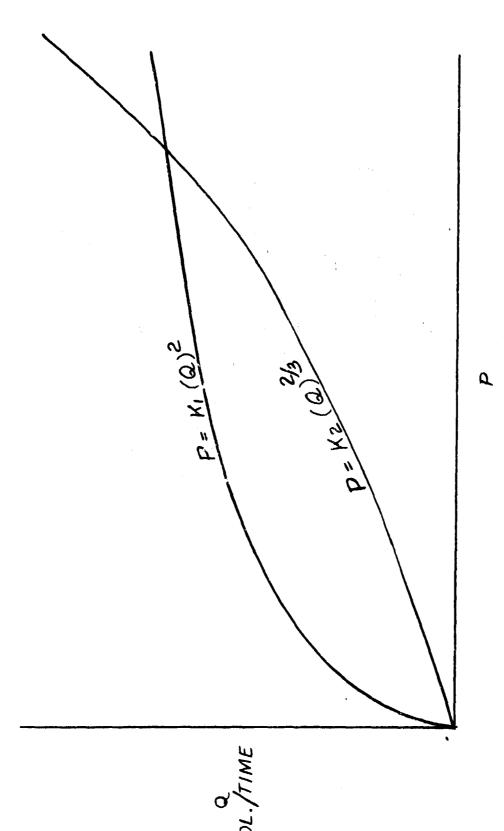VS FLOW RESPONSE OF A TWO STAGE VARIABLE ORIFICE
ASSEMBLY CONTAINING FIXED ORIFICE PARALLEL FLOW PATHS

PRESSURE LBS/SQ.IN.	CALCULATED FLOW GPM	DESIRED FLOW GPM	FIRST VARIABLE ORIFICE DEFLECTION INCHS	SECOND VARIABLE ORIFICE DEFLECTION INCHS
5	.80	.75	.0035	.0000
10	1.45	1.50	.0069	.0000
15	2.15	2.25	.0103	.0000
20	2.91	3.00	.0135	.0000
25	3.70	3.75	.0167	.0000
30	4.54	4.50	.0198	.0000
35	5.41	5.25	.0228	.0000
40	6.10	6.00	.0245	.0000
45	6.72	6.75	.0245	.0013
50	7.43	7.50	.0245	.0030
55	8.16	8.25	.0245	.0046
60	8.90	9.00	.0245	.0063
65	9.64	9.75	.0245	.0079
70	10.40	10.50	.0245	.0095
75	11.16	11.25	.0245	.0111
80	11.93	12.00	.0245	.0126
85	12.71	12.75	.0245	.0142
90	13.49	13.50	.0245	.0157
95	14.28	14.25	.0245	.0172
100	15.08	15.00	.0245	.0187

Fig. 75 - Typical Computer Printout

Fig. 76 - 2 Stage Variable Orifice Assembly

123

a deviation of approximately 2% from the ideal pressure-flow response curve over the 15 GPM range of the device.

The analytical expressions contained within the computer program take into account the reduction in the drive area in each variable orifice poppet as a function of the stroke of the poppet and the change in the constriction area in the orifice assembly as a function of the stroke of the poppet. Fig.77 is a plot of the ideal pressure-flow response versus the calculated and actual measured pressure-flow response of the evaluation hardware.

A major achievement of the program was the development of the machined spring concept clearly illustrated in the test hardware shown in Fig. 76. The machined springs permit an accurate and readily reproducible spring rate to be attained. This is accomplished by control of the rectangular cross-sectional area formed by machining a groove through the cylindrical wall of the poppet body. Furthermore, the machined spring may be modified to reduce the effective spring rate by increasing the internal diameter of the spring or cylindrical cavity.

The machined spring concept also avoids the problem related to the inability of the spring manufacturer to close the end coils of a normal wound spring. The problem exists when an opening in the end coil of a ground spring end termination results in that coil acting in an active manner. This causes a significant lowering of the effective spring rate until the small clearance gap is closed as a result of the application of load. Another important salient characteristic of the machined spring is the fact that the outside diameter and concentricity of the machined spring can be accurately maintained. A hand wound spring has considerable deviation in both concentricity and O.D. or outside diameter variance for each wound coil. Therefore, the machined spring may be more closely fitted to a supporting sleeve than would be possible with a normal hand or machine wound spring.

Electronic Linearization

In this concept the flow developed differential pressure signal which is proportional to the square of the flow rate times a numerical constant is sensed by a differential pressure transducer and converted into an electrical signal which may be shaped to produce the desired linear output.

124
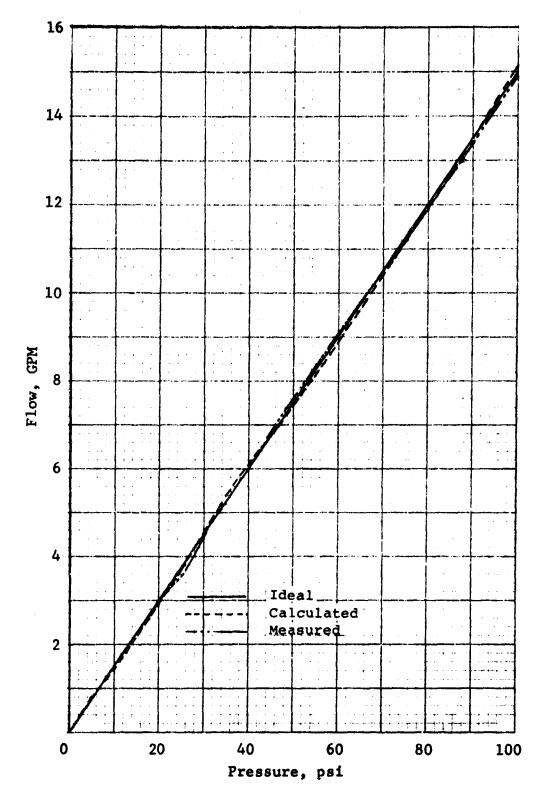
Fig. 77 - P-Q Comparison Curves

The various electronic schemes which could be utilized to extract the square root of the differential pressure signal were analyzed for linearity, accuracy, hysteresis, and resolution. Upon completion of this trade off study, the square root circuit shown in Fig.78 was selected for this application. This circuit utilizes a four quadrant multiplier in the feedback loop of a standard operational amplifier. The input of the circuit is a high level negative going signal derived from the differential pressure signal across a fixed orifice assembly in the supply or return line. The nominal output of the circuit is equal to the square root of 10 times the input. However, the input to the circuit includes a 1/10 voltage divider which causes the output of the circuit to be equal to the square root of the input. A four quadrant multiplier multiplies the output signal by itself which results in a positive going input signal to effectively cancel the input and close the control loop. Thus, the inputs to the quarter square multiplier are two signals equivalent to the square root of the input signal to the circuit (the square root of x). The output of the multiplier is equal to the multiplican divided by 10. Since this output has a positive polarity, it effectively cancels the negative input to the square root network as required for proper circuit operation.

The electronic square root circuit shown in Fig.78 was implemented in the hardware form using commercial integrated circuit modules shown in Fig.79B. Although only two active devices are illustrated in the square root circuit shown in Fig.79B a third active element was included in the actual hardware to provide the capacity to scale the input or output signal as required for proper circuit interfacing. Subsequent tests revealed that this module was not necessary for proper operation of this circuit. Fig.79A also illustrates the hardware form of the variable detection level and time delay network with solenoid valve driver and latching circuit shown in Fig. 80. This circuit compares the linearized differential pressure signal which is proportional to flow rate to a fixed reference signal. For demonstration purposes, this was made analagous to the signal which may be developed by a similar flow sensing element installed in the other line of the branch actuation subsystem.

The two electrical signals thus developed are electronically compared by an open loop operational amplifier module which switches to the high level (+) state when the incoming differential pressure signal exceeds the reference signal by approximately

Fig. 78 - Square Root Circuit

127

B - Multiplier Board

A - Detection Circuit

Fig. 79

128
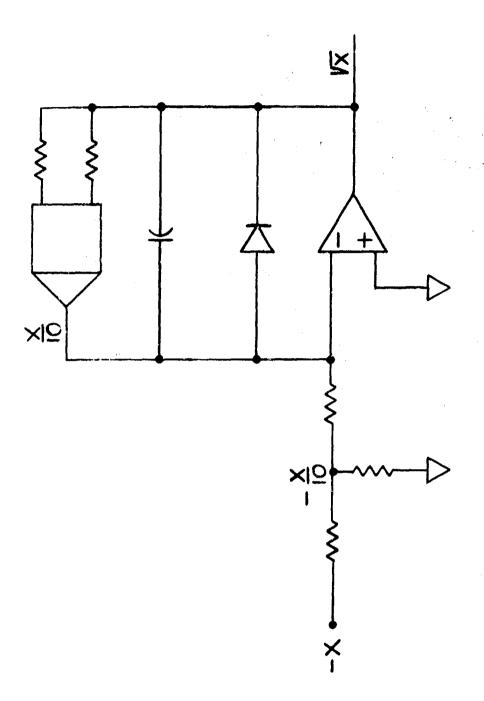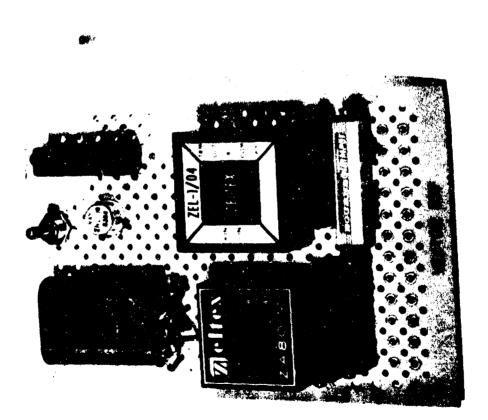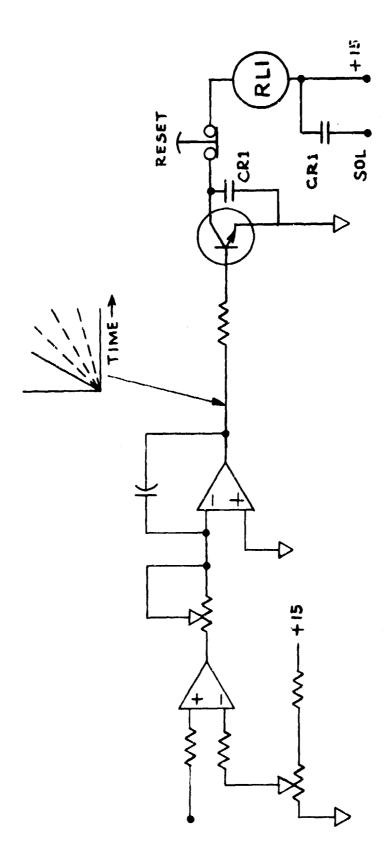
Fig. 80 – Detection Level Circuit

129
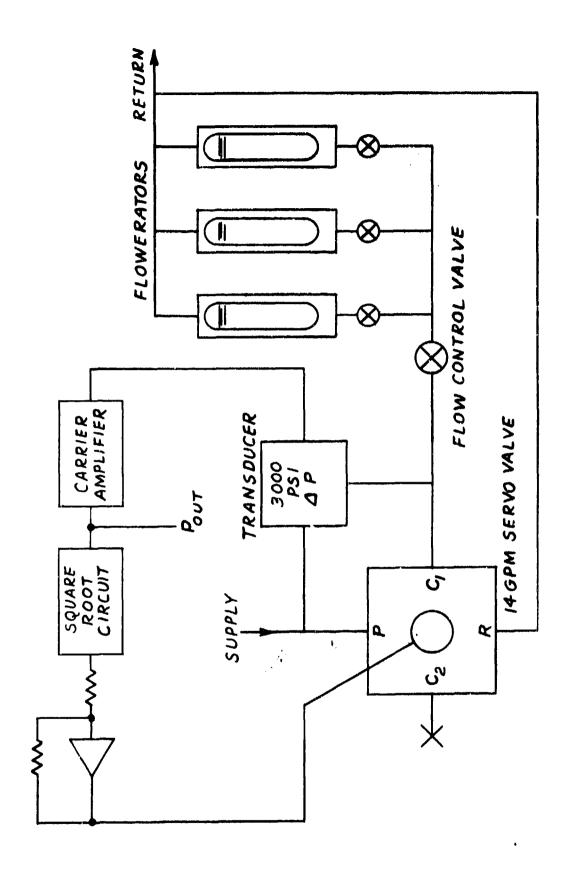
Fig. 81 - Test Schematic

20 millivolts. This high level step signal is applied as an input to a free-running integrator network which produces a ramp function proportional to the RC time constant of the network. In this circuit the time constant was designed to be adjusted over a range of 10 - 100 milliseconds.

The positive going ramp function is applied as an input to an NPN transistor amplifier which will cause a relay to be energized when the current through the transistor approaches a saturation current of the relay coil. The relay is self watching around the transistor and a second normally open contact provides a high level signal to operate a shutdown valve in the supply line of the branch actuator subsystem.

The two plug in cards containing the square root module and the level detection and shutdown logic circuitry were mounted on a chassis containing ± 15 volt supplies and the necessary input potentiometers to provide reference signals to test the associated circuitry.

A fixed orifice was sized to yield a differential pressure of 100 psi for a flow rate of 15 GPM. This fixed orifice was inserted in a test block and a differential pressure gauge and reluctance type differential pressure transducer were connected across the fixed orifice. This produced a visual indication of the developed differential pressure and an electrical signal which would be used as an input for the square root module. The output of the differential pressure transducer was applied to a transistorized carrier amplifier which yielded a full scale output of 10 volts at 100 psi.

Fig. 81 is a hydraulic schematic of the electronic square root test stand. The flow passes through a shutdown solenoid valve, the flow test block containing the fixed orifice and the flow control valve and a series of flow rater instruments to monitor the fluid flow. A leak simulation solenoid valve was inserted in a "T" in the line immediately downstream of the test block. The valve solenoid was connected to a 28 volt DC source and a normally open switch to permit a leak to be simulated when the solenoid was energized.

The initial analysis of the square root circuit was conducted utilizing a variable DC input voltage which could be accurately set to a known level. The output was monitored with a

131

differential volt meter and compared to the calculated actual
square root of the input to determine the error of the electro-
nic computation. The following data set is a result of this
analysis.

Input	Actual	Output	Error
1.011	1.0049	1.020	+.015
2.008	1.4142	1.423	+.009
2.991	1.7291	1.732	+.004
4.000	2.0000	2.002	+.002
4.994	2.2338	2.235	+.0012
6.007	2.4490	2.451	+.002
6.990	2.6438	2.642	-.0018
8.015	2.8284	2.829	+.0006
8.957	2.9933	2.992	-.0013
10.024	3.1654	3.165	-.004
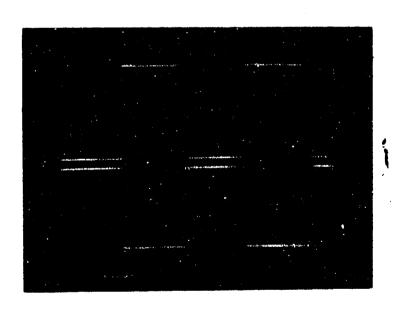
The maximum error in the output of the square root circuit
was equal to 1.5% of the lowest output level or less than 1/2
of 1% of the full scale output. It is also important to note
that the input to the actual square root circuit was reduced
to 1/10 of the initial value. Therefore, the range of signal
level applied to the actual input to the circuit is 0.1 to 1.0
volts, verifying that the circuit will function with very small
inputs. Furthermore, if the full flow range of the instrument
is 0 - 15 GPM and this flow range is represented by a zero error
signal from the pressure transducer of 0 - 10 volts, this square
root network should be capable of an ultimate detection level
of less than 0.15 GPM on a flow comparison basis.

Dynamic operating characteristics of the square root net-
work were investigated, observing the input to output relation-
ship of the square root network when it was subjected to a series
of electrical inputs which varied in frequency, amplitude, and
wave shape. The results of this investigation are shown in Fig.
32 through 87. In each case, the upper trace is the input and
the lower trace is the output of the square root circuit.

The top photograph of Fig. 82 illustrates the input-output
relationship of the square root circuit with a square wave input

132

Input   18V PK-PK @ 1000Hz
Output   3V PK-PK @ 1000Hz

Input   18V PK-PK @ 100Hz
Output   3V PK-PK @ 100Hz

Fig. 82 - Dynamic Characteristics of Square Root Network

at a frequency of 1000 Hz. In this illustration and in all sub-
sequent illustrations, the output of the square root circuit as
shown by the lower trace will remain at some value slightly be-
low the zero reference level until the input crosses the zero
reference level and begins the negative excursion of the wave-
form. The output is determined by the negative half of the peak
to peak value of the applied input.

In this illustration, the input is equal to an amplitude
of -9 volts peak and the resulting output is equal to the square
root of the input or 3 volts peak. The slight excursion of the
output signal below the zero reference axis in the result of
the clamping action of a diode which is positioned between the
input and the output of the forward loop operational amplifier.
It prevents the circuit from locking up or saturating in the
event that a positive input signal is applied.

The diode around the forward loop operational amplifier
cannot clamp the positive inputs to the zero reference because
there is a small forward voltage drop associated with germanium
or silicon diodes. A germanium diode having a forward voltage
drop of approximately 2/10 of a volt was selected for this ap-
plication. Therefore, a 2/10 of a volt negative excursion below
the zero reference axis for the output signal will occur due to
the nominal conversion characteristics of the square root cir-
cuitry.

The lower photograph of Fig. 32 illustrates the input-
output relationship of the square root circuit when it is sub-
jected to a ± 9 volt peak 100 Hz square wave signal. It is im-
portant to note that the leading and trailing edge and slopes
and the rounding of the leading edge corner of the first scope
tracing is not evident in this illustration. Furthermore, the
output is once again equal to the square root of the negative
peak value of the input signal or 3 volts.

Fig. 83 illustrates the input-output relationship of the
square root circuit for an 18 volt peak to peak triangular wave
and sine wave. The action of the square root circuit is very
evident in the output waveform. The output is the square root
of the negative excursion of the 18 volt peak to peak input sig-
nal.

Fig. 84 and 85 are essentially duplicates of Fig. 82 in
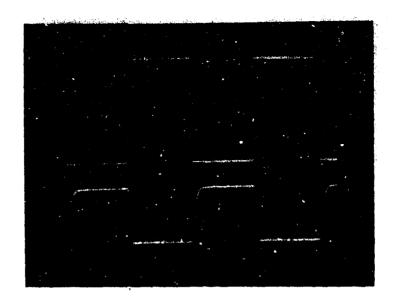
Input   18V PK-PK @ 100Hz
Output   3V PK-PK @ 100Hz
(Triangle Wave Form)
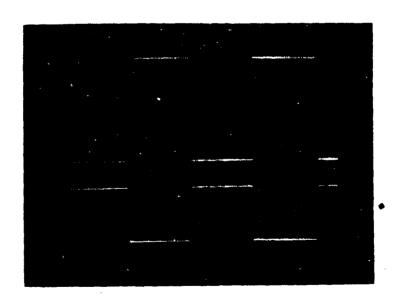
Input   18V PK-PK @ 100Hz
Output   3V PK-PK @ 100Hz
(Sine Wave Form)

Fig. 83 - Sq. Root Network Response to Sine & Triangular Waves
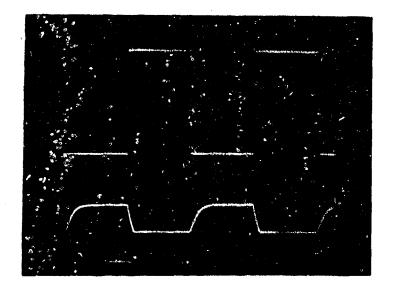
Input   8V PK-PK @ 1000Hz
Output   2V PK-PK @ 1000Hz
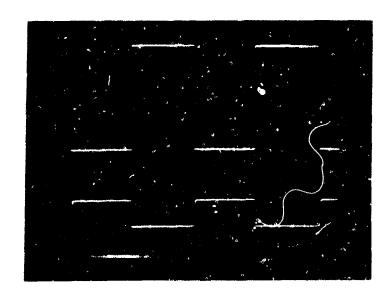
Input   8V PK-PK @ 100Hz
Output   2V PK-PK @ 100Hz

Fig. 84 - Sq. Root Network Response - Medium Amplitude

Input   2V PK-PK @ 1000Hz
Output   1V PK-PK @ 1000Hz

Input   2V PK-PK @ 100Hz
Output   1V PK-PK @ 100Hz

Fig. 85 - Sq. Root Network Response - Small Amplitude

regard to the test frequency and waveform. However, the peak to peak amplitude for Fig. 84 is 8 volts and for Fig. 85 the peak to peak input is 2 volts. Therefore, the output of the square root circuit for the inputs utilized in Fig. 84 is 2 volts peak, and the output for the inputs used in Fig. 85 is 1 volt peak.
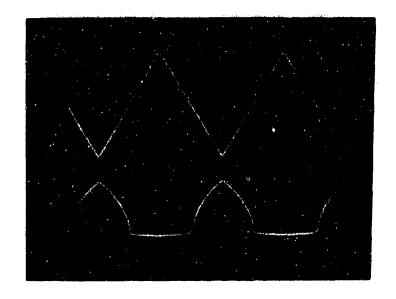
Fig. 86 and 87 are duplicates of Fig. 83 in regard to the frequency and waveform of the input signal. The peak to peak amplitude of the input signal for Fig. 86 is 8 volts and the resulting output is equal to 2 volts peak and the peak to peak input for Fig. 87 is 1 volt and the resulting output is 1 volt peak.

The final test of the electronic square root system or circuit was to determine the overall pressure-flow characteristic of the flow sensor formed by connecting the fixed orifice output to the square root circuit. Fig. 88 illustrates the results of this test. It may be observed that excellent linearity has been achieved over the flow range of 0.375 to 14 GPM. Subsequent analysis of these results indicated that the non-linearity in the high flow range was due to a flow saturation phenomenon within the test block. This phenomenon was verified by observing that the developed differential pressure that exists across the fixed orifice was approximately 5% high at the 15 GPM operating point.
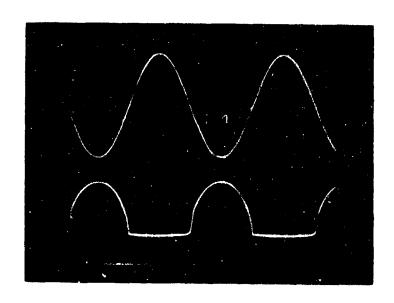
The non-linearity below 0.375 GPM was attributed to the improper performance of the square root circuit at this very low input level. The full scale output of the circuit is 10 volts at 15 GPM, while the output signal at a flow rate of 0.375 GPM is 0.250 volts. This means the square root circuit was actually operating with an input of less than 62 millivolts from the pressure transducer.

Subsequent analysis of the square root circuit with inputs ranging from 50 - 100 millivolts did verify that the electronic circuit is not capable of true square root performance with an input level of less than 75 millivolts.

The output from the fixed orifice flow sensor was applied to the electronic circuitry to demonstrate the ability to detect a small difference in the flows from two such flow sensors installed in the pressure and return lines of an actuator subsystem.
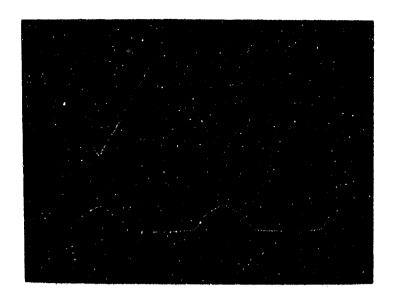
Input   8V PK-PK @ 100Hz
Output   2V PK-PK @ 100Hz
(Triangle Wave Form)
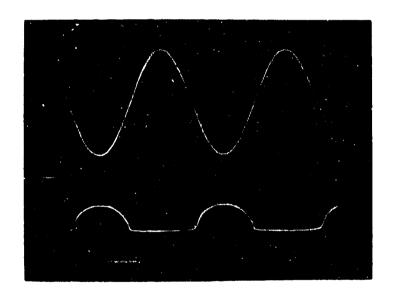
Input   8V PK-PK @ 100Hz
Output   2V PK-PK @ 100Hz
(Sine Wave Form)

Fig. 86 - Sq. Root Sine & Triangular Response - Medium Signal Level

139

Input   2V PK-PK @ 100Hz
Output 1V PK-PK @ 100Hz
(Triangle Wave Form)

Input   2V PK-PK @ 100Hz
Output 1V PK-PK @ 100Hz
(Sine Wave Form)

Fig. 87 - Sq. Root Sine & Triangular Response - Small Signal Level

140
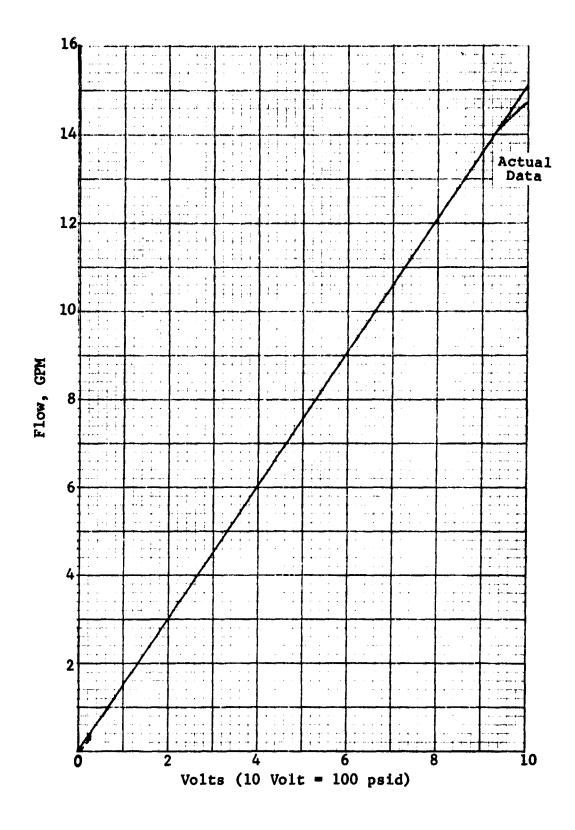
Fig. 88 - P-Q Curve - Electronic Sq. Root Device

141

The electrical signals are analagous to a relative leakage rate or flow imbalance between the pressure and return lines.

The electronic comparator circuit was capable of detecting a voltage difference signal equal to 0.03 GPM (10 volts at 15 GPM). The comparator circuit would switch to the high state any time the input from the square root circuit exceeded the fixed reference setting by 20 millivolts.

This detection level is obviously impractical for any conceived linearization technique that may be developed in the near future. However, it is a fairly simply matter to provide an adjustable deadband of 0.1 - 0.25 GPM to insure that the hydraulic branch isolation device that may result in the implementation of these techniques will not shutdown inadvertently under transient flow conditions.

The output from the detection level comparator circuit was measured as $\pm$ 11.7 volts with a supply voltage of $\pm$ 15 volts. The free running integrator was adjustable over a range of 10 milliseconds to 92 milliseconds. In other words, the output of the free running integrator would reach the saturated condition after a time delay of 10 - 92 milliseconds depending on the setting of the input potentiometer.

The transistor amplifier (relay driver) effectively disregards the negative input from the free running integrator which only causes the amplifier to be driven further into the cut-off region. However, positive going excursions of the free running integrator will cause the amplifier to pull in the relay when the input to the transistor amplifier exceeds a level of approximately 9 volts established by the current limiter resistor in the base lead of the amplifier.

In general the operation of the circuit was exactly as anticipated. The variable time delay of 10 - 90+ milliseconds should be adequate to prevent the leak detection circuitry from initiating a false shutdown due to transient flows or transmission lines phenomena within the branch actuator hydraulic system.

Active Orifice Techniques

As originally conceived, the active orifice technique would act as a remotely adjustable spring rate for a variable

142
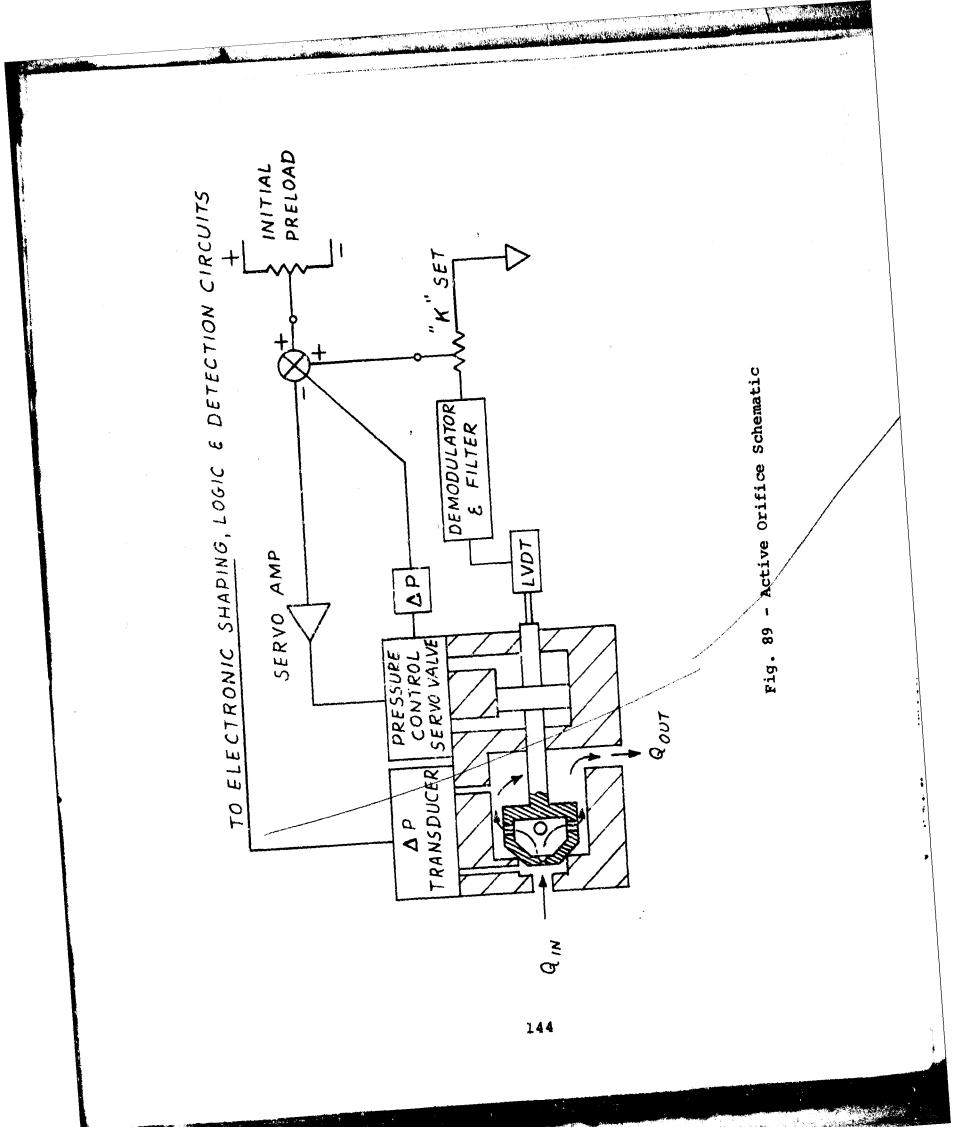
orifice assembly. The variable spring rate effect would be achieved by varying the effective static stiffness of a very small drive area actuator as shown in Fig. 89. The flow developed forces related to the variable orifice seat diameter and the differential pressure across the variable orifice cause the small drive actuator to be displaced away from the seat in proportion to the gain of the position loop. The position loop in turn provides a command input to the pressure control loop which, therefore, creates a linearly increasing pressure or load as a function of the position of the variable orifice poppet.

The active orifice technique was determined to be too expensive for practical purposes. The system was originally conceived to eliminate many of the problems associated with machined or hand wound springs such as lack of ability to close and grind square the end coils of the spring, etc. However, the introduction of the machined spring concept eliminated many of these problem areas. Therefore, the active orifice technique was abandoned in favor of the hydromechanical linearization technique previously discussed in this section of this report.

Square Root Linkage

This concept is based on the relationship that the flow rate through any sharp edge orifice is equal to the discharge area multiplied by a numerical constant and the square root of the differential pressure. To obtain a linear relationship between the flow rate and the differential pressure, it is necessary to remove the differential pressure from under the radical in the analytical expression. This may be accomplished by making the area proportional to the square root of the differential pressure.

The mechanism shown in Fig. 90 was conceived as a technique that could be utilized to cause the discharge area of the variable orifice to vary as a function of the square root of the flow developed differential pressure. In this technique, the pressure is converted to a displacement which is directly proportional to the applied differential pressure. This displacement is then transformed by the square root linkage. The output of the square root linkage restrains the orifice poppet in a manner to cause the displacement of the variable orifice to be linearly related to the flow developed differential pressure. Thus, the pressure-flow response of this mechanism would be linear throughout the design flow range.

143

Fig. 89 - Active Orifice Schematic

144
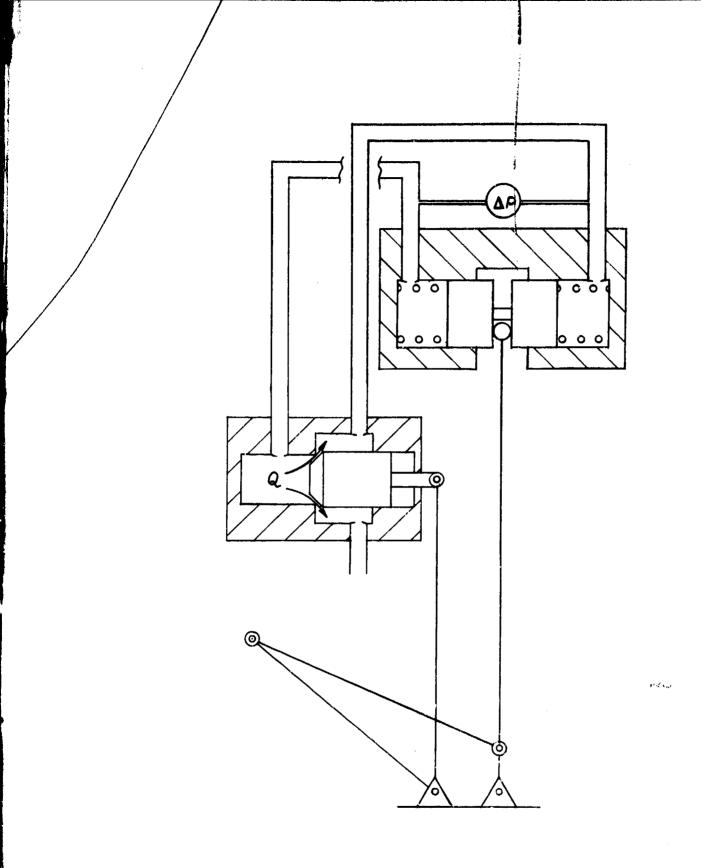
Fig. 90 -- Sq. Root Linkage

A mechanization design analysis was undertaken and evolved to the point that it was determined that the basic square root linkage could be fabricated from one solid piece of material utilizing flexure pivots to provide the limited motion at the linkage pivot points. Furthermore, a force analysis revealed that the stiffness or mechanical compliance of the linkage members could be maintained at a sufficiently high level to prevent errors caused by flexure of the linkage members.
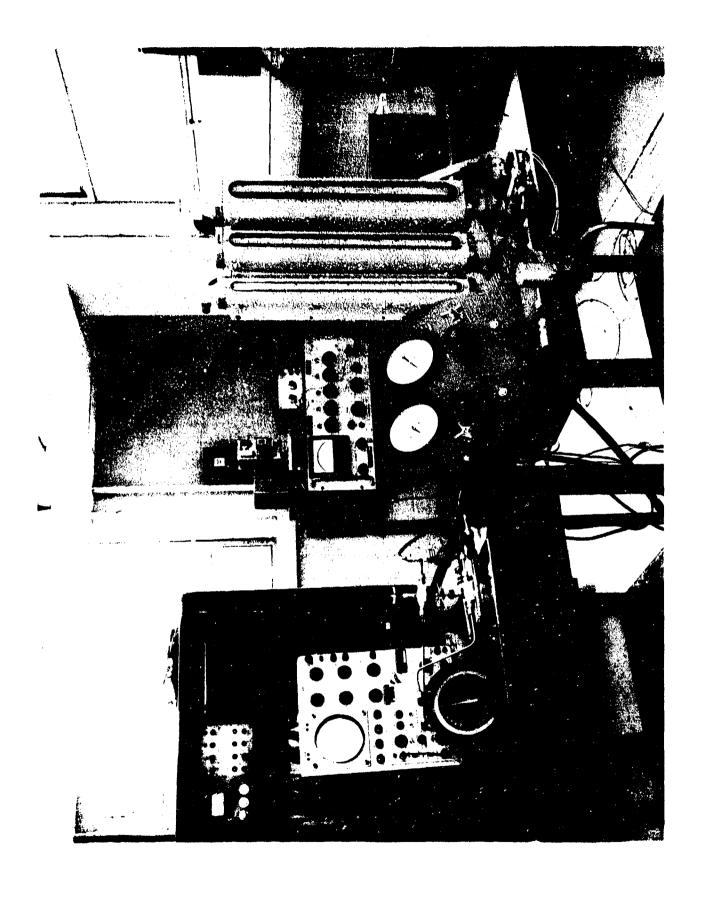
It was decided to perform a simulation of the square root linkage by utilizing hardware previously created for the electronic square root linearization technique.

Fig. 91 is a photograph of the square root linkage simulation test setup. A flow control servovalve provided the variable orifice characteristic by utilizing the variable orifice between the pressure and the C_1 cylinder port. The C_2 port was capped and the return port was connected downstream of the flow instrumentation such that only the flow through pressure to the C_1 port was measured. The flow developed pressure drop was sensed with a reluctance type differential pressure transducer. A high level (10 volt) electrical signal from the demodulator was applied to the square root circuit shown in Fig. 78 of this report.

The output of the square root circuit represents an electrical signal linearly proportional to the flow through the pressure and C_1 ports of the servovalve. This voltage was applied as an input to an amplifier which drives the torque motor of the servovalve. The amplifier is phased to open the servovalve and reduce the developed differential pressure. A 3000 psi differential pressure transducer was used for the square root linkage simulation test setup, since it is exposed to system pressure at zero flow.

Fig. 92 is an illustration of the pressure-flow response of this control system with the servoamplifier gain adjusted to produce 1000 psi across the P and C_1 ports of the servovalve at 14 GPM.

The results indicate that the pressure-flow response is very linear from approximately 0.4 GPM to 12 GPM. At flow rates below 0.4 GPM, the electrical signal developed by the differential pressure transducer is too low for proper operation of the

Fig. 91 - Sq. Root Linkage Simulation Test Set-up

147
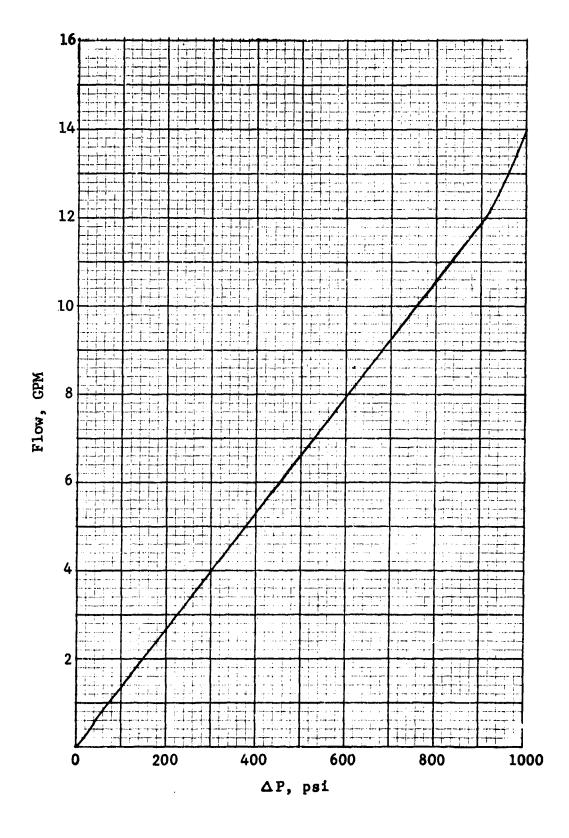
Fig. 92 - P-Q Curve for Simulated Sq. Root Linkage

148

square root circuit. The rise in the pressure-flow response
curve above 12 GPM was attributed to a flow saturation pheno-
menon in the servovalve.

Additional tests were conducted in which the flow con-
trol valve was set for a given nominal flow rate. The valve
upstream of the flow instrumentation was shut off and then
rapidly reopened to cause a flow surge in the test system.
The output of the carrier amplifier was monitored to determine
if any overshoot or significant instability exists in the con-
trol loop. The output exhibited the expected undershoot typi-
cal of a low loop gain.

Non-Linear Spring

The non-linear spring was conceived as a technique to li-
nearize the pressure-flow response of a variable orifice. To
obtain a linear pressure-flow response from a variable orifice
assembly, the discharge area should be made to vary in propor-
tion to the square root of the differential pressure. To ac-
complish this, the displacement may be made to vary in propor-
tion to the square root of the force developed against the spring.
Ref. 2 presents the derivation of the stated functional rela-
tionship.

The mechanization illustrated in Fig.93 was proposed as
a means of obtaining the desired non-linear spring effect. In
this approach a constant strength cantilever beam effectively
changes in length as a function of the stroke of the poppet.
This causes an increased stiffness or increased force propor-
tional to the square of the poppet deflection. The change in
the effective length of the cantilever beam is effected by a
cam surface which is asymptotic with the base of the beam at the
beam restraint. It is contoured to cause the beam to increase
in stiffness as a result of the decrease in the effective free
length of the beam.

An initial analytical evaluation of this technique dis-
closed that the cantilever beam must be of a constant strength
design in which the section properties of the beam vary in pro-
portion to the bending moment of the nominal cantilever beam.
This results in a constant strain or stress throughout the length
of the beam. The laboratory test fixture shown in Fig. 94 was
developed for a laboratory evaluation of this mechanization. A

149
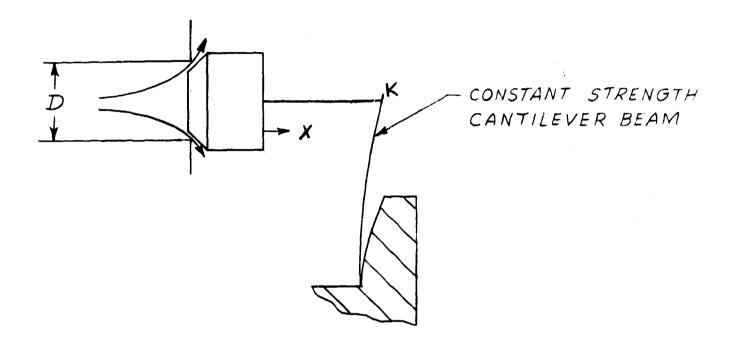
Fig. 93 - Non-Linear Spring
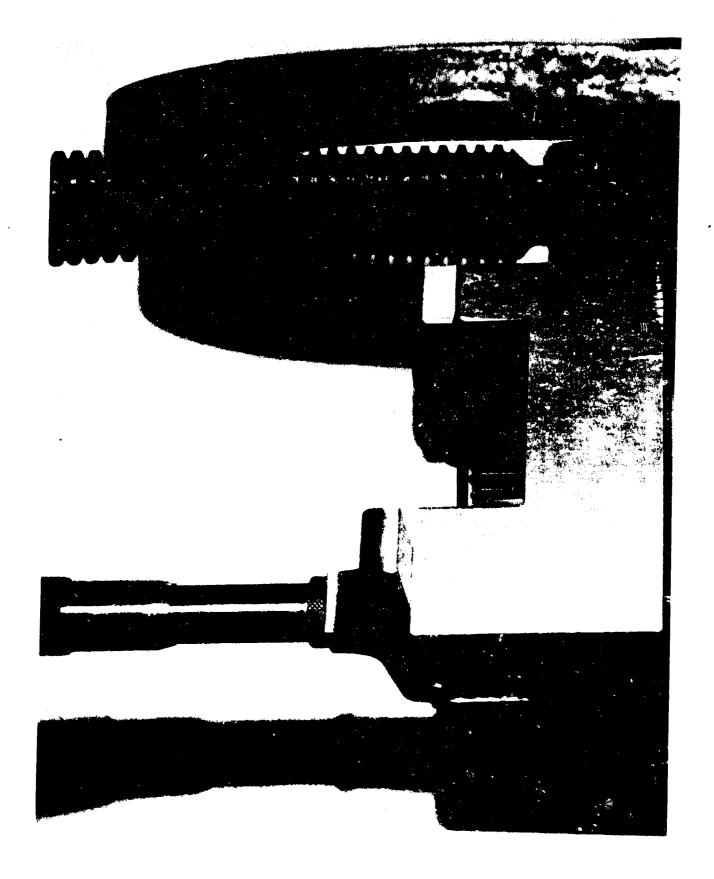
Fig. 94 - Photograph of Non Linear Spring

constant strength beam which would create a load of approximately
10 pounds at the desired deflection was clamped in a holding fix-
ture. Incremental loads were applied to the end of the beam by
attaching them to a cable suspended through a hole in the end
of the beam and terminated with a half-round cable end swaged
into position. In this manner the cable would not transmit a
torque to the end of the cantilever beam as the beam was deflec-
ted by application of the loads. The flattened top of the cable
termination was utilized as a reference point for the measure-
ment of the deflection of the beam relative to the top of the
enclosure which encircles the end of the beam.

The cam surface was formed by a series of linearly spaced
small rounded end screws. The screws were spaced at equal dis-
tances along the last 1/3 of the length of the beam prior to the
point at which the beam is restrained in the fixture.

The beam deflection of 0.0316 inches at 10 pounds was se-
lected for this evaluation. The deflections corresponding to
the loads ranging from 0.1 - 10 pounds were then calculated with
the analytical expression that the beam deflection is propor-
tional to the square root of applied force. The beam was then
incrementally loaded with known weights and the cam screws were
adjusted from the point nearest the point of clamping of the
beam and proceeding towards the front of the beam until the de-
sired deflection relating to a given load was obtained. Fig. 95
presents the results of this evaluation.

Fig. 95 illustrates that the beam deflection was propor-
tional to the square root of applied load over the range of 1.0
to 10.0 pounds. As anticipated, it was possible to adjust each
cam screw only one time to achieve a given loading condition.
In other words, each screw was individually adjusted beginning
with the screw nearest the end restraint of the beam and proceed-
ing toward the front of the beam until the desired cam curve was
obtained. Once the proper cam curvature was established, it was
possible to flex the beam back and forth without any necessity
of readjusting.

The discontinuity shown in Fig. 95 in the region from 0 -
1 pound of applied force per load is caused by the fact that the
square root of numbers less than 1 results in a larger number.
Therefore, while it was possible to set the cam curvature to
produce the desired relationship from 0 - 1 pound, it was not
possible to adjust over the whole range resulting in a dis-
continuity.
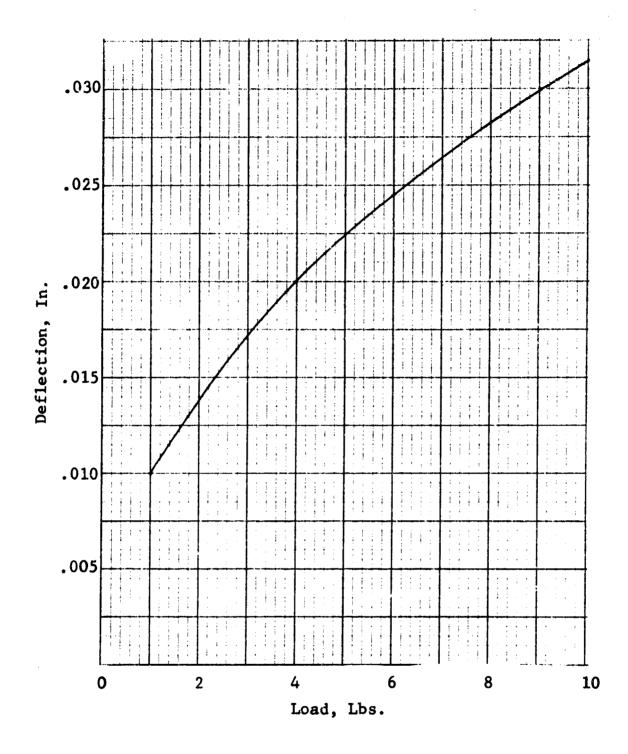
Fig. 95 - Constant Stress Beam Deflection

RECOMMENDATIONS

It is recommended that the hydromechanical linearization technique and the electronic linearization technique be concurrently evaluated by constructing a flow difference sensor utilizing each technique. Each flow difference sensor thus created should be designed utilizing the latest state-of-the-art techniques to achieve a detection level ranging from 0.25 GPM to 0.5 GPM.

The performance characteristics of each flow difference sensor mechanization should be thoroughly evaluated and each device should be subjected to a flight qualification test schedule.

It is recommended that a second breadboard version of electronic flow difference sensor be fabricated for use as a working test bed. To enhance the effectiveness of the flow difference sensor, it would be desirable to provide an automatically variable detection level which would increase in proportion to the flow of fluid through the device. Thus, at variable flow rates or under quiescent operating conditions, the sensor would exhibit maximum sensitivity and would be capable of detecting leaks in the neighborhood of 0.25 to 0.5 GPM.

It would be desirable to develop a flow difference sensor mechanization which did not require an inherent time delay system to provide for transient flow or delay line phenomena. It is recommended that logic techniques be investigated to prevent the device from operating until the pressure and return flows are fully developed and determined to be at the proper ratio for nominal operation of the system. This logic network may be incorporated as part of the detection level network or as a separate system which would operate each time the flow was reduced to the quiescent levels.

It is recommended that a hybrid hydromechanical-electrical technique be considered which would electronically linearize the nominal pressure-flow relationship. The differential pressure would be nominally equal to the 2/3 power of the flow rate through the variable orifice assembly multiplied by some numerical constant. If the square root of this signal is extracted

154

and summed with the initial signal, the resulting output will
be linearly related to the flow rate through the device. Again
it is recommended that this technique be implemented or simulated
on an electronic basis for initial evaluation.

The differential pressure signal from the normal variable
orifice assembly does not exhibit as low signal levels at low
flow rates as with a normal fixed orifice curve. Instead, the
effective pressure gain of the variable orifice assembly is high
at low flow rates, enhancing the resolution of the pressure trans-
ducer.

It is also recommended that consideration be given to se-
parating the pressure and return portions of any flow difference
sensor in such a manner that the individual flow sensors may be
inserted in pressure and return lines which are not necessarily
in close proximity. This packaging concept would also aid the
installation of the hardware in the aircraft system, since it
would reduce the size of the individual flow sensor and logic
packages necessary to create a flow difference sensor.

The pressure side or supply line flow sensor and the nec-
essary valve closure mechanism to occlude the supply line may
be included in one package and the return side flow sensor out-
put may be hydraulically or electronically coupled to the pres-
sure side mechanism.

SECTION V

SUPPLEMENTARY EVALUATION OF AN INTEGRATED

SERVOPUMP ACTUATOR PACKAGE

INTRODUCTION

The objective of the tests discussed in this section of the report was to supplement those conducted by Vickers, Inc. on an integrated servopump actuator package. It was fabricated under Air Force contract F33615-70-C-1088 entitled "Research and Study on Application of the Feasibility of Servopump to an Integrated Servoactuator Package." The actuator was designed to satisfy the following nominal F4 stabilator actuator performance criteria:

1. Actuator area: $A3 = 5.890$ sq. inch for retract motion, $A4 = 6.189$ sq. inch for extend motion

2. Total actuator stroke = 10.5 inches

3. Maximum slew rate = 8.6 inches/second

4. System pressure = 2200 psi maximum

5. Electrical input power, 3-phase, 208 volts, 400 cps

The package is shown installed in the FGL load test system in Fig.96 and 97. It is a self-contained integrated actuator incorporating an electrical motor servopump, reservoir, position feedback transducer, wobble plate position feedback transducer and servovalves for wobble plate actuator positioning. The pump is a variable displacement piston pump with the variable displacement controlled by a wobble plate or yoke actuator. An auxiliary pump is connected to the electric motor drive shaft and supplies pressure for operation of the servovalve. This is shown in the Vickers servopump schematic of Fig.98. A detailed description of the unit may be found in Technical Report AFFDL-TR-71-19 , "Research and Feasibility of an Integrated Servopump Actuator for Aircraft Flight Control" by K.F. Becker and M.F. Pedersen, Vickers, Inc.

PROCEDURE

Vickers Integrated Servopump

The test actuator was mounted in the FGL load test fixture
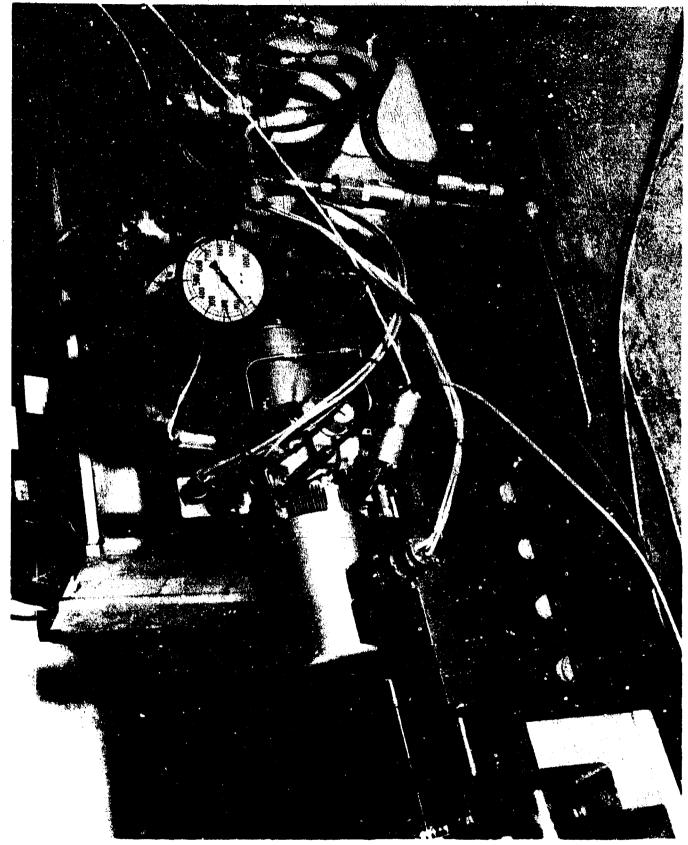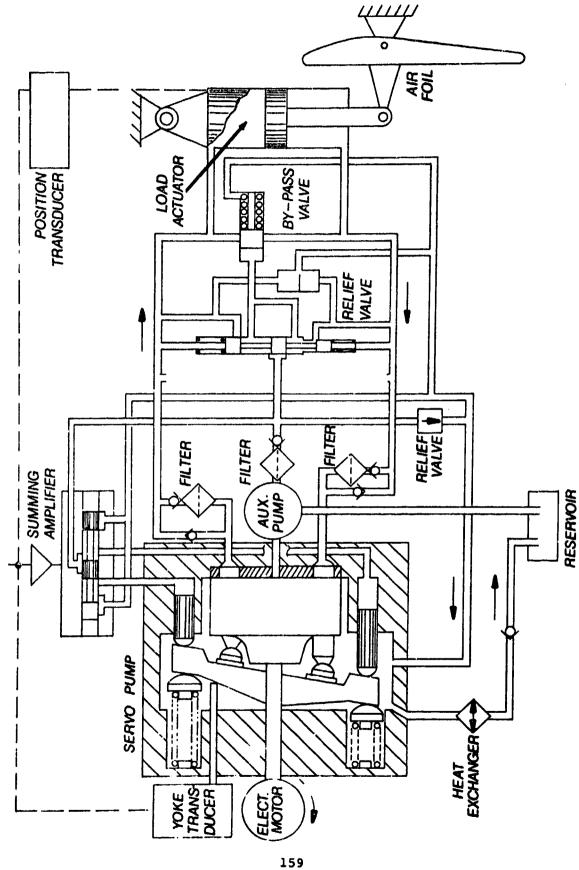
Figure 96 FGL Load Test System

157

Figure 97 - Vickers Integrated Servopump in FGL Load Stand

Figure 98 Vickers Integrated Servopump Actuator Schematic

159

and positioned so that mid-stroke of the actuator (null position) corresponded to the null position of the load system. Meters were installed at the input of the servopump motor in order to monitor power factor, voltage, and current on a continuous basis. A thermocouple was installed in the fluid chamber to allow continuous monitoring of oil temperature. The thermocouple was connected to a Brown recorder. A reservoir pressure gauge and auxiliary pump supply pressure gauge were connected. A pressure transducer was connected to each side of the actuator piston and pressure was recorded on an 8-channel Brush recorder. Limit switches were installed such that when actuator stroke exceeded $\pm$ 4.75 inches from null, the motor was shut down.

The main ram LVDT was excited by a 28 volt, 400 Hz supply. The output was demodulated and filtered by an active filter which exhibited no amplitude attenuation up to 50 cps and 20° phase shift up to 15 cps. The yoke RVDT was excited by a 5 kilocycle signal. Its output was demodulated and filtered by a second order lag network with break frequency at 340 cps. The demodulated actuator rod position and servopump yoke position signals were summed in an operational amplifier whose output was connected to the servovalve. This closed loop system is shown in the block diagram of Fig., 100.

The yoke and actuator loop gains used by Vickers in their tests were not available. It was, therefore, necessary to set amplifier gains by curve matching. The Vickers data is shown reproduced in Fig. 101 and 102 for the .5% and 5% amplitude command signals respectively. The corresponding data obtained by HR&M in the current series of tests utilizing the amplifier gains shown in the block diagram of Fig. 99 are presented in Fig. 103 These plots were for the unloaded actuator. The Vickers data was for an actuator with a spring load. The level of loading was considered to be negligible and, as can be seen, correlation is adequate. A no load slew rate of the actuator was then conducted to compare with the previously established value for validation of the results.

The loading cylinder was connected in a closed loop fashion using ΔP feedback as shown in the block diagram of Fig. 104. It was then possible to program any desired loading condition to the servopump. The static stiffness and dynamic stiffness of the actuator were then determined as described in the detailed test procedure shown in the Appendix of this report. This first series of tests employed MIL H 5606 hydraulic fluid. Upon completion of the series, the actuator was drained and refilled with

160
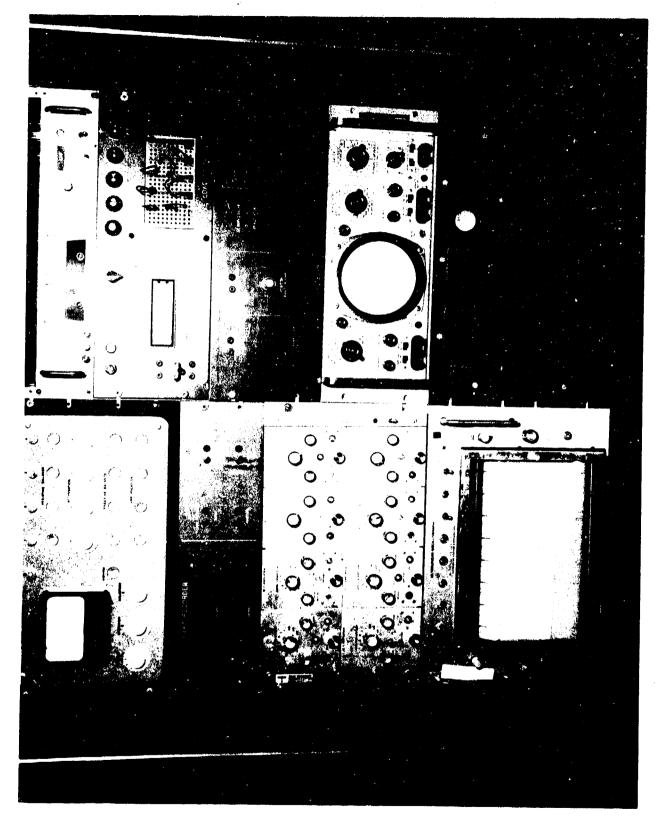
Figure 99 Instrument and Control Console - FGL Load Test System

161
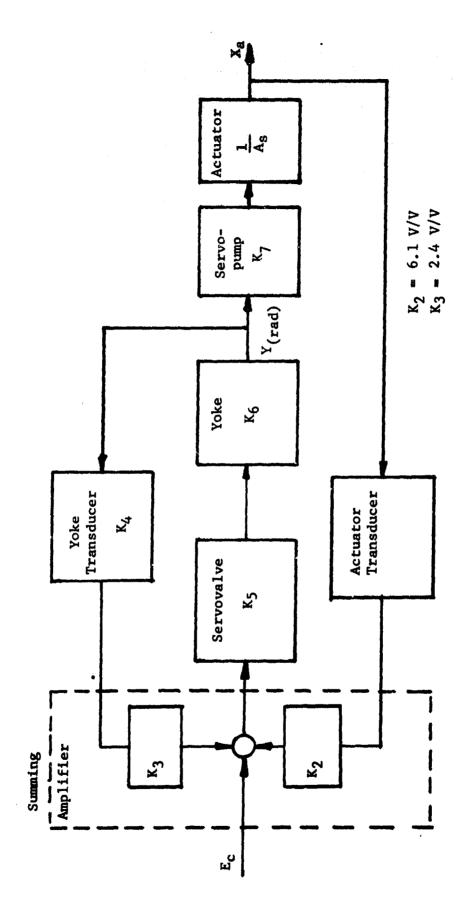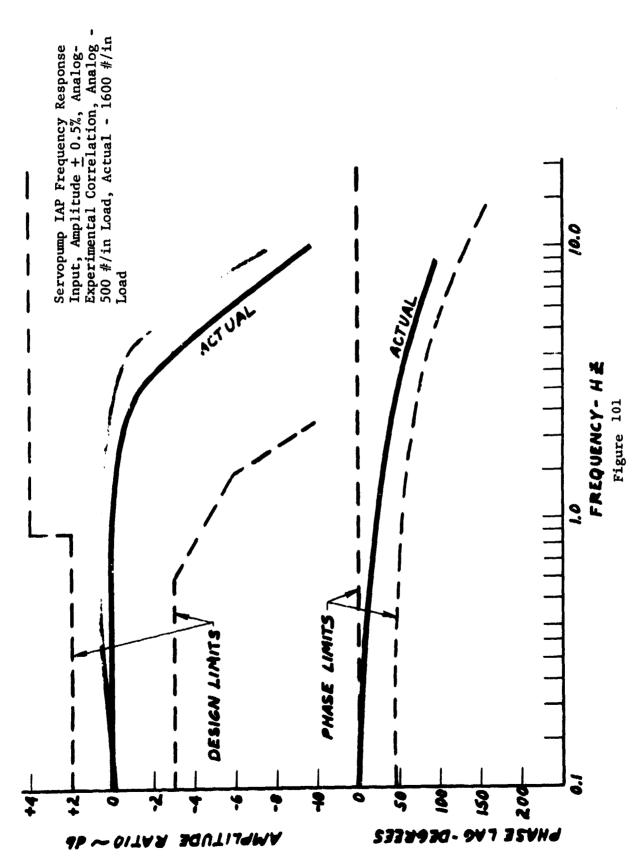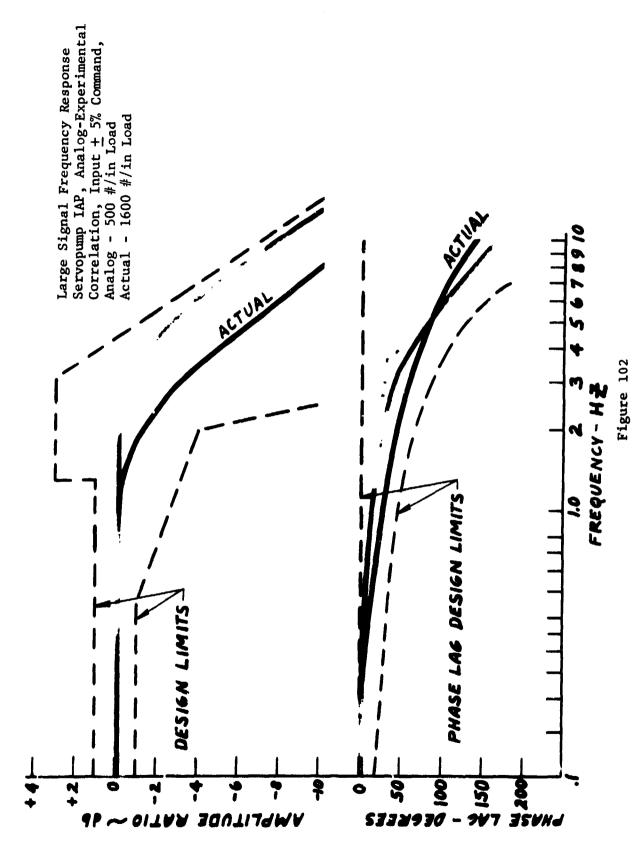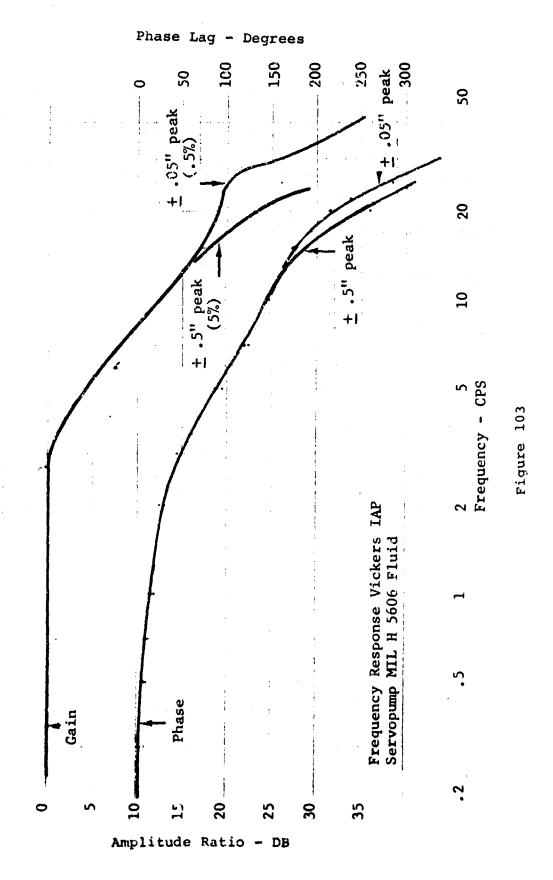
Figure 100 Integrated Servopump Block Diagram

$K_2 = 6.1$ V/V
$K_3 = 2.4$ V/V

Servopump IAP Frequency Response
Input, Amplitude ± 0.5%, Analog-
Experimental Correlation, Analog -
500 #/in Load, Actual - 1600 #/in
Load

FREQUENCY- HZ

Figure 101

163

Large Signal Frequency Response
Servopump IAP, Analog-Experimental
Correlation, Input ± 5% Command,
Analog - 500 #/in Load
Actual - 1600 #/in Load

Figure 102

164

Phase Lag - Degrees

Frequency Response Vickers IAP
Servopump MIL H 5606 Fluid

Frequency - CPS

Figure 103

Amplitude Ratio - DB

± .05" peak
(.5%)

± .5" peak
(5%)

± .05" peak

± .5" peak

Gain

Phase

165

Figure 104 Load System Block Diagram

166

MIL H 83282 hydraulic fluid. The actuator was alternately opera-
ted and flushed six different times. Upon completion of the
flushing procedure, the entire series of tests was re-run with
the new fluid. After completion of the tests with MIL H 83282
the actuator was again flushed using the same procedure to re-
fill with MIL H 5606. A no load frequency response test was
then conducted on MIL H 5606.

F4 Stabilator Actuator Testing

The F4 stabilator actuator was installed in the FGL load
test system. This is shown in Fig. 105 in the moving body con-
figuration. An auxiliary driver was connected to the mechani-
cal input to provide positioning capability. A no load fre-
quency response test was conducted with P_1 pressurized to 3000
psi and P_2 at 0 psi. This simulates the conditions of the Vic-
kers servopump test.

The auxiliary input driver was removed and the pilot's
input linkage was connected and grounded back to the fixed
shaft. This configuration permits tests of static and dynamic
stiffness with bearing end play removed from within the servo-
loop. P_1 and P_2 cylinders were pressurized to 3000 psi and
static stiffness was conducted using the test procedure of Ap-
pendix A. A tensile load bias of 4500 pounds was applied. The
dynamic stiffness was measured at sinusoidal load of 1700 pounds
peak and 3400 pounds peak about the bias level. The tensile
load bias was changed to a compressive one of 3900 pounds. The
dynamic stiffness was again measured by applying 1700 pounds
peak and 2800 pounds peak sinusoidal loads about the bias.

An extremely fine filtration system was installed in the
actuator supply line. As shown in Fig. 106 this provided filtra-
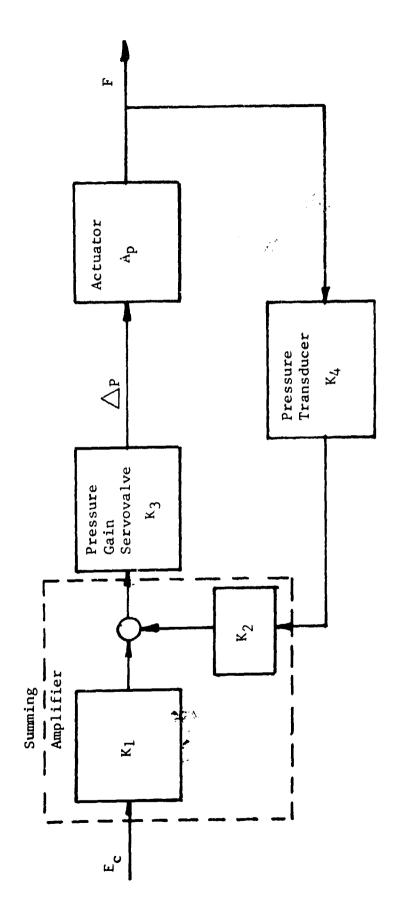tion down to the 1 micron level. With P_1 pressurized to 3000
psi MIL H 5606 and P_2 left at 0 psi, a static stiffness test
was conducted. A tensile load bias of 4500 pounds was applied
and dynamic stiffness was measured using 1700 pound and 3400
pound peak sinusoidal loads. The tensile load bias was changed
to a compressive load bias of 3900 pounds and the dynamic stiff-
ness was again measured, using the same peak load values. P_1
was depressurized and P_2 was pressurized to 3000 psi. Static
stiffness tests were conducted. Dynamic stiffness tests were
performed for both tensile and compressive load biases using
peak sinusoidal loads of 1700 and 3400 pounds.

The F4 stabilator actuator was reversed in the load test
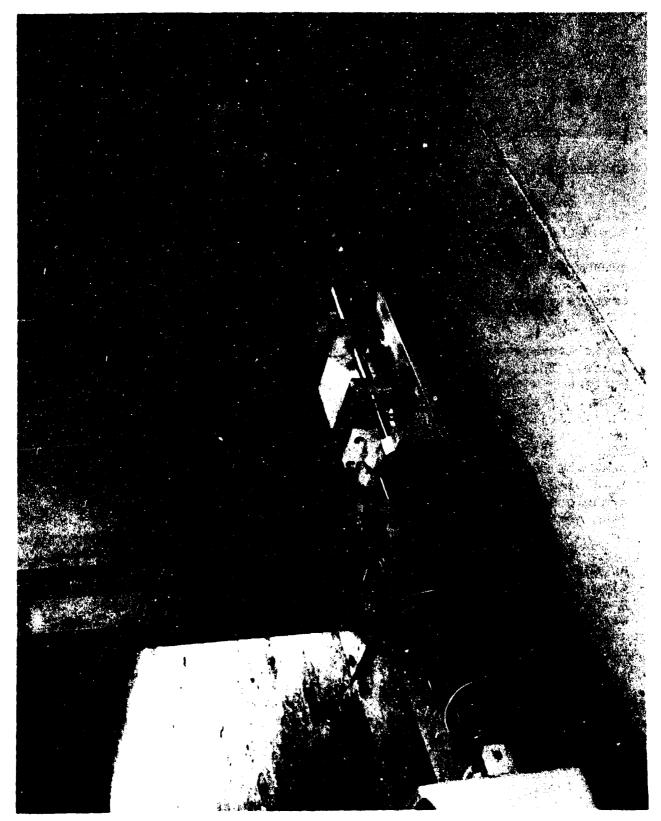
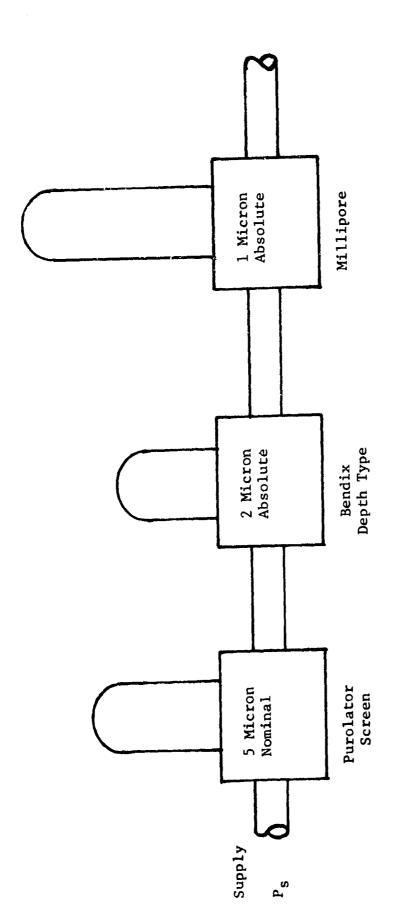Figure 105 F-4 Base Line Actuator in FGL Load Test System

Figure 106   Fine Supply Filtration System

system in order to permit tests of the unit in a fixed body con-
figuration. Static and dynamic stiffness tests were performed
using the same tensile compressive load biases with 1700 and
3000 pounds peak sinusoidal loads.

SUMMARY OF RESULTS

The servopump actuator was operated for approximately 70
total hours over a test program which lasted 2-1/2 weeks. During
that period, there was little observed degradation in perfor-
mance. Reservoir oil temperature stabilized at approximately
$245^{\circ}F$ to $250^{\circ}F$ after 30 minutes of operation and remained at
that level for test duration. Toward the end of testing, a
reservoir leak developed; however, this was not considered sig-
nificant enough to interfere with the completion of testing.
No load frequency response data correlated well with that ob-
tained by Vickers for both the 5% and .5% peak amplitude levels.
The F4 response data obtained for use as a base line exhibited a
lower frequency response than the servopump. Measured servopump
threshold was less than .002". A yoke loop limit cycle was ob-
served of approximately 5% minimum at a frequency of approxi-
mately 7 cps. The limit cycle frequency was basically constant,
independent of yoke loop gain; however, amplitude could be varied
with gain adjustments. In establishing the final loop gains
for system tests, the yoke loop gain was adjusted to minimize
the limit cycle amplitude. The static spring rate was determined
for both tensile and compressive load conditions. In all cases
and at all actuator positions up to 4 inches from null, the
spring rate was in excess of 300,000 pounds/inch. This compares
with the desired value of 167,000 pounds/inch. The complete
stiffness hysteresis loop was measured with the actuator in the
null position. This indicated that the spring rate is not con-
stant for all loads. The effective linear value of static spring
rate was found to be a function of the load used in determining
it with compressive values exhibiting the largest rate. Com-
parisons are not possible with the F4 base line actuator due to
an apparent silting condition which precluded static stiffness
measurements. The servopump dynamic spring rate indicated a
minimum value of approximately 70,000 pounds/inch in the neigh-
borhood of 8 Hz. This compared to a minimum F4 dynamic spring
rate of approximately 210,000 pounds/inch.

Servopump tests were made replacing the MIL H 5606 fluid
with MIL H 83282 fluid. A 5% increase in the response was ob-
served for the 5% signal and a 15% to 20% response increase was

observed for the .5% signal. This was observed with the same
loop gains that were used for MIL H 5606 tests. An 8% increase
in compressive static spring rate was noticed. Tensile static
spring rate remained the same within the limits of instrumen-
tation accuracy. Null stiffness characteristics appeared sig-
nificantly more linear than on the comparison 5606 tests. This
increase in stiffness was also observed in dynamic spring rate
tests where the minimum dynamic spring rate was raised to 80,000
pounds/inch and the frequency was now approximately 10 cps. The
no load frequency response tests conducted utilizing MIL H 5606
fluid after tests with MIL H 83282 correlated closely with ini-
tial measurements.

DISCUSSION OF RESULTS

The no load frequency response tests indicate 3 db atten-
uation at 4.4 cps and 45° phase shift at 3 cps for both the large
and small amplitude tests. Vickers data indicated 3 db point
at 4 cps and 45° at 2.5 cps. The Vickers data was conducted
with a load on the actuator; however, the maximum value would
be only 160 pounds and was not significant. The F4 base line
actuator indicated 3 db attenuation at 2.3 cps and 45° phase
lag at 2.2 cps for the large amplitude signals. The small am-
plitude signal indicated the 3 db point was at .58 cps. This
was attributed to linkage bearing end play. The servopump loop
response appeared to be significantly greater than the base line
F4 comparison.

A noticeable increase in servopump no load response was ob-
served when testing was accomplished with MIL H 83282 fluid.
For the large amplitude signals the 3 db point was raised to 5
cps with 45° phase shift occurring at 4.8 cps. For small am-
plitude signals, the 3 db point was at 15 cps with 45° phase
shift at 4.6 cps.

The actuator static spring rate measured for compressive
load exhibited a minimum at null for both 5606 and 83282 fluids.
The amount of increase as a function of position was signifi-
cantly more pronounced with the MIL H 83282 fluid. For tensile
loads, the spring rate with both fluids was quite similar. A
larger applied load was used for the 5606 tests than for the
83282 tests. In view of the variable stiffness characteristics
exhibited for the 5606 tests, it would appear that the lower
loaded tests, i.e. 83282 fluid, may have been influenced by other
than fluid properties. The null stiffness characteristics exhi-
bited with MIL H 83282 was slightly less variable than that

exhibited in tests with MIL H 5606. Compressive tests above 6400 pounds for the 83282 fluid could not be obtained due to a hunting condition which developed at the higher levels.

Static stiffness and null stiffness data for F4 base line actuator could not be determined. When a load was applied a slow drift type random motion of the output actuator occurred. This motion was of the same order of magnitude as the load deflections being measured. This phenomena was attributed to an apparent silting condition on the control valve which caused the effective flow areas to change. A fine level of supply filtration, 1 micron nominal, was installed. The amount of hunting decreased measureably. However, it was not enough to obtain a valid static stiffness plot. Attempts to measure F4 static stiffness by reversing the actuator in the load test system and treating it as a fixed body actuator were also not successful.

To minimize the effect of rod end bearing end play, the servopump dynamic stiffness was measured by applying a bias load and then sinusoidally cycling within the bias load condition. Fig.109 presents this stiffness for 4500 pounds tensile load bias. For two levels of peak applied load, the minimum spring rate is the same and occurs at approximately 10 cps. The spring rate value at .1 cps can be correlated with the 1700 pound peak applied load. This can be seen from the null stiffness plot, Fig. 103. For a $\pm$ 1700 pound sinusoidal load applied about the 4500 pound tensile level, the spring rate would be 486,000 pounds/inch. For a 3400 pound peak load about the same bias, the spring rate would be 389,000 pounds/inch. The dynamic spring rate measured at .1 cps was approximately 405,000 pounds/inch for the small peak load and 320,000 pounds/inch for the large load. In both cases, these rates would continue to increase until they reach the static value. A similar correlation can be observed for the dynamic spring rate tested with a compressive static load bias. The null stiffness plot for the actuator tested on MIL H 83282 fluid appears more linear, implying that the dynamic spring rate should be approximately the same for both load conditions. This is shown in Fig. 114 for the dynamic spring rate under compressive load bias. The tensile load bias, however, does show a deviation in the low frequency areas. All eight servopump dynamic stiffness plots have exhibited a minimum actuator dynamic stiffness in the range of 70,000 to 80,000 pounds/inch at approximately 10 cps.

The base line dynamic stiffness plots for the F4 stabilator actuator are presented in Fig.119 for both P_1 and P_2 pressurized

with no additional supply filtration. It can be seen that below 1 cps, stiffness decreases with decreasing frequency.

For the large load, the spring rate starts at 220,000 pounds/inch at 1 cps, increases to 620,000 pounds/inch and then decreases again above 10 cps. The small amplitude dynamic spring rate exhibits a similar characteristic. This shaped curve is true for both the compressive and tensile load biases and did not seem consistent with previous data and experiments. Consequently, the discrepancy was attributed to an apparent silting condition and supply pressure was filtered with a 1 micron filtration level. Tests were again conducted and the results seemed to validate the assumption since all other dynamic stiffness tests exhibited high stiffness at low frequencies, dropping to a constant or minimum value. This data utilizing 1 micron filtration on the supply is presented in Fig. 121 through 126 for both fixed body and moving body configurations. It was not possible to get a test with both P_1 and P_2 pressurized due to the limitations of available filters. The minimum observed value of dynamic spring rate was approximately 220,000 pounds/inch and occurred with the P_1 system only pressurized. This is a direct correlation with the servopump condition.
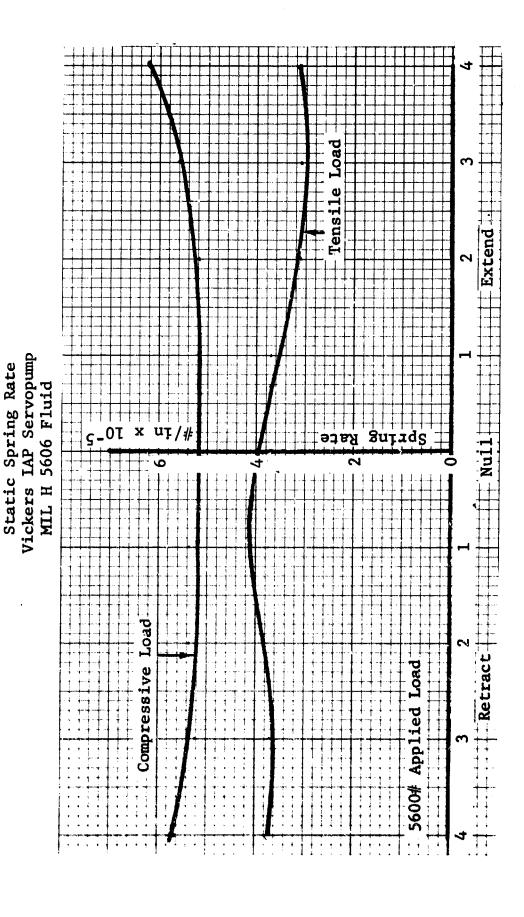
P_2 pressurized tests provided a minimum dynamic spring rate of approximately 280,000 pounds/inch. In any case, all tests of the base line F4 actuator satisfied the 167,000 pounds/inch stiffness requirement.

CONCLUSIONS AND RECOMMENDATIONS

The servopump integrated actuator package performed satisfactorily during the tests. Static spring rate measurements and null static stiffness characteristics could not be compared with the base line F4 actuator; however, it appeared that they did meet required values. The servopump dynamic stiffness plots indicated that the minimum value of stiffness was one-third that of the base line actuator. It is recommended that further investigation be undertaken to determine whether this is inherent in the specific design under consideration, or whether improvements can be made.

Performance comparisons at ambient and high temperature, i.e. 250°F, of MIL H 5606 and MIL H 83282 fluid indicate that performance will be at least as good with the high temperature fluid, MIL H 83282, as with conventional MIL H 5606. However, it is recommended that additional tests be conducted on an F4

type actuator utilizing both fluids. Additionally, it would appear desirable to investigate performance differences in the low temperature area due to viscosity differences in the fluid itself. Since stiffness with MIL H 5606 was found to vary with load, some of the observed spring rate increase may be attributed to test technique. (Different applied loads were used on 5606 and 83282.) Further investigation would appear justified using more precise techniques in an attempt to explain this phenomena. Development of an analytical model would appear warranted.

Static Spring Rate
Vickers IAP Servopump
MIL H 5606 Fluid

Figure 107

Null Stiffness
Vickers IAP Servopump
MIL H 5606 Fluid

Compressive Load - Pounds x 10^{-3}

Inches x 10^3
Extend Deflection

Inches x 10^3
Retract Deflection

Tensile Load - Pounds x 10^{-3}

Figure 108

Figure 109

177

Dynamic Spring Rate
Vickers IAP Servopump

Static Load Bias - 3900# Compressive
MIL H 5606 Fluid

± 1700# Peak Load

± 2800# Peak Load

Frequency - CPS

Spring Rate - #/in x 10^{-5}

Figure 110

Figure 111
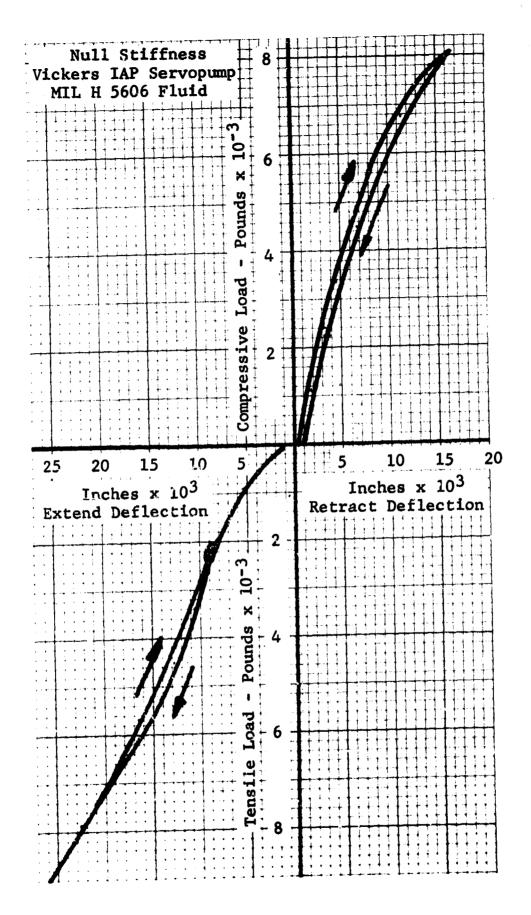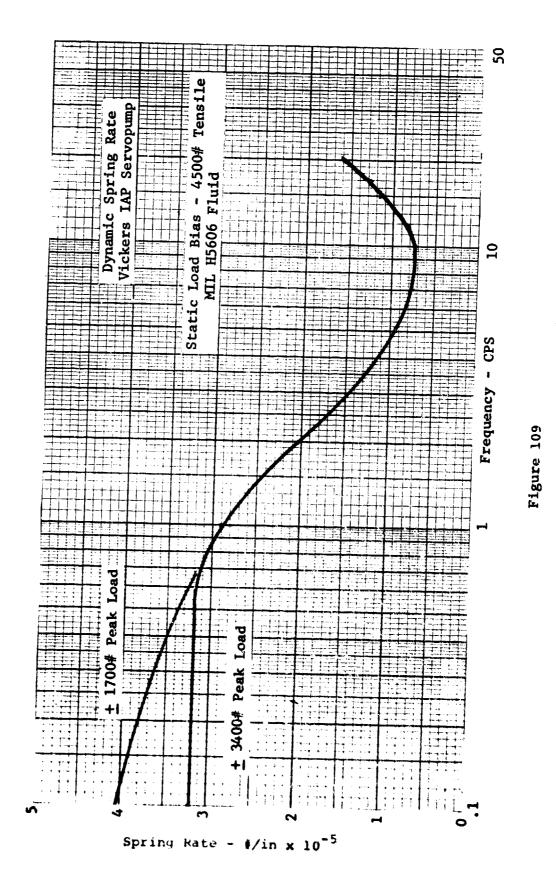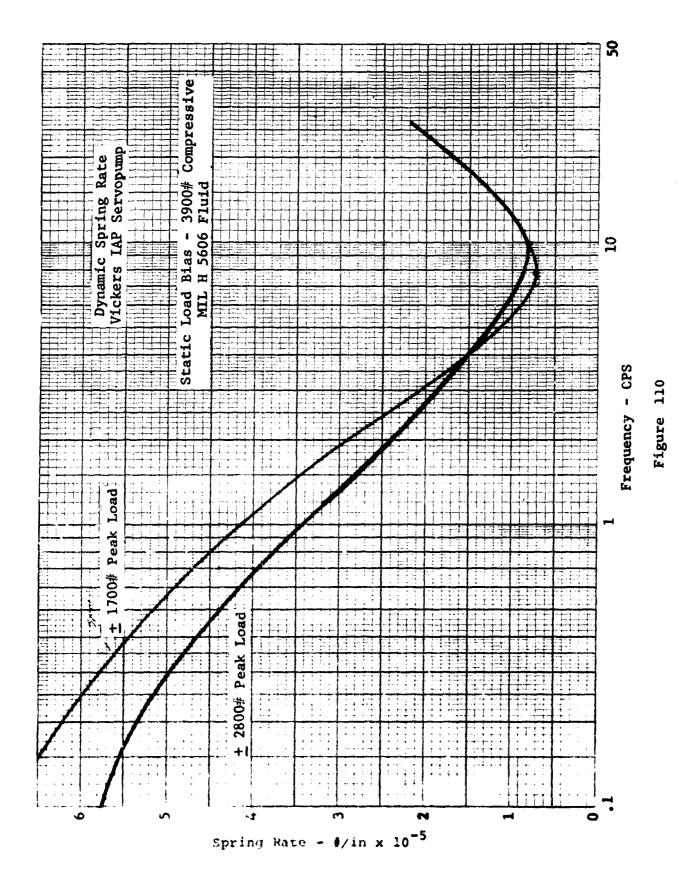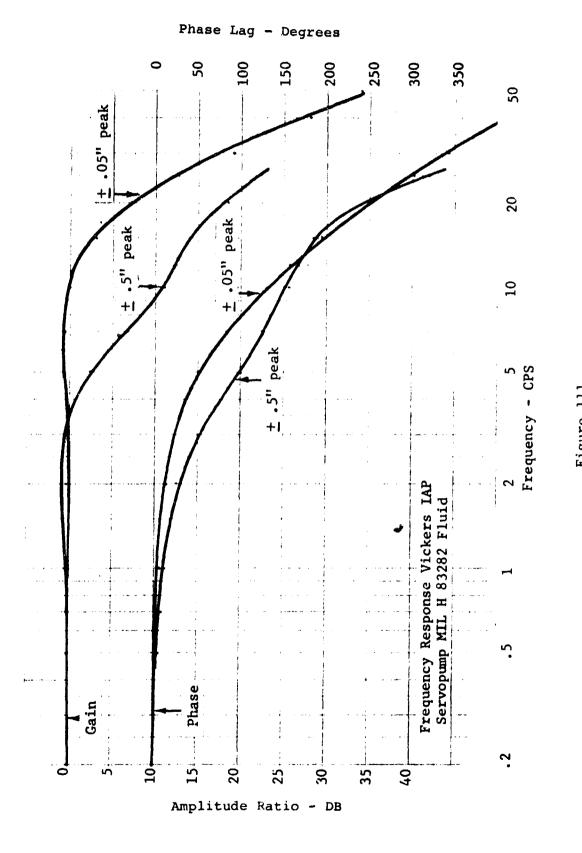
Frequency Response Vickers IAP
Servopump MIL H 83282 Fluid

Figure 112

Figure 113

181

Dynamic Spring Rate
Vickers IAP Servopump

Compressive Static Load Bias
MIL H 83282 Fluid

$3400\# \pm 2300\#$
and
$3900\# \pm 3400\#$

Frequency - CPS

Figure 114

Spring Rate - #/in x 10^{-5}

Figure 115

183

Figure 116.

Frequency Response
Vickers IAP Servopump

MIL H 5606 Fluid After Tests
with MIL H 83282 Fluid

Figure 117

185

Figure 118

186

Moving Body Dynamic Spring
Rate F4 Stabilator Actuator

P1 = 3000 psi
P2 = 3000 psi

MIL H 5606 Fluid
Tensile Load Bias = 4520#

No additional supply
filtration provided

Frequency - CPS

Figure 119

Spring Rate - #/in x 10^{-5}

$\pm$ 1700# Peak Load

$\pm$ 3400# Peak Load

Figure 120

Moving Body Dynamic Spring
Rate F4 Stabilator Actuator

$P_1 = 3000$ psi
$P_2 = 0$ psi
MIL H 5606 Fluid
Tensile Load Bias = 4520#

$\pm$ 1700# Peak Load

$\pm$ 3400# Peak Load

$\pm$ 3400# Peak Load

Spring Rate - #/in x 10^{-5}

Frequency - CPS

Figure 121

189

Figure 122

Figure 123

191

Moving Body Dynamic Spring
Rate F4 Stabilator Actuator

$P_1 = 0$ psi
$P_2 = 3000$ psi
MIL H 5606 Fluid
Compressive Load Bias = 3940#

$\pm$ 2800# Peak Load

$\pm$ 1700# Peak Load

Frequency - CPS

Spring Rate - #/in x 10^{-5}

Figure 125

193
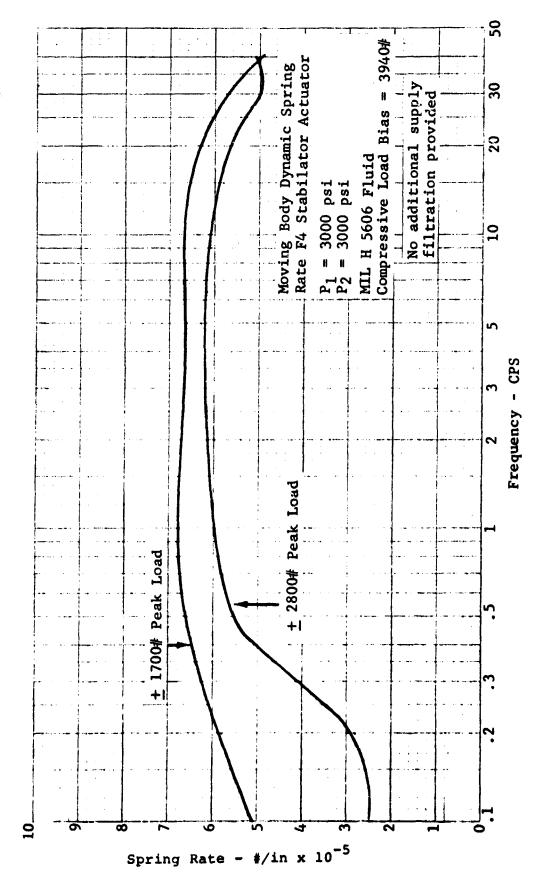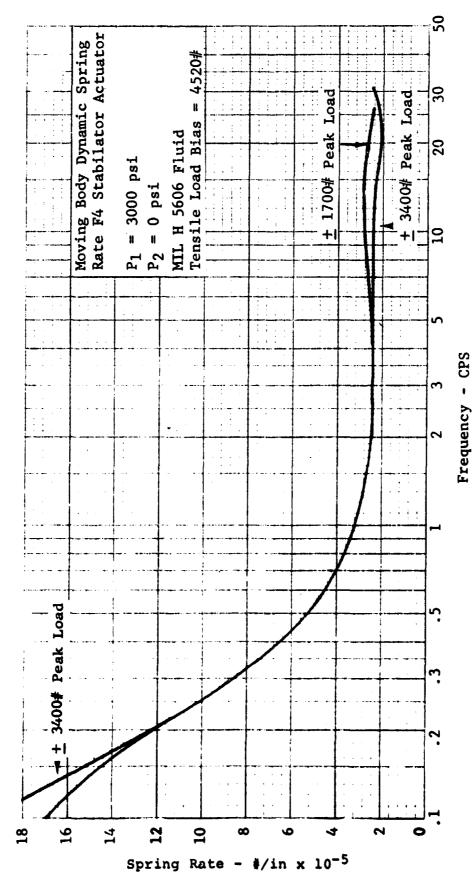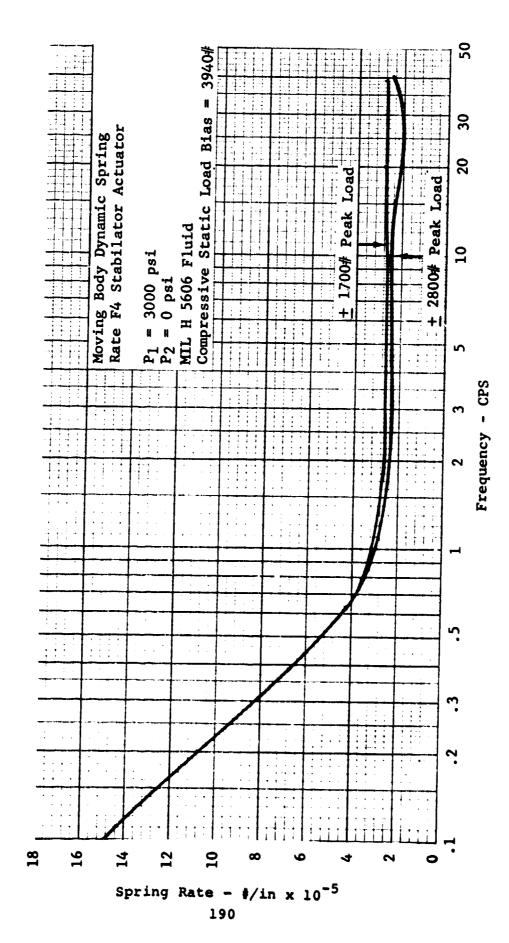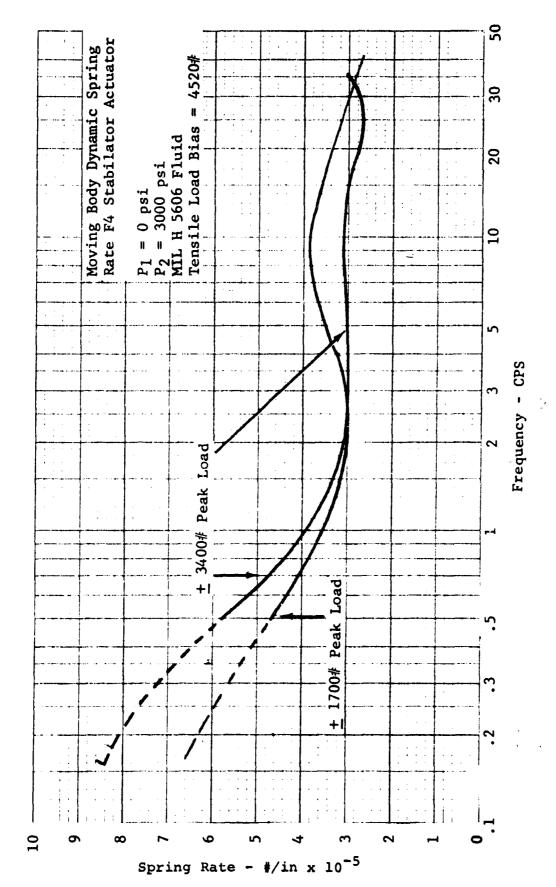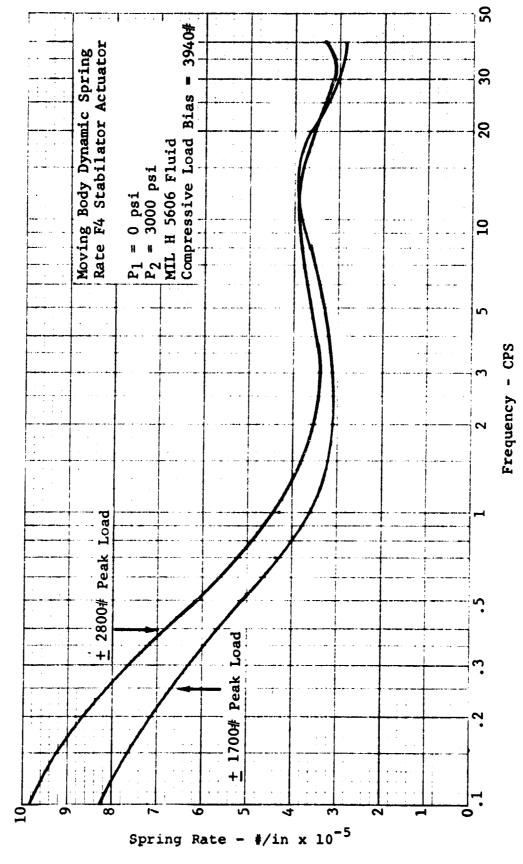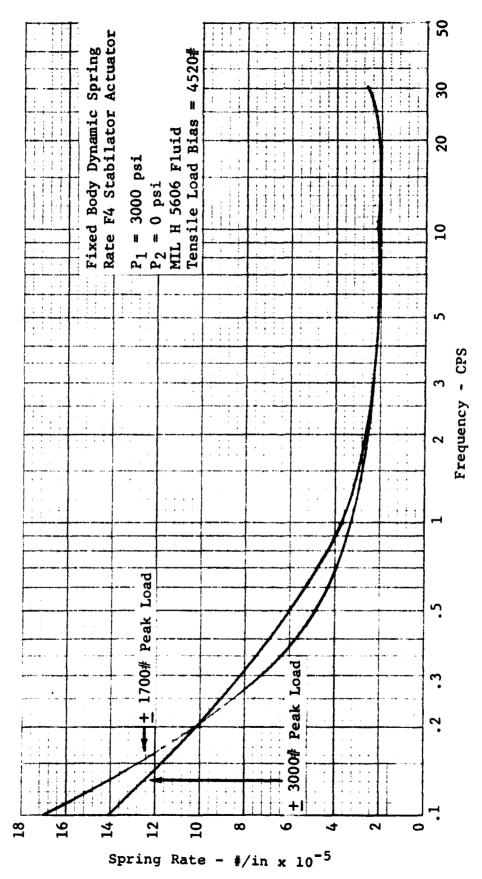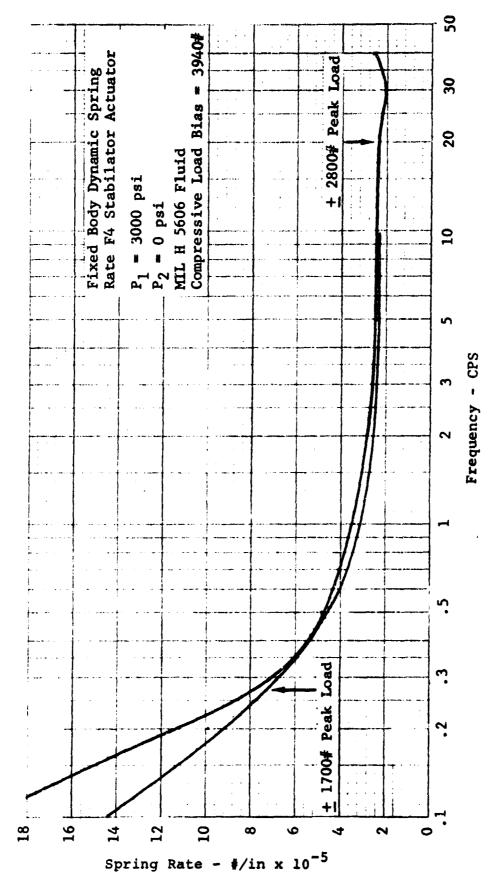
Figure 126

TEST PROCEDURE FOR THE VICKERS INTEGRATED
SERVO PUMP

I. Installation

A. Place the Vickers test actuator in the load test bed,
    positioning the test actuator so that the mid-stroke
    or null position corresponds to the null position of
    the load system.

B. Install capability for inserting ± DC or sinusoidal
    command voltage to the test actuator and/or the active
    load actuator.

C. Install instrumentation to excite and record the out-
    put signals of the linear, rotary and pressure trans-
    ducers.

D. Instrument the electric motor that drives the Vickers
    servo pump, in order to monitor power factor, voltage,
    and current.

E. Install instrumentation necessary to monitor fluid
    temperature in the vicinity of the servo pump through-
    out the test operation. This temperature is not to
    exceed 275°F.

F. Observe the suggested "fill and bleed" procedures.

G. Install limit switches to shut down electrical power
    if the actuator stroke exceeds ± 4.75 inches about
    the null position.

H. Sum the actuator rod position and the servo pump yoke
    position signals through the operational amplifier.
    These signals should apply a negative feedback, enabling
    the actuator to accurately assume the commanded posi-
    tion. The amplifier gain is established as that which
    will yield data matching the reported Vickers frequency
    response data.

II. Performance Testing

A. Establish the slew rate of the test actuator and com-
    pare this rate with that reported by the manufacturer.

195

B. Determine the unloaded frequency response.

1. Drive the unloaded test actuator with a 0.1 CPS
    signal of sufficient amplitude to effect a ± .050
    inch actuator rod deflection. Maintain this in-
    put amplitude and increase the frequency in incre-
    ments small enough to establish smooth amplitude
    ratio and phase shift curves. Record data from
    0.1 CPS to 25.0 CPS. Adjust the amplifier gains
    to "curve match" this data with the original re-
    ported manufacturer's response data.

2. Repeat the above procedure with an input ampli-
    tude necessary to produce a ± 0.5 inch actuator
    rod deflection. This data should also match the
    manufacturer's response data.

C. Determine the static stiffness.

1. Apply a 2000 lb. load to the nulled test actuator.
    Record the deflection and continue to increase
    the load, recording the test actuator deflection
    at 2000 lb. increments. Record data in the above
    manner, starting at 0.0 lbs. load and increasing
    to +10000 lbs., then decreasing the load back
    through 0.0 lbs. to -10000 lbs. and back to 0.0
    lbs. This data, complete with hysteresis infor-
    mation, indicates the linearity of the actuator
    stiffness over a broad load range.

2. Select a load value within the linear stiff-
    ness range established by the preceeding test.
    Apply this load to the test actuator while it
    is at the null position. Measure the actuator
    deflection and calculate the spring rate. Repeat
    this procedure, using the same load and varying
    the actuator rod position from mid-stroke to ±90%
    of full stroke in 1.0 inch increments. This data
    determines static spring rate deviation related
    to actuator position. Compare this data to the
    manufacturer's reported static stiffness data.

D. Determine the dynamic stiffness.

1. Apply a 6000 lb. bias load in the retract direction
    of the test actuator. This bias will eliminate

error introduced by reciprocating couplings. Measure the deflection and calculate the static spring rate.

2. Drive the load actuator with a 0.1 CPS signal of sufficient amplitude to apply a sinusoidally varying load to the test actuator of 2500 lbs. peak. Record the peak to peak deflection of the test actuator and calculate the dynamic spring rate. At low frequencies the dynamic spring rate should approximate the static spring rate. Maintain the $\pm$ 2500 lb. load and increase the frequency in small increments, recording the deflection at enough points to plot a smooth "dynamic spring rate vs. frequency" curve. Record data out to 25.0 CPS if possible.

3. Repeat (2) while applying a $\pm$ 5000 lbs. peak load to the test actuator. (6000 lb. retract bias).

4. Repeat (2) and (3) while applying a 6000 lb. bias load in the extend direction of the test actuator.

SECTION VI

EVALUATION OF GENERAL ELECTRIC 666A ACTUATOR

INTRODUCTION

Apparent limit cycling had been observed in the pitch axis of
the F4 aircraft involved in the AFFDL Optional Train Following
program. A series of tests were conducted on the G.E. 666A
pitch actuator to determine whether the limit cycling was at-
tributable to the actuator characteristics. These tests in-
cluded actuator loaded and unloaded frequency response, single
degree of freedom aircraft simulation with and without actuator
load, and a two degree of freedom simulation with and without
load.

PROCEDURE

The 666A actuator was mounted in the FGL test fixture as shown
in the photograph of Fig. 127. A no-load frequency response
test was conducted with .5% and 5% of rated stroke amplitude.
A tensile load of 4350 pounds was applied and frequency response
was rerun at both .5% and 5% stroke amplitudes. Closed loop
testing was conducted in conjunction with General Electric
Company personnel utilizing their pitch axis electronics and
TR-48 analog computer. The single degree of freedom block dia-
gram is shown in Fig. 128. The hardware and computer are shown
in the photograph of Fig. 129.

The initial single degree of freedom tests were conducted with
no load on the actuator. The pitch rate coefficient $M\delta$, was
increased in ten increments from 25 to 100. Pitch rate ampli-
tude (Peak to Peak) and limit cycle frequency were recorded. A
tensile load of 3350 pounds was then applied to the actuator
and the pitch rate coefficient $M\delta$ was varied in five steps
between 50 and 84. Again, pitch rate and limit cycle frequency
were recorded. The tensile load was increased to 4350 pounds
and $M\delta$ was varied in three steps between 33 and 84.

Pitch rate coefficient, $M\delta$, was varied in steps from 39 to 155
for a two degree of freedom simulation. No load, 3350 pound
tensile load and 4350 pound tensile load conditions were investi-
gated for a heavy weight and light weight aircraft model. In all
cases pitch rate and limit cycle frequency were recorded.
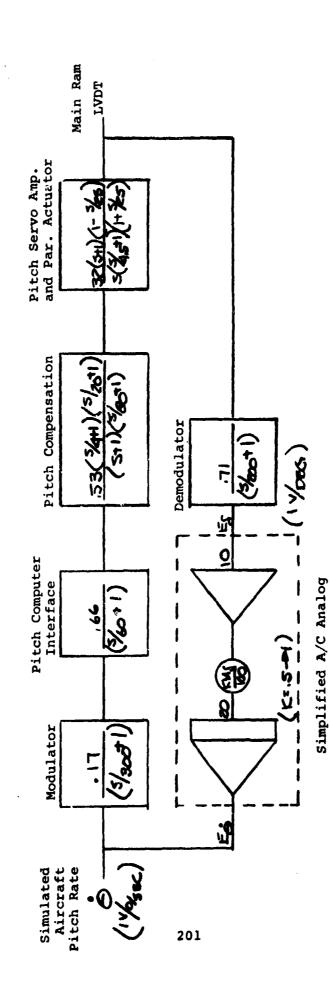
SUMMARY
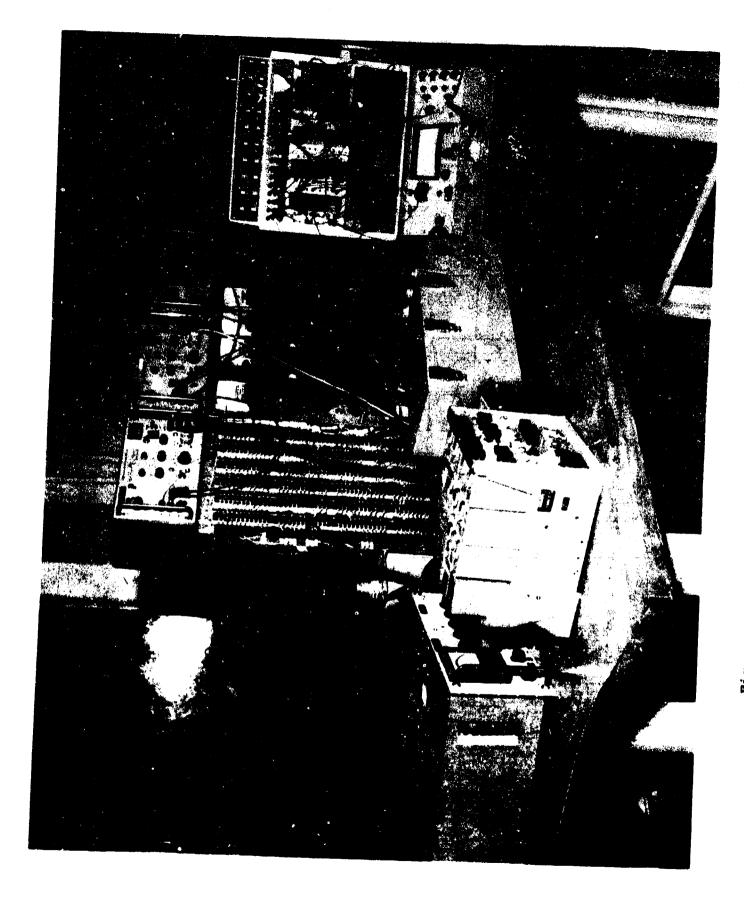
The loaded and unloaded frequency response plots are shown in
Fig. 130 and 131 respectively. The limit cycle data is presented
in Tables III and IV for the single degree of freedom model and

the two degree of freedom investigation. The maximum limit cycle frequency observed was approximately 4 cps and did not approach the 4.7 cps observed during supersonic flight tests of Phase I. A detailed analysis of results has been presented in a General Electric Company project memorandum, Memo Number 71-51-2716 by R. J. Freedman dated June 30, 1971.

Fig. 127 - 666A Actuator in FGL Load Fixture

Fig. 128 - 666A Pitch Rate Loop Block Diagram

201

Fig. 129 - 666A Pitch Axis Electronics and Computer

Phase Lag - Degrees
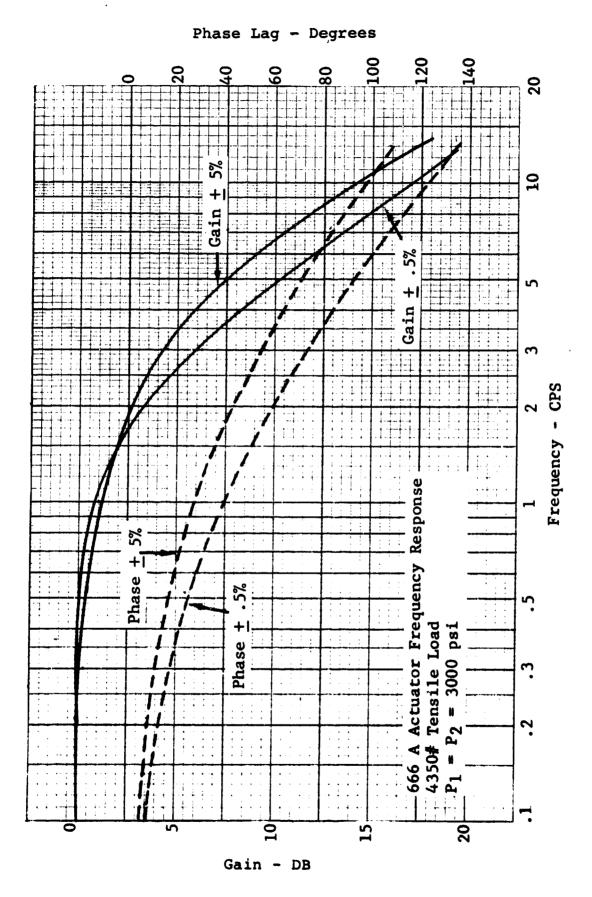
Fig. 130 - Loaded Frequency Response

666 A Actuator Frequency Response
4350# Tensile Load
$P_1 = P_2 = 3000$ psi

Frequency - CPS

Gain - DB
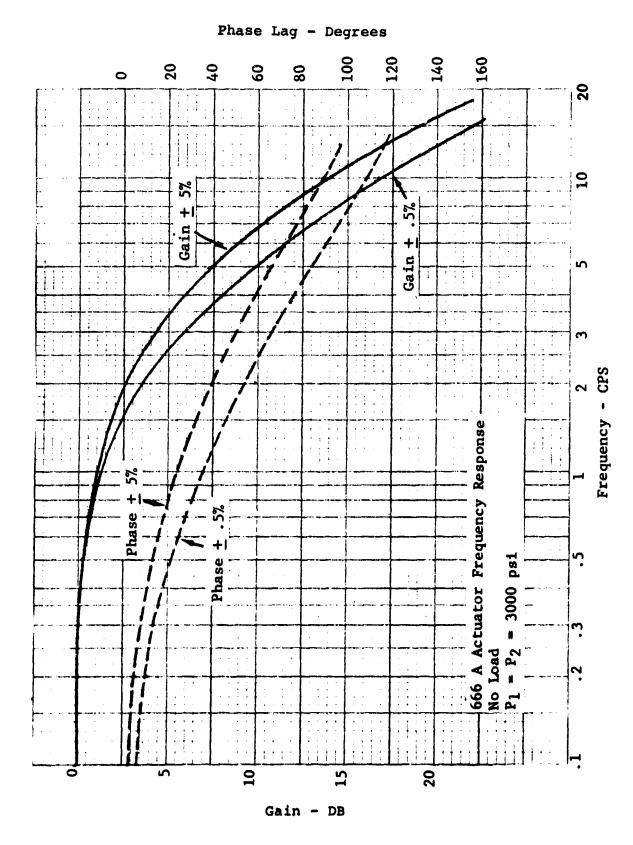
Fig. 131 – Unloaded Frequency Response

TABLE III

666A LIMIT CYCLE TEST

.

SINGLE DEGREE OF FREEDOM AIRCRAFT SIMULATION

M δ	No-Load		3350#TENSILE Load		4350#TENSILE Load	
	θ^O(PK-PK)	f(CPS)	θ^O	f(CPS)	θ^O	f(CPS)
25.2	.008	1.28	–	–		
33.6	.01	1.47	–	–	.005	1.79
42	.01	1.89	–	–		
50.5	.01	2.38	.004	2.32		
58.8	.01	2.5	.018	2.56	.017	2.27
67.3	.017	2.5	.019	2.52		
75.7	.021	2.56	.027	2.70		
84.2	.043	2.94	.055	3.12	.035	2.94
92.5	.07	3.32				
100	Unstable		Unstable			

TABLE IV

666A LIMIT CYCLE TESTS

2 DEGREE OF FREEDOM AIRCRAFT SIMULATION

1.2 M/HW-5 K SIMULATION				$M\delta$(NOM) = 93		
$M\delta$		No-Load		3350#TENSILE		4350#TENSILE
	$\dot\theta$	f(CPS)	$\dot\theta$	f(CPS)	$\dot\theta$	f(CPS)
39.1	.028	2.12	.025	2.7	.02	2.86
58.8	.046	2.17	.035	3.92	.05	2.67
78.2	.05	2.63	.085	2.71	.07	2.86
118	.07	3.57	.11	3.45	.13	3.33
155	.135	3.57	–	–		

666A LIMIT CYCLE TESTS

2 DEGREE OF FREEDOM AIRCRAFT SIMULATION

1.2M/LW-5K SIMULATION				$M\delta$(NOM) = 56		
$M\delta$		No-Load		3350#TENSILE		4350#TENSILE
	$\dot\theta$	f(CPS)	$\dot\theta$	f(CPS)	$\dot\theta$	f(CPS)
25.2	–	–	.055	2.03	.035	1.99
37.8	–	–	.055	2.65	.050	2.43
50.5	–	–	.072	3.03	.105	2.84
75.7	–	–	.140	3.43	.160	4.03

SECTION VII

EVALUATION OF ACTUATORS

DEVELOPMENT OF TEST EQUIPMENT

A portable hydraulic flow stand was assembled. This unit is
shown in the photograph of Fig. 132 and provides a capability
of measuring flow rates between .25 and 20 gpm. System supply
and return pressure gages are also provided to 3000 psi.

A self contained transducer range and balance panel was de-
signed and fabricated for use with strain gage type transducers.
This unit is shown in the photograph of Fig. 133 and contains
provisions for four transducers. Additionally, the panel con-
tains a single ended investing D.C. operational amplifier.
Amplifier gain is adjustable through the use of 100 k potenti-
ometers. The range and balance schematic is shown in Fig. 134.

Fig. 132 – Portable Hydraulic Flow Measurement Stand
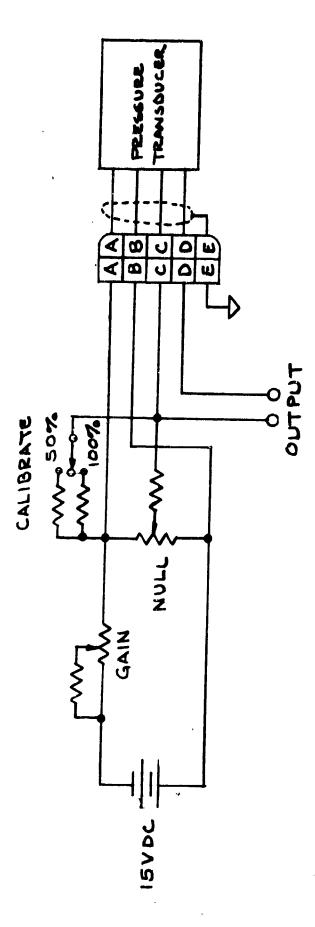
Fig. 133 - Transducer Range and Balance Panel

Figure 134

RANGE & BALANCE SCHEMATIC DIAGRAM

SECTION VIII

CONTAMINATION PARTICLE COUNTING

There are two basic methods of counting the contaminate particle in a fluid. The first method is manual or microscope counting. The second method is the automatic particle counting system.

The manual method is performed by filtering an exact quantity of fluid through a membrane filter. With the aid of a microscope, the collected particles are measured with a reticle and counted in defined group sizes.

Advantages of the Microscope Method are:

1) Basic equipment cost is low.

2) Technicians are easily trained.

3) Definite shape or structure can be seen.

4) An approximate composition of the particle can be seen.

Disadvantages of the Microscope Method are:

1) Counting is very slow, 5-6 hours per sample count.

2) Operator fatigue is high; possiblity of injecting errors into the counts. This error is not predictable.

3) High possibility of coincidence error (one particle on top of the other) because of the two dimensional viewing.

4) More than one technician is required to obtain a reasonable counting rate.

5) Fluid can only be monitored in small quantities.

Automatic particle counters are based on particles interrupting a light beam, creating an electrical impulse or reflecting a sonic tone. (These methods will be discussed in detail later in this text. The sonic method was not evaluated due to lack of response from vendors)

Advantages of the Automatic Counting Method are:

1) Counting can be completed rapidly. (30 minutes per batch)

2) In line monitoring is possible.

3) Operator fatigue is very low.

4) Size groups can be counted simulantaneously.

5) Counts small particles accurately.

211

Contamination Particle Counting (Continued)

    6)   Counting errors can be predicted.

Disadvantages of Automatic Particle Counters are:

    1)   Equipment cost is high.

    2)   A relative shape or composition of the
         particles is unknown.

    3)   "Log Jamming" (counter clogging) can occur.

An attempt has been made to emphasize that there is relative
justification to employ an automatic particle system in a
laboratory where contamination studies are conducted.

A literature search was conducted to attempt to recommend
which automatic counting method is the most satisfactory.
Response was received from the following manufacturers of
particle counting systems. A brief description of each
counter studied is as follows:

    A.   HiAc Counter

        1.   The HiAc particle counter may be equipped
            to count four or five size ranges of
            particles simultaneously. Using inter-
            changeable microcells, particles from two
            microns to 2500 microns may be counted.
            The instrument may be used for in-line-
            monitoring or for laboratory batch testing.
            Fluid flows through a passage of such di-
            mensions that the foreign particles pass
            by a window one by one. Light is collimated
            into a parallel beam by the long passageway
            which is at right angles to the fluid stream
            and impinges on a phototube on the opposite
            side of the tube. As a foreign particle in
            the fluid stream passes the window a portion
            of the light beam is interrupted. This
            causes a change in the output signal from the
            phototube proportional to the size of the
            particle passing through the light beam. The
            counter measures the area of each particle
            rather than the longest dimension as usually
            measured in the microscope method. Since the
            particles are recorded on the basis of cross-
            section area, a particle approximately 20 mi-
            crons long and four microns wide and a parti-
            cle 10 x 8 microns, would both be recorded as
            approximately 10 microns, particles or equi-
            valent to the area of a circle with a 10 micron
            diameter.

Contamination Particle Counting (Continued)

>For laboratory testing the HiAc counter
requires good sampling techniques. Once
a good representative sample is obtained
there is little chance of contamination
since the initial amount of fluid passing
through the apparatus serves to remove
completely any residual contamination
from the fluid previously tested. The
same sample of fluid may be recirculated
in order to obtain additional verifying
tests. The particle counting may be done
in any clean laboratory area provided that
the sampling is done in a "clean room"
atmosphere.

B.   Royco Nepholometer

The Royco Nepholometer uses the same basic princi-
pal as the HiAc, i.e., the interruption of a light
beam. The essential difference is that the light
measured is that deflected by the particle at 90°
to the light source. The instrument measures
particles from 0.5 to 160 microns. Fifteen dif-
ferent sizes may be counted and various sizes
included or excluded by means of a switch. Selected
particle sizes or total particles larger than the
selected size can be counted. The Royco instrument
makes possible a rapid sampling rate and appears to
be very good for in-line monitoring.

C.   Coulter Counter

This instrument measures the volume of individual
particles suspended in an electrically conductive
fluid. Since petroleum fluids are non-conducting
a miscible electrolyte must be added. The fluid
sample is drawn through a calibrated aperture of
such dimensions that particles pass through one
by one. The electrical resistance across the
aperture is measured by means of positive and nega-
tive electrodes on either side of the aperture.

The Coulter counter is essentially a laboratory
instrument and is not readily adaptable to in-line-
monitoring. Sizes from 0.5 to 500 microns may be
counted. Since the petroleum fluid must be diluted
with four parts electrolyte only a small amount of
fluid can be tested during each operation. The
instrument samples 2 mls per trial run which is
equivalent to 0.5 mls of the test fluid.

Contamination Particle Counting (Continued)

The instrument can be used in any clean laboratory
area, however, the solvents used as electrolytes
must be kept free from particulate contamination.

The following reports compare the microscope to automatic
counting methods. "NAEC-AML-2267, Bristol Aircraft LAB.
REF. MG/R/RFC/17., and a reprint 'Evaluating the HiAc PC-101
Automatic Particle Counter", from the Journal of American
Association for Contamination Control, January 1964."

None of these reports indicated absolute correlation between
the microscope and automatic counting methods. The largest
discrepencies were in the 5-10 micron ranges. This may indi-
cate that the automatic counters are not fatigued by the large
quantity or small particles to be counted. Therefore, they
may be giving a more accurate count in this size range.

This survey was restricted to literature available from vendors
of contamination monitoring equipment and published reports.
Actual experience has been gained only with the HiAc counter at
Wright-Patterson Air Force Base and HYDRAULIC RESEARCH. This
unit appears satisfactory for laboratory use. The only deficiency
found is that it can be tempermental due to log jamming; poor
results can be obtained if not operated by an experienced
technician.

HYDRAULIC RESEARCH recommends that for final selection of a
contamination counting system contact be made with the candidate
manufacturers asking for an "in house" demonstration. During
the manufacturers "in house" demonstrations a selected experienced
technician should operate each unit individually. A test under
these conditions should prove to be the most satisfactory for
final selection of a laboratory instrument.

DOCUMENT CONTROL DATA - R & D

(Security classification of title, body of abstract and indexing annotation must be entered when the overall report is classified)

1. ORIGINATING ACTIVITY (Corporate author)	2a. REPORT SECURITY CLASSIFICATION
Hydraulic Research & Manufacturing Company Valencia, California 91355	UNCLASSIFIED
	2b. GROUP NA

3. REPORT TITLE

Test and Development of Flight Control Actuation System Components for Military Aircraft

4. DESCRIPTIVE NOTES *(Type of report and inclusive dates)*

Final Report - December 1970 to November 1971

5. AUTHOR(S) *(First name, middle initial, last name)*

Goldstein, Stanford M.
Schreadley, Harry W.
Bazill, Dale G.

6. REPORT DATE	7a. TOTAL NO. OF PAGES	7b. NO. OF REFS
February 1971	214	

8a. CONTRACT OR GRANT NO. F33615-71-C-1124	9a. ORIGINATOR'S REPORT NUMBER(S)
b. PROJECT NO. 8225	NA
c. Task No. 822510	9b. OTHER REPORT NO(S) *(Any other numbers that may be assigned this report)*
d.	AFFDL-TR-72-13

10. DISTRIBUTION STATEMENT Distribution limited to U. S. Government Agencies only; test and evaluation; statement applied 1 February 197? Other request for this document must be referred to AF Flight Dynamics Laboratory (FGL), W-PAFB, Ohio   45433

11. SUPPLEMENTARY NOTES	12. SPONSORING MILITARY ACTIVITY
NA	Air Force Flight Dynamics Laboratory Wright-Patterson AFB, Ohio 45433

13. ABSTRACT Test and development activities were conducted in the following nine areas:

1. Evaluation of a breadboard multiplexing system driving a fly-by-wire actuator.

2. Evaluate actuation system of six-degree of freedom motion base.

3. Evaluation of a general purpose actuator test stand.

4. Various design concepts were explored for the improvement of branch isolation techniques.

5. Evaluation of a Vickers Inc. integrated servopump actuator package.

6. Investigation of limit cycle characteristics of a General Electric 666A actuator.

7. Literature search and recommendation for a laboratory contamination measurement system choice.

8. Fabrication of a portable flow measurement stand.

9. Design and Fabrication of a transducer range and balance panel.

DD FORM 1473 NOV 65

14. KEY WORDS	LINK A		LINK B		LINK C	
	ROLE	WT	ROLE	WT	ROLE	WT
Flight Control						
Servoactuator						
Integrated Actuators						
Flow Difference Sensors						
Flight Control Actuators						
Actuator Test Stand						
Hydraulic Fluid Contamination						
Signal Multiplexing						